mgr Sonia Maria Dębek

Discovery and Characterisation of the Epigenetic Function of PIM Kinases in Diffuse Large B-Cell Lymphoma

Rozprawa na stopień doktora nauk medycznych i nauk o zdrowiu

w dyscyplinie nauki medyczne

Promotor: prof. dr hab. n. med. Przemysław Juszczyński

Promotor pomocniczy: dr Dorota Komar

Studium Medycyny Molekularnej

INSTYTUT HEMATOLOGII
I TRANSFUZJOLOGII

Obrona rozprawy doktorskiej przed Radą Dyscypliny Nauk Medycznych

Warszawskiego Uniwersytetu Medycznego

Warszawa, 2023 r.

Słowa kluczowe: kinazy PIM, chłoniak rozlany z dużych limfocytów B, epigenetyka, regulacja transkrypcji

Keywords: PIM kinases, diffuse large B-cell lymphoma, DLBCL, epigenetics, regulation of transcription

Acknowledgements

I would like to thank:

- **Przemysław Juszczyński, MD, PhD**, my supervisor, for letting me conduct this project in his lab, for substantive consultations, for his time, and for the help with writing grant applications based on the results of the described PhD project.
- **Dorota Komar, PhD**, the co-supervisor, who is the most inspiring, bright and positive scientist I know. When I grow up, I want to be like Dorota Komar.
- **Filip Garbicz, MD.** Working with Filip has been a pleasure and a true intellectual feast. Thank you for the inspirations, for the excitement with our Sleeping Beauty project, and for being a great friend.
- **Aleksandra Żołyniak, MSc** (my best partner in crime!), **Paulina Laskowska, MSc; Anna Rams, MSc; Piotr Mrówka, PhD,** and **Marta Pelon, MSc,** for the laughs and friendly atmosphere in the Toucan Nest.
- **Eliza Głodkowska-Mrówka, MD, PhD,** and again **Piotr Mrówka, PhD,** for caring about me as if I was your family.
- **Julia Ostrowska, MSc** who helped me with logistics.
- **Marcin Kaszkowiak, MD**, **MSc** for his bioinformatic and statistical comments.
- And other lab members who were kind to help me find my way when I joined the lab, especially **Emilia Białopiotrowicz-Data, PhD** and **Ewa Jabłońska PhD.**

This work is scientific, but I would have never been able to write it, or finish it if not for the indescribable support from the following wonderful people - although they are not directly connected with the laboratory, they were equally important for the work:

- **My parents**, **Irena and Krzysztof Dębek,** who raised me to be a person capable of carrying a PhD project, and were a remarkable help during the 5 years of the PhD, and all the 30 years of my life.
- **My boyfriend, Piotr Łukasiewicz,** who supported me and believed in me absolutely every second.
- **Jazz Point dance school team: the owner - Joanna Gralińska, the teachers: Magdalena Tandek, Helena Hajkowicz and Julia Kozioł, and other fellow dancers,** who all provided me with enormous loads of fun and self-confidence, and helped me achieve a healthier mind and a healthier body by making me focus on pointe feet, high jumps, and balanced pirouettes, instead of being frustrated with scientific conundrums.
- **and all my friends and family** – your support was really felt. Thank you.
- as well as **Magdalena Gąssowska-Szmidt, Magdalena Flaga-Łuczkiewicz, MD, and Marta Kowalczyk,** psychologists and a psychiatrist who supported me when things got very dark.

Sincerely, without the help from all the people above this thesis would never come to life.

Thank you all from the bottom of my heart.

Research conducted within The Foundation For Polish Science TEAM Grant

POIR.04.04.00-00-5C84/17

Doctoral studies realised within The National Centre for Research and Development

POWR.03.02.00-00-I041/16-00

Contents

Figures and Tables

Figures:

Tables:

Abbreviations

of phrases used more than twice

7AAD - 7-aminoactinomycin D

ABC - activated B-cell-like

AID - activation-induced cytidine deaminase

AML - Acute myeloid leukaemia

CAR-T - chimeric antigen receptor T-cells

cHL - Hodgkin lymphoma

CLL - chronic lymphocytic leukaemia

ChIP - chromatin immunoprecipitation

COO - Cell-Of-Origin

CTD – C-terminal domain

DMSO - dimethyl sulfoxide

DNA – deoxyribonucleic acid

DLBCL – diffuse large B-cell lymphoma

FBS – foetal bovine serum

FC – fold change

FITC - fluorescein isothiocyanate

g - relative centrifugal force

G1 (phase) – growth 1

GCB – germinal centre B-Cell-like

GSEA - Gene Set Enrichment Analysis

HEPES - 4-(2-hydroxyethyl)-1-piperazineethanesulfonic acid

KD – knock down

KO – knockout

lncRNA – long non-coding RNA

MTS - 3-(4,5-dimethylthiazol-2-yl)-5-(3-carboxymethoxyphenyl)-2-(4-sulfophenyl)-2H-tetrazolium

ncRNA – non-coding RNA

NHL – non-Hodgkin Lymphoma

NTC – non-targeting control

P_{adj} – adjusted p_{value}

PE – phycoerythrin

PI - propidium Iodide

PIM – serine/threonine protein kinase PIM 1-3 (Proviral Integration site for Moloney murine leukaemia virus)

PS - phosphatidylserine

P_{value} – probability value

RNA – ribonucleic acid

RNAPII - RNA Polymerase II

R/R – relapsed and refractory

S (phase) – DNA synthesis

SCR – scrambled RNA

SHM – somatic hypermutation

shRNA – short hairpin RNA

SE – super enhancer

seRNA – super-enhancer RNA

TE – typical enhancer

TF - transcription factor

TSS – transcription start site

Streszczenie

Odkrycie i charakterystyka epigenetycznej funkcji kinaz PIM w regulacji ekspresji genów w chłoniaku rozlanym z dużych limfocytów B

Rodzina kinaz PIM składa się z 3 protoonkogennych białek: PIM1, PIM2 i PIM3, ulegających ekspresji w wielu nowotworach, w tym chłoniaku rozlanym z dużych limfocytów B (DLBCL). Kinazy PIM regulują kluczowe procesy komórkowe, takie jak proliferacja, apoptoza, metabolizm i migracja, dlatego ich zahamowanie zyskało zainteresowanie jako potencjalna strategia terapeutyczna. Nad małocząsteczkowymi ihibitorami pan-PIM prowadzone są badania kliniczne, np. SEL24/MEN1703, który obecnie przechodzi II fazę badania w leczeniu AML. Choć ostatnie badania nieprzerwanie dostarczają nowych danych o biologicznej roli PIM w nowotworach limfoidalnych, szczegóły i mechanizmy działania onkogennego PIM oraz konsekwencje ich hamowania w DLBCL pozostają niewystarczająco poznane. Ponadto dotychczasowe badania wykazały potencjalną epigenetyczną rolę PIM poprzez fosforylację histonu H3S10, opisaną jednak tylko w pojedynczym *locus*. Genomiczna rola PIM w modulowaniu transkrypcji w komórkach chłoniakowych pozostaje niejasna.

Wpływ hamowania PIM na modyfikacje histonów i proliferację potwierdzono przez użycie małocząsteczkowych inhibitorów oraz przez wyciszenie genetyczne kinaz PIM w liniach komórkowych DLBCL. Inhibicja kinaz PIM wpłynela na globalne ilości modyfikacji histonów, czemu towarzyszyła niższa fosforylacja polimerazy RNA II, co sugeruje udział PIM w fazie elongacji transkrypcji. Zidentyfikowano również lokalne zmiany acetylacji histonów w obszarach enhancerów (H3K27ac) i promotorów (H3K9ac) w odpowiedzi na traktowanie inhibitorem SEL24/MEN1703, oraz przeprowadzono profilowanie ekspresji genów w liniach DLBCL. Zestawienie wyników analiz epigenomicznych i transkryptomicznych tłumaczy zmiany w ekspresji genów związanych z wieloma ścieżkami, m.in. metabolizmem RNA lub uszkodzeniami DNA. Indukcję uszkodzeń DNA dodatkowo potwierdzono przez badanie poziomu znacznika pęknięć DNA (γH2AX) w następstwie traktowania inhibitorem. Ponadto inhibicja PIM osłabiła ekspresję genów kontrolowanych przez super-enhancery (SE), czyli rozległe regiony regulatorowe odpowiedzialne za wysoki poziom ekspresji najważniejszych dla komórki genów, w tym onkogenów. Analiza zasugerowała również nowe procesy biologiczne kontrolowane przez PIM, w tym redukcję niekodujących RNA generowanych z regionów SE.

Przeprowadzone badania potwierdzają rozległą, epigenetyczną rolę kinaz PIM oraz wskazują, że zahamowanie aktywności PIM prowadzi do potencjalnie cytotoksycznych zaburzeń transkrypcji DLBCL. Wskazują również, że SEL24/MEN1703 może być nową opcją terapeutyczną w DLBCL, a także dostarcza danych do optymalizacji terapii ukierunkowanej na PIM w klinice.

Abstract

The PIM kinase family consists of 3 proto-oncogenic proteins: PIM1, PIM2 and PIM3, expressed in numerous cancers, including DLBCL. PIM kinases regulate crucial processes, such as proliferation, apoptosis, metabolism, and migration, therefore their inhibition is of great interest as a potential therapeutic strategy. In fact, pan-PIM inhibitors have been studied in clinical trials, e.g. MEN1703, which currently undergoes II phase trial in AML. Although recent studies have shed new light on the biological role of PIM in lymphoid cancers, the details and mechanisms of PIM's oncogenic effects and the consequences of their inhibition in DLBCL remain insufficiently understood. Earlier studies have demonstrated a potential epigenetic role of PIM through histone H3S10 phosphorylation, however, described only at a single locus. The broad genomic role of PIM in modulating transcription in lymphoma cells remains unclear.

The effect of PIM inhibition on histone modifications and proliferation was confirmed by treatment with small molecule inhibitors and by genetic silencing of PIM kinases in DLBCL cell lines. Pan-PIM inhibitor SEL24/MEN1703 changed the global amounts of histone modifications, accompanied by lower phosphorylation of RNA polymerase II, suggesting the involvement of PIM in the elongation phase of transcription.

Local histone acetylation changes in the enhancer (H3K27ac) and promoter (H3K9ac) regions in response to treatment with the SEL24/MEN1703 inhibitor were also identified, coupled with gene expression profiling in DLBCL lines. The integrated results of epigenomic and transcriptomic analyses explain the changes in expression of genes associated with many pathways, including RNA metabolism or DNA damage. The induction of the latter was further confirmed by examining the level of DNA break marker (γH2AX) following treatment with the inhibitor. In addition, PIM inhibition decreased the expression of genes controlled by super-enhancers (SE), i.e. wide regulatory regions responsible for the high level of expression of the most important genes for the cell, including oncogenes. The analysis also suggested novel biological processes controlled by PIM, such as the reduction of non-coding RNAs generated from SE regions.

The conducted studies document a vast epigenetic role of PIM kinases, and suggest that inhibition of PIM activity leads to potentially cytotoxic disturbances of DLBCL epigenetic patterns, and transcription. They also indicate that SEL24/MEN1703 can be a therapeutic

option in DLBCL, and provide information for optimisation of PIM-targeted therapy in the clinic.

1. Introduction

1.1. Diffuse Large B-Cell Lymphoma

1.1.1 DLBCL pathogenesis and diagnosis

Diffuse Large B-Cell Lymphoma (DLBCL) is the most common lymphoid malignancy in adults, characterised by high heterogeneity in terms of phenotype, molecular background, prognosis and response to treatment [1]. The malignant cells reside mostly in lymphoid organs, such as lymph nodes and spleen, however, extranodal localisations are encountered in up to 30% of patients; advanced DLBCL can spread to bone marrow, liver, peritoneum, pleura, and central nervous system [2]. Clinical symptoms are nonspecific, and include enlarged lymph nodes, unexplained weight loss and fever, night sweats and elevated level of lactate dehydrogenase (LDH) [3]. In the USA, the median age of diagnosis is 66 years, and an average of 64.6% of patients survive 5 or more years after being diagnosed (based on data from 2012-2018; SEER).

DLBCLs originate from cells undergoing germinal centre (GC) reaction, or from post-GC cells unable to terminally differentiate (plasmablasts). Germinal centres are functional compartments formed in secondary lymphoid organs by antigen-encountered B-cells, which proliferate and edit their immunoglobulin genes to diversify the repertoire of antibodies and increase their affinity to the antigen that initiated the GC reaction. During the GC reaction, the cells circulate between the so-called “dark zone”, where cells rapidly proliferate, and “light zone”, where they undergo selection and antibody class switching. In the dark zone, variable regions of the immunoglobulin chains are subject to somatic hypermutation (SHM). In this physiologic process, immunoglobulin locus is heavily mutated through deamination of cytosine to uracil by activation-induced cytidine deaminase (AID), followed by repair by base excision repair enzymes and error-prone polymerases. The introduction of mutations in the robustly proliferating cells results in large amounts of B lymphocytes, all of which have different receptors and varying affinity to the antigen. In the light zone, the cells are quiescent, but undergo selection for the best affinity to the antigen, and the cells with non-productively edited Ig genes are eliminated. B cells circulate between these two states, and epigenetically alter gene expression programme, including chromatin remodelling, histone modifications, DNA methylation or mRNA modifications [4]. After several

rounds of transitions between the zones, the successful cells cease the divisions and differentiate to become memory or antibody-producing plasma cells. Given the processes that take place in the GC, and the physiologically blunted DNA damage response due to BCL6 activity, GCs are particularly conducive to acquisition of oncogenic driver mutations [5]. For example, *PIM1*, *MYC, Rho/TTF, FAS, BCL2* are known to be frequently mutated by AID in DLBCL cells [6]. More recent studies demonstrated that AID mutational signature is present in 20% of driver genes [1], but the most prevalent mutational signature associated with DLBCL is ageing (i.e. spontaneous deamination of CpG dinucleotides).

Early attempts to understand the molecular heterogeneity of DLBCLs and identify molecular substructure of this malignancy utilised microarray-based analysis of DLBCL transcriptomes. In a study by Alizadeh *et al.,* different DLBCLs were shown to share transcriptomic similarities with either normal GC cells (GCB-like DLBCLs), or anti-IgM/IL-4/CD40L-activated naive B-cells (ABC-like DLBCLs) [7]. Importantly, this cell-of-origin (COO) based classification conferred prognostic information: patients with GCB tumours have a significantly better prognosis than those with ABC-type tumours. However, consistent with a biased principle of the COO classification, certain number of tumours remained unclassified, indicating that there was an additional substructure that cannot be captured with this approach.

To obtain unbiased, comprehensive transcriptional profiles and subtype of DLBCLs, M. Shipp's group utilised a consensus cluster classification (CCC) algorithm, finding agreement between 3 independent clustering methods. Three biologically robust, discrete clusters were defined: "oxidative phosphorylation (Ox-Phos)," "B-cell receptor/proliferation (BCR)," and "host response (HR)". Importantly, the CCC classification was largely independent of COO [8].

Given the simplicity of the methodology developed for identifying COO clusters and the important clinical information provided by this classification, it is included in the current WHO classification of lymphoid malignancies [9]. Additional studies on the COO classification demonstrated that the GCB and ABC tumours arise *via* different pathogenic mechanisms and have different therapeutic vulnerabilities. For example, the GCB subtype is enriched in IGH::BCL2 fusion due to the t(14;18)(q32;q21), and mutations in fundamental genes for GC development, dark-light zone transitions and microenvironmental interactions, such as *EZH2*, *GNA13*, *MEF2B*, *KMT2D*, *TNFRSF14*, *B2M* and *CREBBP*. The ABC subtype is dependent on BCR

signalling and NF-κB activity, has lost most of the GC markers, expresses *IRF4/ MUM1*, and is characterised by mutations in the BCR pathway proteins, such as CD79B, CARD11, MYD88, and PIM1, as well as aberrations that block the B-cell differentiation program, e.g. *BCL6* rearrangements and *PRDM1/BLIMP1* mutation/deletion [9].

More recent classifications included low-frequency mutations, somatic copy number alterations, and structural variants analysed genome-wide. Such multi-omic, multi-layered analyses allowed for identification of additional complexity within DLBCLs [1,10,11]. These newer studies that focused on deciphering the molecular heterogeneity in DLBCL were performed by two groups: M. Shipp's and L. Staudt's teams at a similar time, and the independently obtained results were largely concordant. The newly characterised DLBCL subgroups are associated with the following defining lesions (listed in the descending prevalence): (i) frequent mutations of chromatin remodelers and BCL2, and overexpression of BCL2, (ii) structural variants of BCL6 and mutations in NOTCH2 signalling pathway components, (iii) CD79B and MYD88 mutations, (iv) JAK/STAT3 signalling and NF-κB activation, (v) TP53 inactivation, (vi) NOTCH1 mutations, or (viii) other alterations that did not resemble any of these groups. The mutations presented above define the clusters, but the groups may be further diversified by numerous other mutations.

Although the novel, multi-omic classifications are not broadly used in the clinic, they comprehensively elucidate DLBCL's oncogenic dependencies, providing robust underpinnings to the understanding of DLBCL pathogenesis. In addition, they define actionable vulnerabilities that can be utilised to design novel therapeutic approaches. Importantly, the fact that the most prevailing subtype of DLBCL utilises chromatin modification emphasises the need to study epigenetic landscape in DLBCL, with prospective therapeutic application.

1.1.2 DLBCL treatment

R-CHOP regimen is the current standard of care in DLBCL, usually administered in 3-6 cycles with or without radiation therapy [12]. R-CHOP consists of 5 drugs: Rituximab is an antibody targeting the B-cell-specific CD20 surface antigen, Cyclophosphamide is a DNA-alkylating agent that represses DNA replication, Hydroxydaunorubicin/Doxorubicin is DNA-intercalating agent that inhibits DNA replication, DNA repair and transcription; Vincristine (Oncovin)

inhibits formation of microtubules and mitotic spindle by binding to tubulin; and Prednisone is a glucocorticoid with immunosuppressive and anti-inflammatory properties. Approximately 50-60% of patients are cured with the standard R-CHOP regimen. However, remaining patients are refractory to R-CHOP or relapse after initial response. These patients can be treated with salvage chemotherapy (e.g. R-DHAP, R-ICE, or R-ESHAP) followed by autologous transplant, if eligible [13,14].

Registration of novel therapies, such as bispecific antibodies, antibody-drug conjugates (ADCs) or chimeric antigen receptor T-cells (CAR-T) brought new hope for DLBCL patients. Numerous clinical trials showed unprecedented response rates to CAR-T in relapsed and refractory (R/R) DLBCL patients, and CAR-T therapy has eventually become a standard of care for R/R DLBCL after at least 2 lines of treatment in the United States [15]. On the other hand, several recent analyses of real-world patient outcomes show that the response or overall survival are not substantially better with CAR-T therapy in comparison to the standard further-line regimens, such as allogeneic hematopoietic cell transplantation (alloHCT)[16–19]. Therefore, there is still an unmet need in DLBCL treatment for patients who do not respond to therapy, emphasising the importance of further basic studies of DLBCL biology, drug discovery, and clinical trials in these refractory cohorts.

1.2. PIM kinases

PIM kinase family comprises three serine/threonine kinases: PIM1, PIM2 and PIM3. The name derives from the genomic site that was frequently activated in murine T-cell lymphomas by Moloney murine leukaemia virus (Proviral Integration site for Moloney murine leukaemia virus) [20]. PIM kinases phosphorylate a broad array of substrates, important in cell proliferation, survival, migration, apoptosis, metabolism, or translation and play important functions in normal haematopoiesis, as well as carcinogenesis, especially of hematologic malignancies (recently reviewed by Bellon *et* Nicot [21]).

1.2.1 Regulation of expression of PIM genes

PIM1 gene is located on chromosome 6 (6p21.2), *PIM2* on the X (Xp11) chromosome, and *PIM3* on chromosome 22 (22q13). Physiological expression of PIM family genes is characteristic for hematopoietic cells (see Figure 1.1), especially in embryonic stem cells and early developmental states, such as foetal: spleen, liver, epithelia, or nervous system [22–25]. While expression of PIM1 and PIM2 is increased in hematopoietic cells and tumours, PIM3 shows a more promiscuous pattern of expression and low levels of this protein are observed in various tissues and solid tumours (Human Protein Atlas, proteinatas.org; and ref. 21). The expression of PIM is propelled mostly via the JAK/STAT pathway, by cytokines and growth factors including: interleukin-2 (IL-2) [26], IL-3 [26,27], IL-4 [26], IL-5 [28], IL-6, IL-7 [26,29], IL-9 [26], IL-12 , IL-15, granulocyte-macrophage colony-stimulating factor (GM-CSF) and G-CSF, alpha interferon [30], gamma interferon [26,31], erythropoietin, thrombopoietin [32], prolactin [33], or lipopolysaccharide [26]. Moreover, PIM proteins are overexpressed in most, if not all, human lymphomas and leukeaemias, and several solid tumours [34–36]. In case of DLBCL, PIM kinases are present in both GCB and ABC subtypes, but their elevated expression is more frequent in the more aggressive ABC subtype [37].

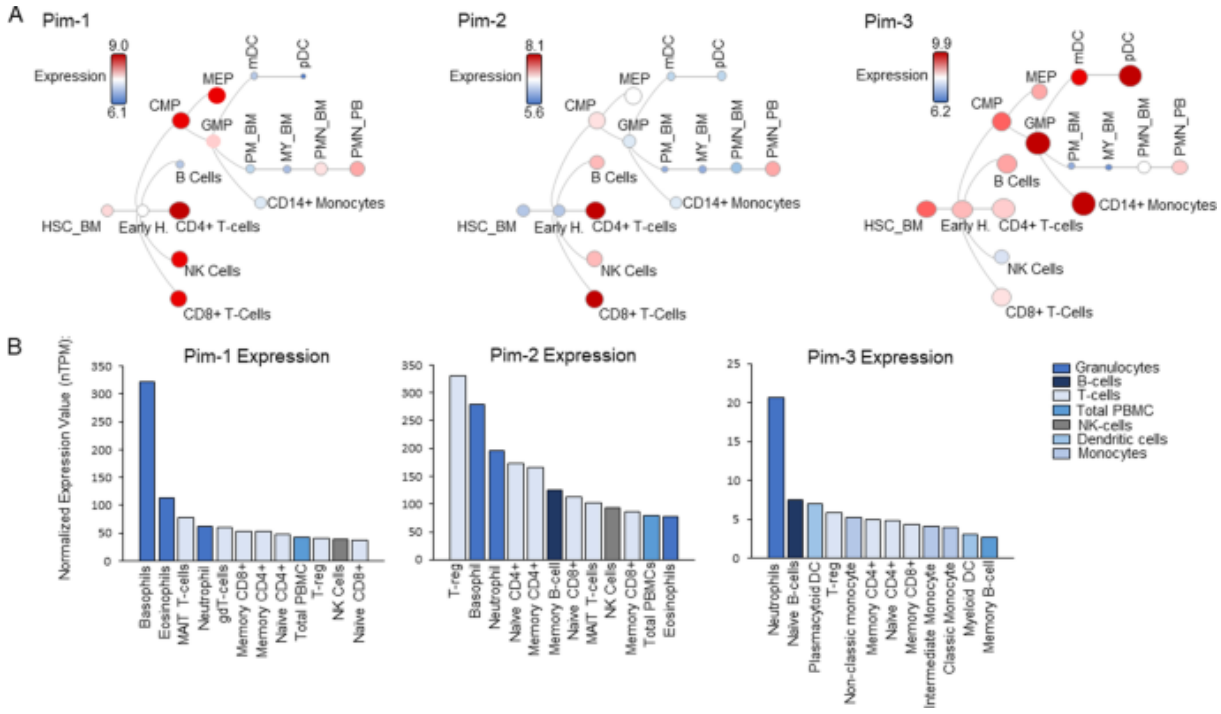

Figure 1.1 Expression of PIM kinases in the development of haematopoietic cells. Source: Bellon *et* Nicot, 2023 (ref. 21), by permission.

PIM mRNA has relatively short half-life ranging from minutes to several hours due to AUUA destabilising motifs in their long 3' untranslated region (UTR) [38] and GC-rich regions in 5' UTRs that require 5'-m7G cap for translation [39]. Additionally, microRNA miR-33a [40] and miR-761 [41] can downregulate PIM expression. Alternative translation initiation sites give rise to two isoforms of PIM1, three isoforms of PIM2, while PIM3 has a single isoform [42].

PIM proteins are constitutively active and their activity depends on the regulation of their transcription, translation, and protein turnover. In other words, their activity corresponds to their level in the cell [43,44]. The stability of PIMs can be regulated by chaperone heat shock protein HSP90, which prevents it from proteasome degradation and maintains correct conformation [45]. Moreover, PIM SUMOylation promotes ubiquitin-mediated degradation, enhances PIM's activity and possibly changes substrate specificity [46].

PIMs do not have fixed subcellular localisation and can change cell compartments. For example, in normal lymph nodes, PIM1 can have cytoplasmic and/or nuclear localisation, while in Burkitt lymphoma, PIM1 is exclusively nuclear [47]. In DLBCL, PIM1 can be localised in both the cytoplasm and the nucleus with a preference for one of the compartments, or have exclusively cytoplasmic localisation, PIM2 has mixed, nuclear-cytoplasmic localisation, while PIM3 is cytoplasmic. Interestingly, the nuclear localisation correlates with non-GCB (i.e. with more aggressive) DLBCLs, high proliferation and advanced disease stage [48]. Therefore, these data suggest that PIM's activity in the nucleus provides survival advantage for DLBCL cells.

The mechanism of PIM nucleo-cytoplasmic shuttling is poorly understood, however, it might be modulated by numerous factors, including isoform, cell differentiation state, cellular context, or protein modification. In prostate cancer, shorter PIM1, ~34 kDa, is localised in the cytoplasm and the nucleus, while the longer ~44 kDa isoform localises to the plasma membrane [49]. In myocytes, PIM1 is localised in the cytoplasm during proliferation, but is translocated to the nucleus upon differentiation. Interestingly, PIM1 with kinase-inactivating mutation K67M did not change its cytoplasmic localisation. This might suggest that the kinase activity and autophosphorylation is required for the nuclear translocation in myocytes. In line with this hypothesis, in differentiated myotubes, nuclear PIM1 is phosphorylated, while the cytosolic protein is unphosphorylated [50]. Other studies, however, suggest that the nuclear localisation is independent of kinase activity, but rather regulated by the C-terminus of the protein [47].

Change of subcellular localisation modulates PIM function – most probably due to the availability of different substrates in various cell compartments. In a study with human cardiac progenitor cells, PIM1 that was engineered to localise in the nucleus antagonised cellular senescence, while PIM1 that was directed to the mitochondria preserved mitochondrial integrity and increased the proliferation rate. In general, optimal progenitor cell traits were achieved upon translocation of PIM1 to specific cellular compartments/organelles [51]. These results show that the nuclear localisation of PIMs might enable specific gene expression programmes modifying cell biology, while the cytoplasmic PIMs participate in maintaining already established phenotypes.

PIM proteins share a considerable similarity of sequences at the amino acid level: PIM1 and PIM2 are 61% identical, PIM1 and PIM3 are 71% identical, while PIM2 and PIM3 share 44% homology [52]. All three PIM kinases share a common phosphorylation consensus sequence (ARKRRRHPSGPPTA), suggesting at least partial functional redundancy [53]. In line with this finding, several studies confirm compensatory overexpression of other PIM kinases in case of a knock out (KO) of one of the family members in mice [54–56], or DLBCL cell lines with single PIM are knockdown (KD) with siRNA [37].On the other hand, no compensation by other PIM proteins has been observed upon PIM1 or PIM2 shRNA KD in acute myeloid leukaemia (AML) [57] or PIM1 shRNA KD in prostate cancer cell line [58]. These experiments point to redundancy of PIM isoforms' function in certain cellular contexts - such as the disease, or the duration of PIM deprivation. It is therefore important from the clinical point of view to verify the dependencies between PIMs, and appropriately adjust treatment and dose to inhibit all three kinases when they can compensate for the loss of one another.

Furthermore, triple knockout of PIM in healthy mice did not cause lethality, infertility, or other severe phenotype. The mice were, however, smaller and exhibited impaired responses of hematopoietic cells to growth factors [38], had lower platelet count, erythrocyte hypochromic microcytosis, and slower proliferation of hematopoietic stem cells [59]. Since PIM kinases are crucial for tumour cells, and cause manageable impairments in healthy tissues (and possibly reversible – but that requires further studies), they are promising targets for clinical use in treatment of blood cancers.

1.2.2 Oncogenic functions of PIM kinases in tumours

PIM kinases are abundantly expressed in multiple haematological malignancies [21]. PIM overexpression leads to leukaemia- and lymphomagenesis in mice, albeit at a low frequency and with a long latency [60]. However, PIM-induced lymphomagenesis is dramatically enhanced when PIMs are co-expressed with MYC [26,58,61,62].

Hypermutation of PIM1 is characteristic for certain subtypes of non–Hodgkin's lymphoma (NHL), including DLBCL [1,63–66]. Although PIM1 is one of the most commonly mutated oncogenes in this disease, consequences of these mutations are unclear. Most of these mutations do not increase enzymatic activity of the kinase, neither lead to its complete loss [67]. Novel, detailed genomic analyses identified that *PIM1* mutations frequently co-occur with *BCL2* gain, concordant *MYD88^{L265P}/CD79B* mutations and additional mutations of *ETV6, GRHPR, TBL1XR1* and *BTG1* [1]. Such non-random distribution of mutations suggests that the proteins encoded by the genes are involved in common, specific oncogenic pathways.

Given the high expression at early developmental stages linked to a plethora of stem-like functions (selectively listed below and graphically summarised in Figure 1.2), and relative steady-state quiescence in adult tissues, constitutive PIM overexpression in tumours is a logical carcinogenic mechanism that renders PIM a promising therapeutic target.

1.2.2.1 PIM-MYC cooperation

MYC transcription factor plays a vital role in lymphomagenesis, and PIM kinases are important regulators of MYC stability and activity [37,68]. For example, phosphorylation of Ser239 or Ser62 by PIM increases MYC's stability and/or blocks proteasomal degradation [68]. Moreover, MYC recruits PIM for phosphorylation of histone H3, which is necessary for the expression of 20% of MYC targets (the mechanism is described in detail in section 1.2.2.8) [69,70]. In turn, MYC participates in the expression of PIMs. Thus, MYC and PIM levels are linked by a feed-forward circuit. The powerful role of PIM and MYC cooperation in oncogenesis has been experimentally confirmed by overexpression of these proteins in murine embryos, which led to accelerated lymphomagenesis *in utero* or shortly after birth [60,61].

MYC regulates transcription of genes involved in key cancer cell functions, such as: cell proliferation, cellular metabolism, growth, angiogenesis, metastasis, genomic instability, stem cell self-renewal, differentiation, and immunogenicity. Since MYC-induced tumours maintain dependency on constitutive MYC expression [71], therapeutic MYC targeting is of great interest. However, up to date the protein remains "undruggable", and numerous studies focus on switching MYC off indirectly. Given the tight cooperation between MYC and PIM, inhibition of PIM will also affect MYC targets, impair cancer cell function and likely lead to apoptosis [37,72]. Therefore, targeting PIMs is a reasonable therapeutic approach in treatment of MYC-driven tumours.

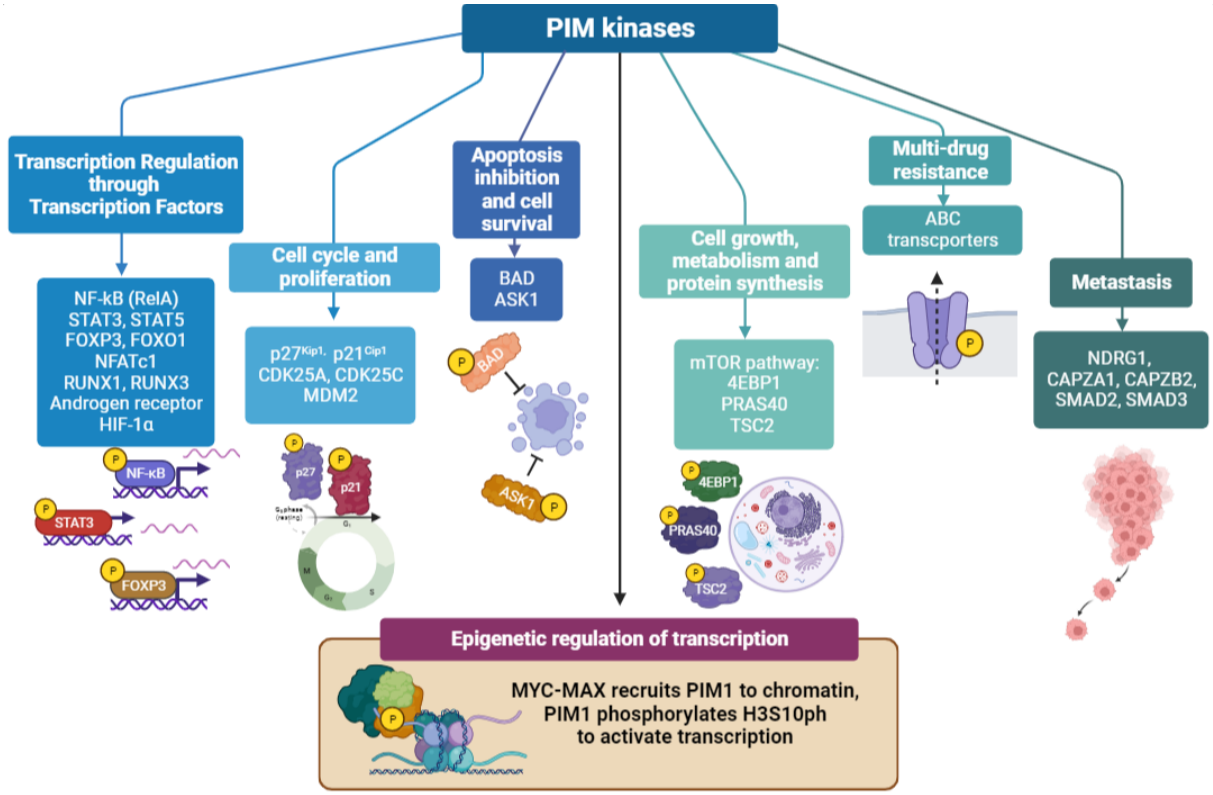

Figure 1.2 Selected functions of PIM kinases in tumours (created in BioRender).

1.2.2.2 Regulation of transcription via factors other than MYC

In addition to MYC, PIMs phosphorylate and regulate a plethora of transcription factors important for lymphoma pathogenesis.

NF-κB pathway participates in cellular responses to various stimuli, such as stress, cytokines, or UV, infectious agents. PIM1 phosphorylates RelA (p65), a subunit of NF-κB, at Ser276, which prevents degradation by ubiquitin-mediated proteolysis, and activates the protein. Moreover, PIM1 contributes to the recruitment of RelA to κB-elements in the promoters of TNF-a-responsive genes, including e.g. *IL-6* [73–75].

STAT3 and STAT5 TFs are other targets of PIMs in numerous cell types [74–77]. Since PIM expression is activated via JAK/STAT and NF-κB pathways, these interactions result in a feed-forward loop.

FOXP3 is a master regulator transcription factor (TF) in regulatory T cells (T_{reg}). Ser^{422} phosphorylation by PIM1 negatively regulates FOXP3 chromatin binding, thus downregulates FOXP3-dependent genes involved in immune response, and inhibits the immunosuppressive activity of T_{reg} [78,79]. PIMs also regulate another protein from this family – FOXO1, important for survival and apoptosis in certain lymphoma cells, including DLBCL and Burkitt lymphoma [80–82].

Taken together, PIMs play an indirect, but crucial role in activation of transcriptional programmes connected to cell survival, proliferation and differentiation, migration and invasion, angiogenesis or immune response, among others. Importantly, all of these pathways are hallmarks of cancer cell biology [83,84].

1.2.2.3 Cell cycle and proliferation

In addition to regulating transcription through TFs, PIMs modulate the activity of effector proteins in many key pathways of proliferation. For example, $p27^{Kip1}$ and $p21^{Cip1}$ are cell cycle inhibitors that prevent cell cycle progression at G1 phase. All three PIM kinases bind and phosphorylate $p27^{Kip1}$ in cells and *in vitro*. This phosphorylation induces $p27^{Kip1}$ binding to the adaptor 14-3-3 protein, resulting in its nuclear export and proteasome-dependent degradation. Moreover, PIMs indirectly downregulate $p27^{Kip1}$ expression by phosphorylation and inactivation of FOXO1a and FOXO3a transcription factors [79]. Similarly, $p21^{Cip1}$ can be phosphorylated by PIM1 and PIM2, what stabilises the protein and exports it to the nucleus, allowing for cell cycle progression from G1/S phases [85,86]. Other studies show that PIMs

activate CDC25A, M-phase inducer phosphatase 1[87,88]. Interestingly, PIMs' role in cell cycle is not limited to progression from G1/S to mitosis, as the function of CDC25C, a G2/M checkpoint phosphatase, is enhanced by phosphorylation by PIM, which allows for G2/M transition [89].

Phosphorylation by PIM kinases stabilise mouse double minute 2 homologue (MDM2), an E3 ubiquitin ligase. PIM kinases phosphorylate MDM2 at S166 and S186, what increases the protein's stability. One of MDM2's important targets is p53, crucial DNA-damage response protein, regulator of apoptosis and cell cycle. Therefore, stabilisation of MDM2 reduces the level of p53, reduces DNA damage responses, promotes cell cycle progression and cell survival [90,91]. Consequently, diminution of PIM levels or its inhibition generates p53 activation, facilitating stress-induced cell death.

1.2.2.4 Apoptosis inhibition and cell survival

PIM-mediated phosphorylation of BAD, a pro-apoptotic BCL2-associated agonist of cell death, inactivates BAD. Phosphorylated BAD binds to 14-3-3 protein, which blocks its association with anti-apoptotic BCL-XL, thus enhancing the escape from programmed cell death [92,93]. In addition, phosphorylation of ASK1, apoptosis signalling kinase 1, enables cells to evade stress-induced apoptosis [94]. Considering the importance of apoptosis evasion in cancer cell survival, inhibition of PIM appears a potent therapeutic target, especially in BCL2-overexpressing tumours such as follicular lymphoma, or subtypes of DLBCL.

1.2.2.5 Cell growth, metabolism and protein synthesis via mTOR pathway

mTOR is a central regulator of growth and metabolism in response to the presence of nutrients. PIM kinases are involved in phosphorylation of mTOR substrate 4EBP1 (eIF4E binding protein 1) leading to cap-dependent translation initiation [95,96]. They also regulate e.g. PRAS40 and TSC2 - mTOR inhibitors of substrate binding. Upon phosphorylation by PIM, PRAS40 and TSC2 dissociate from mTORC1 and activate the kinase complex [97,98]. Thus, since PIM regulates elements both upstream and downstream of mTOR, inhibition of PIM impedes cancer cell growth, even in the presence of nutrients.

1.2.2.6 Multi-drug resistance

ATP-binding cassette (ABC) transporters are established factors conferring drug resistance, involved in transmembrane drug efflux. PIM kinases phosphorylate ABC transporters, and increase their expression, thus leading to multi-drug resistance [99–101]. Inhibition of PIM blocks the efflux, retains the antitumor drug in the cell and increases toxicity. Moreover, elevated PIM3 level was found to induce cisplatin resistance in hepatoblastoma, while PIM inhibition re-sensitised cells to this drug, and reversed stem-cell-like phenotype of the cells [25,102].

1.2.2.7 Metastasis

Involvement of PIM kinases in tumour metastasis has been characterised in certain solid tumours, including hepatocellular carcinoma, prostate cancer and lung adenocarcinoma [96,103–105]. In the latter, metastatic cells exhibited predominantly nuclear localisation, suggesting that PIM-associated metastasis is driven by transcriptional reprogramming rather than by phosphorylation of cytoplasmic cytoskeleton/motility proteins [96,105]. In line with this, in renal cell carcinoma, PIM1 was observed to interact with and phosphorylate signalling proteins SMAD2 or SMAD3 in the nucleus to induce the expression of transcription factors promoting epithelial-mesenchymal transition and metastasis [106]. Moreover, in prostate cancer, PIM1-dependent phosphorylation attenuates NDRG1, a suppressor of metastasis [107]. It also regulates actin capping proteins CAPZA1 and CAPZB2, and reduces their ability to protect polymerised actin from disassembly, thus enhancing prostate cancer cell migration or adhesion [108]. In renal cell carcinoma, PIM1 was observed to interact with and phosphorylate signalling proteins SMAD2 or SMAD3 in the nucleus to induce the expression of transcription factors promoting epithelial-mesenchymal transition and metastasis [106]. A fraction of DLBCL involves extranodal sites (such as central nervous system, gastrointestinal tract, breast, mediastinum, testis, skin or bone), therefore, blocking cellular migration is one of the desired effects in the therapy of this disease.

1.2.2.8 Beyond PIM canonical pathways: Epigenetics and chromatin remodelling

In addition to the "canonical" functions of PIM kinases in regulation of key tumour functions (enumerated above), PIMs also function as indirect modulators of transcription. At MYC-regulated genes, PIM1 is recruited to the enhancers by dimerisation with MBII domain of MYC-MAX (MYC-associated factor X) complex. Upon serum treatment, MYC-MAX recruits PIM1 to E-boxes of its targets to regulate approximately 20% of MYC-dependent genes. Although a mechanism of their regulation has not been elucidated on a genomic scale, single-locus studies suggest that PIM1 modifies epigenetic landscape of MYC-MAX-PIM1-bound regulatory regions [69,70]. For example, the MYC-MAX-PIM1 complex is recruited to *FOSL1*'s canonical E-box enhancer, where PIM1 phosphorylates H3S10 at pre-acetylated H3K9acK14ac histones. Subsequently, the adaptor protein 14-3-3 binds the H3S10-phosphorylated nucleosomes and recruits the histone acetyltransferase MOF to the enhancer regions, where MOF is responsible for the acetylation of histone H4 at lysine 16 (H4K16ac). Thus, H3K9ac/S10ph/H4K16ac creates a docking platform recognised by bromodomain-containing protein 4 (BRD4), a chromatin reader and established marker of enhancers, including super-enhancers (SE; see section 1.3.3). BRD4 then recruits positive transcription elongation factor b (P-TEFb) - a dimer of CDK9 kinase with a regulatory subunit Cyclin T. CDK9 phosphorylates Ser2 at C-terminal domain (CTD) of RNA Polymerase II (RNAPII) and releases the promoter-proximal paused RNAPII into elongation phase (see Figure 1.3). Thus, PIM1-induced H3S10ph initiates the cascade of events that leads to transcriptional activation of *FOSL1* [69]. On a side note, according to a SE database SeDB, *FOSL1* is regulated by a SE in HUVEC cells, in which the experiments were performed [109].

It has been demonstrated that factors such as NF-κB, Androgen receptor, MyoD and MYC can recruit P-TEFb to specific loci [69]. Interestingly, PIM kinases interact with most of these TFs [50,70,73,74,110,111]. Whether PIM employ a similar mechanism of transcriptional activation in case of genes regulated by these TFs, remains to be elucidated.

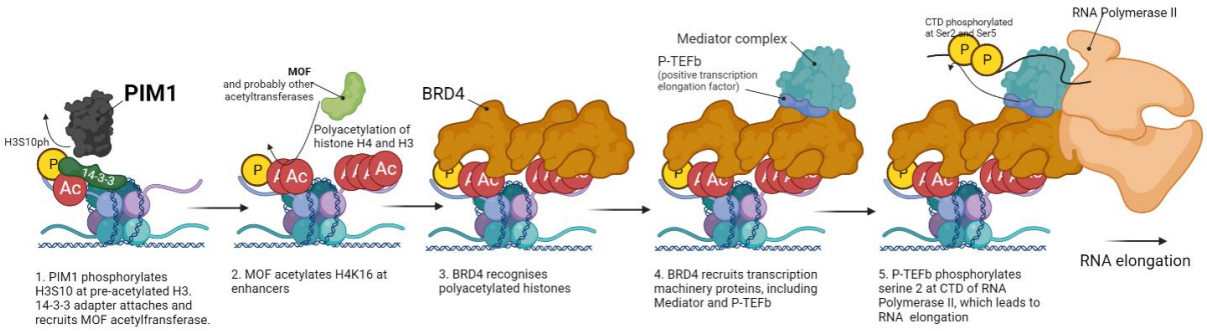

Figure 1.3 Transcriptional activation of FOSL1 gene by PIM1-induced H3S10ph (Created in BioRender.com)

MYC and PIM1 cooperate in several oncogenic mechanisms, but it is the recruitment of the MYC-PIM1 complex to the chromatin that seems to be crucial in carcinogenesis. Introduction of PIM1 fused with MYCΔC, a mutant unable to bind to the DNA, to fibroblasts did not cause transformation, nor phosphorylation of H3S10 at the target genes analysed. In turn, fusion of PIM1 to the transformation-defective MYCΔMBII (with mutation in MBII domain, responsible for MYC-PIM1 complex formation) could rescue the carcinogenic potential and H3 phosphorylation at MYC-binding sites, while co-expression of PIM1 and MYCΔMBII separately did not lead to rescue [69].

In addition, all three PIMs regulate the level of long non-coding RNA H19, involved in stem cell and pluripotency phenotype. Interestingly, the effect was MYC-independent, even though H19 is a target of MYC. Instead, Singh et al. suggest that in addition to regulation of transcription factors that target H19 locus, PIM induce epigenetic changes by controlling the level of DNA methylation of regulatory regions that modulate H19 expression, and/or through phosphorylation of heterochromatin protein 1 gamma (HP1) [25,112]. Other studies confirm PIMs' role in DNA methylation through destabilising phosphorylation on UHRF1, a E3 ubiquitin ligase that acts as a key epigenetic regulator by bridging DNA methylation and chromatin modification [113]. Therefore, PIMs regulate epigenetic landscapes in both direct (H3S10ph) and indirect (chromatin modellers, level of H19) ways.

1.2.3. PIM inhibitors

Several PIM inhibitors have reached clinical trials, mostly in hematologic malignancies. At first, many studies were terminated after the I phase due to off-target toxicity or insufficient therapeutic effect. However, preliminary results of more recent trials are indeed promising.

1.2.3.2 First generation of PIM inhibitors

Despite promising preclinical results, the first-generation PIM inhibitor SGI-1776 showed off-target effect associated with unfavourable cardiotoxicity profiles, which led to the termination of phase I trial recruiting patients with either castration-resistant prostate cancer or R/R NHL[114]. Another pan-PIM inhibitor - AZD1208, was well tolerated, but exhibited poor on-target activity and efficacy in single-agent therapy for advanced solid cancers or refractory AML [115]. Nevertheless, PIM447 (LGH447) was well tolerated and exhibited moderate therapeutic efficacy in R/R multiple myeloma (MM) [116,117]. The trials with PIM447 were, however, eventually terminated due to disease progression in the majority of patients, leaving the conclusion that PIM447 acts as a cytostatic rather than cytotoxic drug [118].

1.2.3.1 Novel PIM inhibitors currently in clinical trials

There are several ongoing phase I/II studies with newer generations of PIM inhibitors. For example, INCB053914 has recently completed a 1b phase trial in DLBCL, in combination with a PI3K inhibitor (NCT03688152, the results are not available yet). Previous trials with this drug were terminated for tolerability reasons (in combination therapy with cytarabine in advanced malignancies; NCT02587598), or withdrawn (NCT04355039, combination therapy with pomalidomide and dexamethasone for R/R MM). Other PIM inhibitors: TP-3654 (NCT03715504, NCT04176198), or ETH-155008, a triple inhibitor of FLT3, PIM3 and CDK4/6 (NCT04840784) are tested as monotherapy in hematologic and solid tumours in very recently commenced clinical trials.

In this study, I used SEL24/MEN1703, a pan-PIM/FLT3 inhibitor, developed by Ryvu Pharmaceutics (formerly Selvita S.A.). Given the dual target kinase profile and our earlier

studies demonstrating promising activity in AML preclinical models [119], the inhibitor is currently tested in a phase II clinical trial in patients with AML (DIAMOND-01/CLI24-001 trial, NCT03008187), where initial results show a manageable safety profile and single-agent activity [120]. In preclinical studies in lymphoid malignancies, SEL24/MEN1703 was effective in inducing apoptosis in DLBCL, primary mediastinal large B-cell lymphoma (PMBL), Hodgkin lymphoma (cHL) and chronic lymphocytic leukaemia (CLL) cell lines and patient samples [37,74,75,121]. Since all DLBCL cell lines used in this work are FLT3-negative [37], the drug's activity in DLBCL can be attributed to pan-PIM inhibition rather than to FLT3.

1.3. Epigenetic regulation of transcription

The term "epigenetics" refers to processes that modulate gene expression, but are independent of DNA-encoded information. The usual modes of this type of control include chromatin architecture, histone modifications, DNA methylation, or RNA modifications. These elements work cooperatively, and direct a fine-tuned change in gene expression patterns [122–126]. Noteworthy, deregulated epigenetic mechanisms have been recently recognised as another hallmark of cancer [83,84].

1.3.1 DLBCL as a disease of dysregulated epigenetics

Since epigenetic regulation is rapid and reversible, it is a crucial mechanism in repetitive switches of GC B-cell phenotype during the several rounds of circulation between the light and dark zone. GC B-cells relatively quickly oscillate between two states: robust proliferation accompanied by the introduction of DNA mutations that are ignored by DNA damage response machinery, and cell selection. Genes that encode chromatin remodellers that participate in light-dark zone transitions are often mutated in DLBCL, and evaluated in diagnostics of DLBCL according to WHO recommendations, e.g. acetyltransferases CBP/p300, methyltransferases KMT2D/C and EZH2 [127,128]. Furthermore, a recent study identified 150 oncogenic drivers of DLBCL through exploratory analysis of 1001 patient samples, followed by an unbiased CRISPR for functional confirmation. Importantly, 21 of the identified 150 drivers are epigenetic

modulators, while 18 of the 21 lie in the top 75 drivers. In this analysis, the most frequently altered gene of all is lysine methyltransferase D2 (MLL2/KMT2D), mutated in 25% of DLBCLs [129]. The substantial representation of malignant mutations in epigenetic modulators accentuates the important role of epigenetics in DLBCL pathogenesis.

1.3.2 H3S10ph in transcriptional regulation

Histone phosphorylation at H3S10 is highly abundant in mitosis (especially metaphase), when it plays a significant role in proper chromosome segregation [135]. For this reason, H3S10ph is regarded as a marker of cell division in molecular research. Although in interphase the representation of H3S10ph is radically smaller, the modification serves a vital function in orchestrating gene expression.

Interphase gene-rich regions are broadly occupied by H3S10ph. The mark negatively correlates with repressive H3K9me2 [130], and frequently occurs on hyperacetylated histones, which indicate active chromatin. Moreover, adaptor protein 14-3-3, which binds phosphoacetylated proteins is recruited to H3S10phH3K9acK14ac with high affinity, while binding of 14-3-3 to H3S10phK14ac protects H3S10 from dephosphorylation and stabilises gene expression [131]. 14-3-3 can also recruit MOF acetyltransferase to H3S10ph-marked enhancers, leading to RNAPII pause release and RNA elongation [69]. Interphase H3S10ph also attracts the SET domain of KTM2A/MLL1 methyltransferase complex, which not only imposes methyl groups at H3K4 (H3K4me3 is a marker of active promoters), but also excludes HP1- and Polycomb-mediated chromatin condensation [132], further supporting the role of interphase H3S10ph in epigenetic activation.

Importantly, before S phase, H3S10ph is imposed on early replicating genes that are directed to “transcription factories” in the inner, active part of the nucleus [133] (note that the term “transcription factory” likely overlaps with the term “super enhancer” [134,135]). This way, H3S10ph prepares the chromatin for replication, but also inevitably renders the chromatin accessible for the interphase transcription machinery. Moreover, H3S10ph protects acetylated histone H4 from deacetylation, and thus maintains a platform for BRD4 [136]. These observations further support H3S10ph involvement in regulation of gene expression.

H3S10 can be phosphorylated by a plethora of kinases, active in different phases of the cell cycle. Interphase kinases include: PIM1, MSK1/2, RSK2, CDK8, IKK-a, JNK, AKT1 and MAP3K8, while in mitosis, Aurora kinases are principally responsible for imposing the mark [131]. There is limited data on whether the interphase kinases are redundant. They most probably differ in substrate specificity – e.g. MSK1/2 phosphorylates only the promoter, and PIM1 only the enhancer of *FOSL1* gene [69].

Despite close homology among the PIM family, to date, the histone writer function has been attributed only for PIM1. Interestingly, PhosphoNET kinase predictor (phosphonet.ca, Kinexus Bioinformatics Corporation) lists the three PIM kinases as top three hits for the kinase of H3S10ph (Figure 1.4). The software predicts kinases responsible for the phosphorylation of the input site, based on the similarity to the consensus amino acid substrate context of the kinase. The high degree of homology between PIMs, and the prediction results may suggest that other PIM kinases might also be able to phosphorylate H3S10, however, to date, there are no studies that confirm the epigenetic role of other PIM kinases in cells. On the other hand, there are reports which show that isolated PIM3 protein is capable of phosphorylating histone H1 *in vitro* [137,138].

Transcriptional function of H3S10ph, as well as other H3S10 kinases have been comprehensively reviewed by Komar *et* Juszczyński [131].

Phosphosite			
Human Protein:	H3F3A		
Human P-Site:	S11		
P-Site Sequence:	TKQTARKSTGGKAPR		
UniProt:	P84243		
Intern. Prot. ID:	IPI00219038		
Protein Kinase Match	Human Kinase Short Name	Human UniProt. ID	Kinase Predictor V2 Score
Kinase 1:	PIM1	P11309	501
Kinase 2:	Pim3 (AL549548)	P58750	470
Kinase 3:	PIM2	Q9P1W9	426
Kinase 4:	CHK2 (CHEK2)	O96017	417
Kinase 5:	RSKL1	B1APS8	390
Kinase 6:	PKCh (PRKCH)	P24723	388
Kinase 7:	PKCe (PRKCE)	Q02156	382
Kinase 8:	MSK1 (RPS6KA5)	O75582	382
Kinase 9:	AurA (STK15)	O14965	381
Kinase 10:	PKCb (PRKCB1)	P05771	376

Figure 1.4 Top 10 hits of H3S10 kinases prediction by PhosphoNET (phosphonet.ca, Kinexus Bioinformatics Corporation). The kinase substrate predictions are based on the deduced consensus of phosphorylated amino acid context.

1.3.3 BRD4 and enhancers and super-enhancers

PIM kinases participate in a cascade of events that leads to transcriptional activation through recruitment of BRD4 [69], a chromatin reader, abundant in active regions, especially SEs. In general, SEs are regulatory regions similar to typical enhancers (TE), but their quantifiable characteristics are usually an order of magnitude higher than TEs', such as the genomic span or processivity [139–141]. The enrichment with elements like BRD4, but also complexes like the Mediator or RNAPII, and active chromatin marks, such as the hallmark H3K27ac, or H3K4me1 [142] are 10- to 28-fold higher at SEs than at TEs [139]. An estimated 1/3 of the chromatin load of these factors gathers at SEs, i.e. in the 3% of the occupied regions [139,143]. Based on these observations, SEs are usually identified computationally with the Rank-Ordering of Super-Enhancers (ROSE) algorithm developed by R. Young's group [139,140]. Briefly, constituent enhancers are stitched together if they locate within a certain distance, followed by ranking the enhancers by signal of active chromatin such as H3K27ac, BRD4, or sometimes cell-specific TFs marker (input-subtracted; the signal data is drawn from ChIP-Seq experiment). Then, the algorithm divides these regions into SEs and TEs by identifying an inflection point of active chromatin signal versus enhancer rank.

In terms of function, SEs activate transcription at distance, independently of their orientation to the target gene. They depend on higher-order structures, such as topologically associating domains (TAD) [144]. Moreover, amassing evidence shows that SEs function as membraneless, phase-separated compartments of nucleus, which stabilise robust transcription [145–150].

SEs usually regulate genes associated with cell lineage, function and survival, including a number of well-defined oncogenes. Importantly, SE landscape is reshaped in carcinogenesis, and tumours exhibit transcriptional addiction to this type of gene regulation [151–153]. Elements of SEs have even become therapy targets, tested in clinical trials. One example of drug from this category is bromodomain inhibitor JQ1, which shows the highest affinity to BRD4. Although very promising in cell line models and xenografts, clinical trials were discontinued due to poor kinetic profile and low bioavailability [154]. Nevertheless, *in vitro* and *in vivo*, JQ1 was able to displace BRD4 from chromatin, and showed anti-tumour activity in numerous solid and haematological tumours [154], and is still used as a potent BRD4 inhibitor in basic research.

Other SE-targeting drugs in clinical trials, as well as SE function, architecture and regulation in haematological malignancies have been systematically reviewed by Dębek *et* Juszczyński [155].

1.4 Summary and rationale

PIM kinases are important players in the pathogenesis of DLBCL, the most common type of non-Hodgkin lymphoma. They participate in numerous fundamental functions of the cell, including proliferation and apoptosis. Interestingly, PIM kinases can be translocated, or primarily localised to the nucleus, where they exert different functions then their cytoplasmic counterparts, seemingly correlating with the cell's identity and tumour's aggressiveness. One of these nuclear functions includes phosphorylation of H3S10 by PIM1 (and perhaps other PIMs). H3S10ph's function has not been widely characterised, yet, in the interphase it is generally associated with chromatin remodelling leading to activation of gene expression, including transcription of key oncogenes. It has been documented, albeit only for the locus of *FOSL1*, that PIM-induced H3S10ph participates in transcriptional activation *via* BRD4 recruitment, the key element of SEs. Importantly, cancer cells have been shown to heavily rely on SE-regulated genes. DLBCL might especially take advantage of this type of regulation, as dysregulated epigenetic mechanisms are one of the key drivers of the disease.

Taken together, PIM kinases are likely involved in the global epigenetic regulation of transcription as epigenetic writers, which potentially has broader effect on gene expression programmes than "merely" phosphorylation of TFs, which is one of the canonical functions of PIM. I hypothesise that PIM inhibition decreases the level of H3S10ph, which disrupts epigenetic patterns and consequently undermines transcription to disturbs key DLBCL cellular pathways. This function can thus be a novel mechanism of cytotoxicity of PIM inhibition in DLBCL.

2. Aims

The aim of this work is to describe the previously uncharacterised role of PIM kinases in broad epigenetic regulation of gene expression, and consequences of its inhibition in diffuse large B-cell lymphoma. Specifically:

1. to describe changes in epigenetic landscape after PIM inhibition,
2. to characterise changes in transcription patterns following PIM inhibition,
3. and to assess the impact of these changes on DLBCL cell viability and proliferation.

3. Materials and methods

3.1 Mammalian cell culture methods

3.1.1 Handling and functional tests

3.1.1.1 Cell culture

Human DLBCL cell lines were purchased from DZSM (German Collection of Microorganisms and Cell Cultures) or ATCC (American Type Culture Collection).

- LY1, HBL1 and TMD8 were cultured in IMDM with 4-(2-hydroxyethyl)-1-piperazineethanesulfonic acid (HEPES) and L-glutamine (Lonza, BE12-722F)

- DHL4, DHL6, RIVA and U2932 were cultured in RPMI1640 medium (Lonza, BE12-167F) supplemented with 1% HEPES (Lonza, BE17-737E) and 1% L-glutamine (Lonza, BE17-605E)

- HEK293T cells were cultured in DMEM (Lonza; BE12-614Q) supplemented with 1% HEPES (Lonza, BE17-737E) and 1% L-glutamine (Lonza, BE17-605E)

Table 3.1 Cell lines used in this work.

CELL CULTURE	DESCRIPTION/GENOTYPE	COO CLASSIFICATION SUBTYPE
LY1	t(14;18) rearrangements, some cryptic, effecting juxtaposition of IGH with BCL2	GCB
DHL4	**Mutations**: EZH2 Y641S; t(14;18) effecting BCL2 (MBR)-IGH fusion	GCB
DHL6	**Mutations**: EZH2 Y641N; t(14;18) effecting IGH-BCL2 fusion	GCB
HBL1	**Mutations**: CD79B; Tyr196Phe (c.587A>T); Heterozygous; MYD88; Leu252Pro (c.755T>C), Heterozygous; t(14,16)	ABC
TMD8	**Mutations**: CD79B; Tyr196His (c.586T>C); Heterozygous; MYD88; Leu252Pro (c.755T>C), Heterozygous	ABC
U2932	DLBCL developed in a patient with relapsing HL; overexpression of BCL2, BCL6 and p53	ABC

All media were supplemented with 10% foetal bovine serum (FBS; Euroclone/Celllab, ECS0180L until August 2021, and Sigma Aldrich, F9665 from August 2021 on) and penicillin-streptomycin (Lonza, DE17-602E), unless otherwise stated in the work. For cell lines transfected with plasmids for doxycycline-inducible expression, tetracycline-free FBS (Takara, 631106) was used.

The cultures were incubated in 37°C, in a humidified 5% CO_2 atmosphere. They were handled in sterile conditions, in a laminar flow cabinet (Thermo Scientific, MCS-Advantage™). For maintenance, the cultures were split with fresh, full medium every 2-3 days, to the density of $0.5*10^6$ cells/ml. The cell culture density was determined with Trypan Blue staining, which penetrates only dead cells, while live cells remain unstained. Live/dead cell counting was done either manually in the Neubauer chamber under an optical microscope, or in an automated cell counter (Nanoentek, Eve™). 24h before any experiment, cells were split so as they were in mid-log phase at the time of the experiment.

3.1.1.2 PIM inhibitors

The dual pan-PIM-FLT3 inhibitor SEL24/MEN1703 was provided by Selvita (Kraków, Poland) in 2018-2019, or Menarini Ricerche (Pomezia, Italy) from 2019 on. Pan-PIM inhibitor PIM447 was acquired from Selleckchem (S7985). PIM1 inhibitor SGI-1776 was acquired from Selleckchem (S2198). The inhibitors were dissolved in dimethyl sulfoxide (DMSO; Sigma-Aldrich, D8418) and stored in -80°C.

3.1.1.3 Induction of shRNA expression

Expression of shRNA from Sleeping Beauty plasmids TST201, and pTRIPZ plasmids was induced by doxycycline in the concentration of 1µg/ml. Since doxycycline is unstable in the culture medium, a fresh portion of the antibiotic was added to the medium daily.

3.1.1.4 Cell freezing and thawing

Cells were frozen in a medium containing 90% FBS and 10% DMSO, in an isopropanol freezing container, at the rate of cooling of approximately -1°C/minute, down to -80°C, and then transferred to a cryostat. Frozen cells were stored in -180 °C. Thawing was done rapidly, by warming the vial in 37°C water bath, immediately followed by dilution of the freezing medium with culture medium, centrifugation at 300 x g for 5 min, and resuspension of the cell pellet in appropriate culture medium to the density of $1*10^6$ cells/ml. The cells were then inspected and split accordingly. If several days after thawing there had still been over 50% of dead cells, the culture was subjected to viable cell isolation with histopaque 1077.

3.1.1.5 Viable cell isolation with histopaque 1077

4 ml of histopaque 1077 (Sigma Aldrich, 10771) was poured to a 15 ml falcon. 8-10 ml of cell culture was carefully layered onto the histopaque and centrifuged at 400 x g for 20 min in room temperature, with no acceleration and break. Viable cells, which form a coat between the histopaque and the medium layers, were collected with a sterile Pasteur pipette, transferred to a new 15 ml tube, washed in PBS, and centrifuged at 300 x g, 5 min, room temperature. The supernatant was discarded, and the cell pellet was then resuspended in appropriate cell culture medium to the density of $0.5\text{-}1*10^6$ cells/ml.

3.1.1.6 Apoptosis assessment

Apoptosis was assessed with either Annexin V-Phycoerythrin (PE) and 7-aminoactinomycin D (7AAD) staining (BD; 559763), or Annexin V-Fluorescein isothiocyanate (FITC) and propidium Iodide (PI) staining (BD; 556547) according to the manufacturer's manual: https://www.bdbiosciences.com/content/bdb/paths/generate-tds-document.tw.559763.pdf (PE-7-AAD) https://www.bdbiosciences.com/content/bdb/paths/generate-tds-document.tw.556547.pdf (FITC-PI). The kits are interchangeable, and the selection of the kit was determined considering fluorescent proteins inside the cells.

One of the first steps in apoptosis is the translocation of phosphatidylserine (PS) from the intra- to the extracellular side of the plasma membrane, what recruits macrophages to the cell. PS is bound by annexin V, therefore, visualisation of early-apoptotic cells is possible by staining cells with annexin V conjugated with a fluorochrome, FITC, or PE. In turn, PI or 7-AAD, penetrate cells with disrupted cell membrane, i.e. dead cells, and bind DNA. Therefore, double staining with annexin V conjugate and the DNA-binding agent enables visualisation of live-apoptotic-dead cells in the culture (see Figure 3.1).

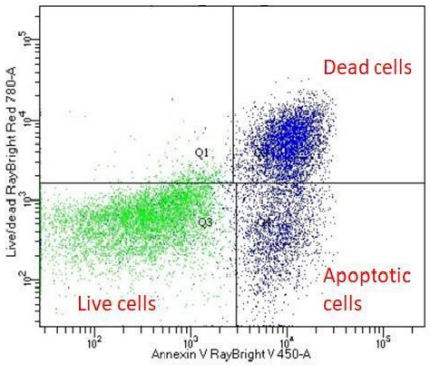

Figure 3.1 Schematic of apoptosis staining results. Cells in the lower left quadrant are alive, and do not bind annexin V, nor are penetrated by the DNA-binding agent. In the lower right quadrant, there are cells which have translocated PS to the extracellular side of the membrane, but the membrane is still intact, hence, they are early apoptotic. Cells in the upper right quadrant bind annexin, and have stained DNA, so they are dead cells. Cells that have disrupted cell membrane, but have not initiated apoptotic PS reversal are necrotic, and are reflected in the upper left quadrant. Image source: https://www.raybiotech.com/raybio-annexin-v-apoptosis-kit-raybright-v450/

3.1.1.7 Cell cycle arrest and PIM inhibitors treatment

Addition of high concentrations of thymidine to the culture medium causes competitive inhibition in the deoxynucleotide metabolism pathway, thus interrupting DNA replication, and arresting the cells in G1/S phase of the cell cycle. The cells were seeded at $0.5*10^6$ cells/ml in full medium with the addition of 2 mM thymidine and incubated for 18h. After that time, the cell cycle arrest was confirmed by Hoechst stain, the medium with thymidine was washed out, and the cells were resuspended in fresh medium containing PIM inhibitor: 1.5 µM of SEL24/MEN1703 or 7 µM of PIM447, for 2 hours. The duration of

treatment has been optimised for the maximal time when the majority of cells were still in G1/S after thymidine washout.

3.1.1.8 Cell cycle assessment – Hoechst stain

Cell cycle phase distribution was assessed by Hoechst 34580 (BD; 565877) staining followed by flow cytometry visualisation. Hoechst solution was added to the culture at concentration of 10 µg/mL, and incubated for 30 minutes at 37°C. Next, the cells were assessed in flow cytometer (CytoFLEX, Beckman Coulter) in PB-450 channel.

Hoechst binds preferentially to adenine-thymine regions of double-stranded DNA. Therefore, G1 phase was attributed to the highest peak in PB-450 histogram for the control sample, i.e. the sample of the same cell line, not treated with any inhibitors. The peak that reflects twice as intensive fluorescence (and thus DNA amount) was deemed G2/M phase. The area between the peaks represents cells in S phase, when DNA is being synthesised, anywhere from 2n to 4n. Peaks of fluorescence below the G1 peak's levels represent dead cells, with fractured DNA, while peaks above G1/M fluorescence levels stand for polyploid cells (see Figure 3.2).

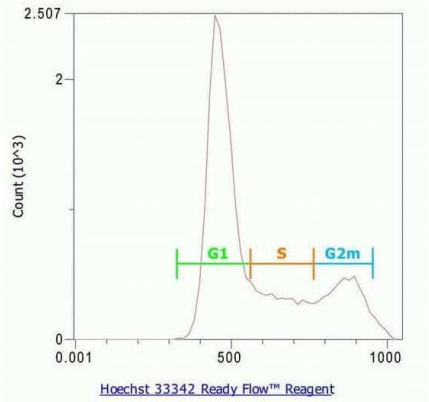

Figure 3.2 Schematic of cell cycle distribution in Hoechst-stained cells. The intensity of fluorescence reflects DNA amount: 2n in G1, 4n in G2M before cell division, and amount between 2n and 4n during DNA synthesis, i.e S phase. Image source: thermofisher.com/order/catalog/product/R37165

3.1.1.9 Proliferation and metabolism assay - MTS

Cell proliferation was assessed with metabolic test using Promega CellTiter 96™ Aqueous One Solution Cell Proliferation Assay (MTS) kit (Promega, G3580) following the manufacturer's protocol: https://pl.promega.com/-/media/files/resources/protocols/technical-bulletins/0/celltiter-96-aqueous-one-solution-cell-proliferation-assay-system-protocol.pdf?rev=3c361e9a413e4bf9a6c94a3d1bfbbbd9&sc_lang=en .

Briefly, the test uses the conversion of a yellow solution of MTS (3-(4,5-dimethylthiazol-2-yl)-5-(3-carboxymethoxyphenyl)-2-(4-sulfophenyl)-2H-tetrazolium) to a purple formazan in the presence of phenazine methosulfate by NADPH-dependent dehydrogenases. These enzymes are active only in viable cells, therefore, the intensity of the solution reflects the number of viable cells. Cell culture, as well as a blank sample containing only culture medium, were incubated with MTS solution for 2-4 hours. The time was determined with regard to the number of seeded cells (from 5 to 10 thousands, depending on the cell line) and was constant throughout the experiment. The absorbance was measured at 490 nm, and was proportional to formazan amount, and thus viable cell number.

3.1.1.10 Proliferation assay – cell count using flow cytometry

Since CytoFLEX is equipped with a peristaltic pump, it maintains even flow and enables precise calculation of cell density in the sample. By staining with PI or 7AAD, which penetrate only dead cells, it is possible to calculate the number of viable cells. This method is very sensitive and does not measure metabolism, thus overpassing the eventual false positive results of MTS assay, as apoptosis can also be an energy-consuming process.

Cell culture was thoroughly mixed. 100 µl of the culture was transferred to a cytometer tube, mixed with 1 µl of PI or 7AAD, and incubated for 10 min at room temperature, in the dark. The population of single cells was determined by gating cells whose FSC-Area to FSC-Height ratio was a linear function. The number of viable cells was determined by counting PI/7AAD negative cells.

3.1.1.11 Phospho-flow

Changes of H3S10ph levels in cell cycle phases after PIM inhibition were assessed by double staining with anti H3S10ph-FITC antibody and Hoechst. The cells were treated with 1.5 µM SEL24/MEN1703, or DMSO. After 6h and 24h, a fraction of cells was collected from the culture, washed in cold PBS, and resuspended in 1.5 ml of cold PBS, to which 3.5 ml of 100% ice-cold ethanol was gradually added to fix the cells. The cells were kept at 4°C until staining.

For staining, the cells were washed twice with cold PBS, and subsequently permeabilised for 20 min with BSA-T-PBS buffer containing PBS, 0,2% Triton X-100 and 1% BSA (100 µl per $1*10^6$ cells), in order to gently perforate the nucleus. The suspension was centrifuged, and 100 µl of BSA-T-PBS with anti-H3S10ph antibody (Cell Signalling Technology, 3377), or rabbit IgG isotype control antibody (Invitrogen, 02-6102), diluted 1:800, was added to the cell solution and incubated in the dark for 1 h, on ice. Then, the cells were washed in BSA-T-PBS, and resuspended in 100 µl BSA-T-PBS with anti-rabbit-Alexa Fluor 488 (Cell Signalling Technology, 4412) diluted 1:600. Washed cells were resuspended in 100 µl BSA-T-PBS with 100 µg of RNAse A and Hoechst and incubated for 15 min, and washed in BSA-T-PBS. The cytometry recording was done with previously compensated matrix corrections.

3.1.1.12 RNA measurement in live cells by flow cytometry

RNA amount was measured in live cells by staining with acridine orange and flow cytometry. Acridine orange interacts with RNA by electrostatic attraction, and emits red fluorescence (>630 nm). Therefore, red fluorescence intensity was measured in stained cells, treated with PIM inhibitor or DMSO.

3.1.1.13 Cell sorting using flow cytometry

Cells expressing fluorescent proteins were sorted with MoFlo Astrios cell sorter (Beckman Coulter) at the Institute of Haematology and Transfusion Medicine. 7AAD was added to the sample 10 minutes before the sort to stain dead cells. The population of live cells expressing the fluorescent reporter protein of interest was then gated and sorted from the sample.

3.1.2 Genetic engineering

3.1.2.1 Lentivirus generation and lentiviral transduction

Cell lines transfected with pTRIPZ were generated by Małgorzata Bajor, Medical University of Warsaw. Cell lines transfected with pSFFV and its derivatives were generated by Sonia Dębek. 24 hours before transfection, HEK 293-T cells were plated in a 10-cm plate. On the day of transfection, at 70% confluence, the medium is replaced with fresh DMEM. PEI at final concentration of 1 mg/ml was mixed with antibiotic-free and serum-free medium, 1.5 ml per transfection, and incubated for 5 min at room temperature. Next, 10.67 µg of the plasmid with the gene of interest, 8 µg of psPAX2 and 5.33 µg of pMD2G were added to the tube, mixed and incubated for 20 min. The PEI-plasmid mix was then added dropwise to the plate with cells, and incubated in 37°C. After 16 hours the medium was replaced with fresh DMEM. The medium, which contained the lentivirus, was collected, filtered through 0.45 µm pores to remove residual HEK293-T, and frozen in – 80°C. Fresh medium was added to the plate. After 24 h medium was again collected, filtered and frozen.

For lentiviral transduction, 2 millions of target lymphoma cells in mid log phase were used per transduction. Polybrene and viral supernatant were added to the cell suspension. The cells were then spin-inoculated for 1 hour at 1000 x g, in 30°C. Extra medium was added to the well after the inoculation. The cells were incubated for 24h in 37°C. After that time, the lentivirus-containing medium was replaced with fresh full medium appropriate for the target cells. After 3 days, GFP-positive cells were separated from the culture by flow cytometry sorting.

3.1.2.2 Lymphoma cell electroporation and antibiotic selection

Sleeping Beauty plasmids pSBX100, TST209 and TST201 derivatives were introduced into lymphoma cell lines via electroporation. The electroporation method, and the method ’s conditions were optimised for each line.

Ly1 was electroporated using the Neon Transfection System (Invitrogen, MPK5000) according to the manufacturer’s protocol, in buffer R, with conditions: 1200 V, 20 ms, 2 pulses. Antibiotic selection began approximately 2 days after the electroporation.

HBL1 was electroporated with GenPulser (BioRad, 165266). 20 mln of cells were collected, centrifuged, resuspended in 500ul electroporation medium containing RPMI1640 medium supplemented with 50% FBS and 50 mM xylitol (serilised by filtration) and transferred to 4 mm electroporation cuvettes. 10 µg of the plasmid of interest and 15 µg of SBX100 plasmid with transposase were added to the suspension and thoroughly mixed. The cells were subject to electroporation with conditions: Square Wave, 1 pulse, 250 V, 20 ms. After the pulse, the cells were gently collected from the cuvette and transferred to a plate with fresh, warm, IMDM medium with 10% FBS, but without antibiotics. The cells were checked every day, and as soon as they regained normal morphology and proliferation (3-7 days), were subject to antibiotic selection.

Doses of antibiotics were experimentally optimised for each cell line. For each selection, parental, not modified cells were also treated with an antibiotic. The selection ended when all parental cells were dead. Puromycin (Sigma Aldrich, P8833) selection lasted 2-3 days. 2 µg/ml was added to Ly1 cell lines. HBL1 was treated with 1 µg/ml. G418 (Pol-Aura, PA-03-2946-A) selection took 10-14 days. Ly1 was treated with 2.5 µg/ml, HBL1 was treated with 1.25 µg/ml.

3.1.3.4 List of genetically engineered cell lines used in this work

Table 3.2 Genetically engineered cell lines used in this work.

#	CELL LINE	DESCRIPTION	SOURCE
1	**Ly1-pTRIPZ-PIM1**	OCI-Ly1 with pTRIPZ-PIM1 for inducible KD of PIM1	This work
2	**Ly1-pTRIPZ-PIM2**	OCI-Ly1 with pTRIPZ-PIM2 for inducible KD of PIM2	This work
3	**Ly1-pTRIPZ-PIM3**	OCI-Ly1 with pTRIPZ-PIM3 for inducible KD of PIM3 (likely not functional)	This work
4	**Ly1-SB-TST209**	OCI-Ly1 with tetracycline repressor (pTST209)	This work
5	**Ly1-SB-shPIM1.2**	OCI-Ly1 with pTST201-shPIM1.2 for inducible KD of PIM1	This work
6	**Ly1-SB-shPIM1.3**	OCI-Ly1 with pTST201-shPIM1.3 for inducible KD of PIM1	This work
7	**Ly1-SB-shPIM1.4**	OCI-Ly1 with pTST201-shPIM1.4 for inducible KD of PIM1	This work
8	**Ly1-SB-shPIM1.5**	OCI-Ly1 with pTST201-shPIM1.5 for inducible KD of PIM1	This work
9	**Ly1-SB-shPIM2.1**	OCI-Ly1 with pTST201-shPIM2.1 for inducible KD of PIM2	This work
10	**Ly1-SB-shPIM2.2**	OCI-Ly1 with pTST201-shPIM2.2 for inducible KD of PIM2	This work
11	**Ly1-SB-shPIM2.3**	OCI-Ly1 with pTST201-shPIM2.3 for inducible KD of PIM2	This work
12	**Ly1-SB-shPIM2.4**	OCI-Ly1 with pTST201-shPIM2.4 for inducible KD of PIM2	This work
13	**Ly1-SB-shPIM2.5**	OCI-Ly1 with pTST201-shPIM2.5 for inducible KD of PIM2	This work
14	**Ly1-SB-shPIM3.1**	OCI-Ly1 with pTST201-shPIM3.1 for inducible KD of PIM3	This work

15	**Ly1-SB-shPIM3.2**	OCI-Ly1 with pTST201-shPIM3.2 for inducible KD of PIM3	This work
16	**Ly1-SB-shPIM3.3**	OCI-Ly1 with pTST201-shPIM3.3 for inducible KD of PIM3	This work
17	**Ly1-SB-shPIM3.4**	OCI-Ly1 with pTST201-shPIM3.4 for inducible KD of PIM3	This work
18	**Ly1-SB-shPIM3.5**	OCI-Ly1 with pTST201-shPIM3.5 for inducible KD of PIM3	This work
19	**Ly1-SB-shSCR**	OCI-Ly1 with pTST201-shSCR, control cell line for Sleeping Beauty system	This work
20	**Ly1-SB-shTRIPLE**	OCI-Ly1 with pTST201-shTRIPLE for inducible KD of PIM1, PIM2, PIM3	This work
21	**HBL1-SB-TST209**	HBL1 with tetracycline repressor (pTST209)	This work
22	**HBL1-SB-shPIM1.4**	HBL1 with pTST201-shPIM1.4 for inducible KD of PIM1	This work
23	**HBL1-SB-shPIM1.5**	HBL1 with pTST201-shPIM1.5 for inducible KD of PIM1	This work
24	**HBL1-SB-shPIM2.1**	HBL1 with pTST201-shPIM2.1 for inducible KD of PIM2	This work
25	**HBL1-SB-shPIM2.4**	HBL1 with pTST201-shPIM2.4 for inducible KD of PIM2	This work
26	**HBL1-SB-shPIM3.2**	HBL1 with pTST201-shPIM3.2 for inducible KD of PIM3	This work
27	**HBL1-SB-shPIM3.4**	HBL1 with pTST201-shPIM3.4 for inducible KD of PIM3	This work
28	**HBL1-SB-shSCR**	HBL1 with pTST201-shSCR, control cell line for Sleeping Beauty system	This work
29	**HBL1-SB-shTRIPLE**	HBL1 with pTST201-shTRIPLE for inducible KD of PIM1, PIM2, PIM3	This work
30	**DHL4-pSFFV-H3wt**	DHL4 with pSFFV-H3 for constitutive overexpression of Flag-tagged histone H3	This work
31	**DHL4-pSFFV-H3S10A**	DHL4 with pSFFV-H3S10A for constitutive overexpression of Flag-tagged histone H3 with H3S10A mutation	This work
32	**DHL4-pSFFV**	DHL4 with pLV-SFFV-MCS-IRES-GFP, control cell line	This work
33	**HBL1-pSFFV-H3wt**	HBL1 with pSFFV-H3 for constitutive overexpression of Flag-tagged histone H3	This work
34	**HBL1-pSFFV-H3S10A**	HBL1 with pSFFV-H3S10A for constitutive overexpression of Flag-tagged histone H3 with H3S10A mutation	This work
35	**HBL1-pSFFV**	HBL1 with pLV-SFFV-MCS-IRES-GFP, control cell line	This work

3.2 Bacterial methods

3.2.1 Bacterial strains and bacteria culture conditions

pTRIPZ and pSFFV plasmids were generated in One Shot™ Stbl3™ Chemically Competent *E. coli*, (Invitrogen, C737303; F-*mcr*B *mrrhsd*S20(r_B^-, m_B) *rec*A13 *sup*E44 *ara*14 *gal*K2 *lac*Y1 *pro*A2 *rps*L20 (Str^R) *xyl*-5 λ^-*leumtl*-1). Since this strain is RecA (recombinase) deficient, the cells are suitable for growing viral vectors with long terminal repeats (LTRs).

Sleeping Beauty vectors TST30, TST201, TST209 and their derivatives were generated in chemically competent DH5α *E. coli* (F- 80d *lac*Z M15 (*lac*ZYA-*arg*F) U169 *rec*A1 *end*A 1hsdR17(r_k-, m_k+) *pho*A*sup*E44 -*thi*-1 *gyr*A96 *rel*A1).

Competent bacteria were stored in -80°C and thawed on ice. Bacteria cultures were propagated in sterilised LB medium (1% (w/v) Tryptone/Peptone ex casein, 0.5% (w/v) Yeast Extract, 1% (w/v) NaCl) supplemented with selection antibiotic (ampicillin (Sigma Aldrich, A9518), in 37°C, overnight. Agar plates were incubated in a steady incubator, and liquid cultures with shaking at 200 rmp.

3.2.2 Bacteria transformation – heat shock

10-50 ng of plasmid DNA, or 10 µl of ligation reaction mixture, was added to 100 µl chemo-competent cells, mixed by flicking the tube, and incubated on ice for 30 min. The tubes were then transferred to a thermoblock warmed to 42°C for 2 min, and placed on ice for 2 min. 500 µl of warm SOC medium (0.5% (w/v) Yeast Extract, 2% Tryptone /Peptone ex casein, 10 mM NaCl, 2.5 mM KCl, 10 mM MgCl2, 10 mM MgSO4, 20 mM Glucose) was added to the heat-shocked bacteria, followed by incubation of the tube for 40 min in 37°C, with shaking. The tube was then centrifuged at 5000 rpm for 5 min. The bacterial pellet was resuspended in 100 µl of sterile LB medium, and plated on a 10-cm LB-agar plate with selective antibiotic (ampicillin; Sigma Aldrich, A9518). The plate was incubated at 37°C overnight.

3.2.3 Colony PCR

Colony PCR was used as a screening procedure for constructs after plasmid cloning. It was done in the same conditions as regular PCR, but instead of DNA template, bacterial colony from agar plate was added to the reaction mixture. The tip that was used to collect the colony was kept in sterile conditions. Colonies which yielded the required product (visible after gel electrophoresis, under ultraviolet (UV) light in a transilluminator) were propagated in LB medium with selection antibiotic by inoculating the medium with the appropriate saved tip,

and incubated overnight at 37°C with shaking at 200 rmp. After 12-16 h, the culture was subject to plasmid isolation.

3.3 Molecular methods

3.3.1 Nucleic acids

3.3.1.1 RNA isolation

Total RNA was isolated from samples using GeneMATRIX Universal RNA/miRNA Purification Kit (EurX, E3599), according to the manufacturer's manual: https://eurx.com.pl/docs/manuals/pl/e3599.pdf , Section II and Section IV. RNA samples were stored in -80˚C.

3.3.1.2 cDNA synthesis

cDNA was obtained from RNA, with Transcriptor Universal cDNA Master (Roche, 5893151001) following the manufacturer's protocol: https://www.sigmaaldrich.com/deepweb/assets/sigmaaldrich/product/documents/340/811/transcriptor-universal-cdna-master.pdf. 1 µg of RNA was used per reaction.

3.3.1.3 qPCR

The reaction was performed of CFX96 (BioRad), and the samples were prepared with iTaq™ Universal SYBR® Green Supermix (Bio-Rad; 1725124), following the manufacturer's protocol: https://www.bio-rad.com/webroot/web/pdf/lsr/literature/10041157.pdf. GAPDH was the reference gene in all described experiments.

3.3.1.4 Polymerase Chain Reaction (PCR)

PCR was performed with Phusion™ High–Fidelity DNA Polymerase (Thermo Scientific, F530) according to the manufacturer's protocol: https://assets.thermofisher.com/TFS-Assets/LSG/manuals/MAN0012393_Phusion_HighFidelity_DNAPolymerase_UG.pdf. Temperature of annealing was adjusted to the melting temperature of the primers. The primers were ordered from Sigma Aldrich, or Oligo.pl (at the Institute of Biochemistry and Biophysics, Polish Academy of Sciences) for Sleeping Beauty oligos. Time of extension was adjusted to the length of the expected DNA product. The product of PCR was subject to electrophoresis in agarose gel with ethidium bromide, and visualised in UV light in a transilluminator.

3.3.1.5 Plasmid isolation - miniprep

Small-scale plasmid isolation was performed with Plasmid Miniprep DNA Purification Kit (EurX, E3500), according to the manufacturer's manual (https://eurx.com.pl/docs/manuals/pl/e3500.pdf). The composition of the buffers is not publicly available, but the protocol follows alkaline lysis of bacteria followed by DNA purification with SiO_2 columns and DNA concentration measurement.

3.3.1.6 Plasmid isolation – endotoxin-free maxi prep

Since residual bacterial endotoxins might induce human cell death, and thus bias the results, plasmids for human cell lines modification were obtained following endotoxin-free maxi prep protocols.

For pSFFV and pTRIPZ, EndoFree® Plasmid Maxi Kit (Qiagen, 12362) was used, according to the manufacturer's protocol (https://www.qiagen.com/us/resources/download.aspx?id=a48e64ab-27cf-4576-bb93-98bbd0e1229e&lang=en). Briefly, bacterial cells were lysed under alkaline conditions, and the lysates were cleared using the "QIAfilter Cartridge". Next, the Endotoxin Removal Buffer was added to the cleared lysate, and the sample was incubated on ice. The mixture was then

transferred to the DNA-binding anion-exchange tip. The tip, with bound DNA, was then washed several times, at which stage bacterial metabolites, RNA, proteins, and other contaminants were removed. The plasmid DNA was then eluted in high-salt buffer, concentrated, and desalted by isopropanol precipitation followed by centrifugation and resuspension in TE buffer.

For Sleeping Beauty, a custom-made kit was used. The procedure followed the same protocol as Qiagen method, with three differences: (i) the buffers were prepared at the laboratory, (ii) instead of "QIAfilter Cartridge", coffee filters were used, (iii) DNA-binding columns, DEAE midi/maxi columns, were purchased from EpochLife Sciences.

Endo-free Maxi prep buffers compositions:

Buffer P1 (resuspension buffer): 50 mM Tris·Cl, pH 8.0; 10 mM EDTA; 100 µg/ml RNase A (RNAse A is added directly before use)

Buffer P2 (lysis buffer): 200 mM NaOH, 1% SDS (w/v)

LyseBlue: 43 mg/ml thymolphthalein (1000x concentrated)

Buffer P3 (neutralization buffer): 3.0 M potassium acetate, pH 5.5

Buffer ER (endotoxin-removal buffer): 750 mM NaCl, 10% Triton X-114 (v/v), 40 mM MOPS, pH 7.0

Buffer QBT (equilibration buffer): 750 mM NaCl; 50 mM MOPS, pH 7.0; 15% isopropanol (v/v); 0.15% Triton® X-100 (v/v)

Buffer QC (wash buffer): 1.0 M NaCl; 50 mM MOPS, pH 7.0; 15% isopropanol (v/v)

Buffer QN (elution buffer): 1.6 M NaCl; 50 mM MOPS, pH 7.0; 15% isopropanol (v/v)

TE: 10 mM Tris·Cl, pH 8.0; 1 mM EDTA

3.3.1.7 Nucleic acid concentration measurement

RNA and DNA content in samples was measured with a µDrop™ plate (Thermo Scientific, N12391), in plate scanner (Thermo Scientific, Multiscan™). Absorbance at 320 nm,

280 nm, 260 nm, and 230 nm was measured, and used to calculate the concentration and purity of nucleic acid samples.

DNA was calculated in the following formula:

$$c=(A260-A320)*((50\ \mu g/ml)/PATHLENGTH\_CM)$$

where: c = dsDNA concentration in µg/ml, A260 = absorbance value at 260 nm after blank subtraction, A320 = absorbance value at 320 nm after blank subtraction, and PATHLENGTH_CM = pathlength value of the µDrop Plate in cm. Since the µDrop Plate has a fixed nominal pathlength of 0.05 cm, the equation used to calculated the concentration was always c=(A260-A320)*((50 µg/ml)/0.05).

260/280 and 260/230 absorbance ratios were used to determine the purity of nucleic acid measurements. The former detects contamination by protein and/or phenol, while the latter – contamination by organic compounds. Samples with the 260/280 ratio which was higher or equal 1.8, and ratio 260/230 of 2.0-2.2 were regarded as pure, however, lower or higher ratios did not discriminate the samples from further handling.

3.3.1.8 Sanger sequencing

DNA samples were prepared for Sanger sequencing with BigDye™ Terminator v3.1 Cycle Sequencing Kit (Thermo Fisher, 4337455). The sequencing was performed at the Department of Molecular Biology, Institute of Haematology and Transfusion Medicine.

3.3.1.9 Enzymes used in subcloning

Cloning was done using standard molecular biology procedures (subcloning).

Table 3.3 Enzymes used in this work.

#	ENZYME	MANUFACTURER, CATALOGUE NUMBER	PURPOSE
1	**BamHI**	Thermo Fisher, ER0055	Restriction digestion for Sleeping Beauty plasmids cloning
2	**BglII**	Thermo Fisher, ER0082	Restriction digestion for Sleeping Beauty plasmids cloning
3	**BstXI**	Thermo Fisher, FD1024	Restriction digestion for Sleeping Beauty plasmids cloning
4	**FastAP**	Thermo Fisher, EF0651	Dephosphorylation of 3’ and 5’ ends DNA after restriction digestion, various plasmids

5	**MluI**	Thermo Fisher, ER0561	Restriction digestion for pSFFV cloning
6	**SacI**	Thermo Fisher, FD1133	Restriction digestion for Sleeping Beauty plasmids cloning
7	**SalI**	Thermo Fisher, ER0641	Restriction digestion for pSFFV cloning
8	**T4 DNA Ligase**	Thermo Fisher, EL0012	Ligation of DNA, all plasmids
9	**T4 Polynucleotide Kinase**	Thermo Fisher, EK0032	Phosphorylation of DNA 5' ends of annealed oligos, pTRIPZ-PIM3 and Sleeping Beauty plasmids

3.3.1.9 List of oligonucleotides/primers used in this work

Table 3.4 Oligonucleotides used in this work.

#	NAME	SEQUENCE 5'-3'	DESCRIPTION
1	**SD1-EcoRI-FLAG-H3F3A-Fw**	ATACCGGAATTCATGGACTACAAAGACGATGACG	Used to introduce Flag tag and EcoRI restriction site at 5' end of *H3F3A*
2	**SD2-BamHI-H3F3A-Rv**	AAACGCGGATCCCTTAAGCACGTTCTCCACG	Used to introduce BamHI restriction site at 3' end of *H3F3A*
3	**SD3-S10Amut-Fw**	GCCCGCAAAGCGACCGGTGGTAAAGCACCC	Used for directional mutagenesis of *H3F3A*, for introduction of T28>G mutation, resulting in H3S10A mutation. Forward primer.
4	**SD4-S10Amut-Rv**	GGGTGCTTTACCACCGGTCGCTTTGCGGGC	Used for directional mutagenesis of *H3F3A*, for introduction of T28>G mutation, resulting in H3S10A mutation. Reverse primer.
5	**SD34_TRIPZ_shPIM3_FW_XhoI**	TCGAGAAGGTATATTGCTGTTGACAGTGAGCGACCGGCGCCTGTCAGAAGATGAACATCTCGAGATGTTCATCTTCTGACAGGCGTTTTTGGTGCCTACTGCCTCGG	Top strand of shPIM3 insert for pTRIPZ
6	**SD35_TRIPZ_shPIM3_RV_EcoRI**	AATTCCGAGGCAGTAGGCACCAAAAACGCCTGTCAGAAGATGAACATCTCGAGATGTTCATCTTCTGACAGGCGCCGGTCGCTCACTGTCAACAGCAATATACCTTC	Bottom strand of shPIM3 insert for pTRIPZ
7	**SD36_SFFV_H3S10A_FW**	AAACGCGGATCCaccatggATGGACTACAAAGACGATGACG	Used to obtain the pSFFV-H3S10A and pSFFV-H3wt plasmids, with Kozak sequence.
8	**SD37_SFFV_H3S10A_RV**	ATACCGTGCGCATTAAGCACgTTCTCCACG	Used to obtain the pSFFV-H3S10A and pSFFV-H3wt plasmids, with Kozak sequence.

Additionally, each of the 15 Sleeping Beauty inserts with shRNAs was designed and ordered as two complementary oligos. Target sequence for each shRNA is listed in the "List of plasmids used in this work" section.

#	NAME	SEQUENCE 5'-3'	DESCRIPTION
9	**Oligo_shPIM1.1_T**	gatctGCCATCAAACACGTGGAGAATTCAAGAGATTCTCCACGTGTTTGATGGTTTTTTgagct	Top strand for shPIM1.1 insert for TST30

10	**Oligo_shPIM1.1_B**	cAAAAAACCATCAAACACGTGGAGAATCTCTTGA ATTCTCCACGTGTTTGATGGCa	Bottom strand for shPIM1.1 insert for TST30
11	**Oligo_shPIM1.2_T**	gatctGTGCAAGATCTCTTCGACTTTCAAGAGAA GTCGAAGAGATCTTGCACTTTTTTgagct	Top strand for shPIM1.2 insert for TST30
12	**Oligo_shPIM1.2_B**	cAAAAAAGTGCAAGATCTCTTCGACTTCTCTTGA AAGTCGAAGAGATCTTGCACa	Bottom strand for shPIM1.2 insert for TST30
13	**Oligo_shPIM1.3_T**	gatctGCAAGATCTCTTCGACTTCTTCAAGAGAG AAGTCGAAGAGATCTTGCTTTTTTgagct	Top strand for shPIM1.3 insert for TST30
14	**Oligo_shPIM1.3_B**	cAAAAAAGCAAGATCTCTTCGACTTCTCTCTTGA AGAAGTCGAAGAGATCTTGCa	Bottom strand for shPIM1.3 insert for TST30
15	**Oligo_shPIM1.4_T**	gatctGAGTGAACTGGTCTTCCTTTTCAAGAGAAA GGAAGACCAGTTCACTCTTTTTTgagct	Top strand for shPIM1.4 insert for TST30
16	**Oligo_shPIM1.4_B**	cAAAAAAGAGTGAACTGGTCTTCCTTTCTCTTGA AAAGGAAGACCAGTTCACTCa	Bottom strand for shPIM1.4 insert for TST30
17	**Oligo_shPIM1.5_T**	gatctGCCTGGAGGTCAATGTTATGTTCAAGAGAC ATAACATTGACCTCCAGGTTTTTTgagct	Top strand for shPIM1.5 insert for TST30
18	**Oligo_shPIM1.5_B**	cAAAAAACCTGGAGGTCAATGTTATGTCTCTTGA ACATAACATTGACCTCCAGGCa	Bottom strand for shPIM1.5 insert for TST30
19	**Oligo_shPIM2.1_T**	gatctGCTTGACTGGTTTGAGACATTCAAGAGATG TCTCAAACCAGTCAAGCTTTTTTgagct	Top strand for shPIM2.1 insert for TST30
20	**Oligo_shPIM2.1_B**	cAAAAAAGCTTGACTGGTTTGAGACATCTCTTGA ATGTCTCAAACCAGTCAAGCa	Bottom strand for shPIM2.1 insert for TST30
21	**Oligo_shPIM2.2_T**	gatctGCTTCATGATGAACCCTACTTCAAGAGAGT AGGGTTCATCATGAAGCTTTTTTgagct	Top strand for shPIM2.2 insert for TST30
22	**Oligo_shPIM2.2_B**	cAAAAAAGCTTCATGATGAACCCTACTCTCTTGA AGTAGGGTTCATCATGAAGCa	Bottom strand for shPIM2.2 insert for TST30
23	**Oligo_shPIM2.3_T**	gatctAGGAGATTCTGGAAGCTGATTCAAGAGAT CAGCTTCCAGAATCTCCTTTTTTTgagct	Top strand for shPIM2.3 insert for TST30
24	**Oligo_shPIM2.3_B**	cAAAAAAAGGAGATTCTGGAAGCTGATCTCTTG AATCAGCTTCCAGAATCTCCTa	Bottom strand for shPIM2.3 insert for TST30
25	**Oligo_shPIM2.4_T**	gatctGCCGGGACTCTTATTCTGATTTCAAGAGAA TCAGAATAAGAGTCCCGGTTTTTTgagct	Top strand for shPIM2.4 insert for TST30
26	**Oligo_shPIM2.4_B**	cAAAAAACCGGGACTCTTATTCTGATTCTCTTGA AATCAGAATAAGAGTCCCGGCa	Bottom strand for shPIM2.4 insert for TST30
27	**Oligo_shPIM2.5_T**	gatctGCCAGGATCTCTTTGACTATTTCAAGAGA ATAGTCAAAGAGATCCTGGTTTTTTgagct	Top strand for shPIM2.5 insert for TST30
28	**Oligo_shPIM2.5_B**	cAAAAAACCAGGATCTCTTTGACTATTCTCTTGA AATAGTCAAAGAGATCCTGGCa	Bottom strand for shPIM2.5 insert for TST30
29	**Oligo_shPIM3.1_T**	gatctGCGACATTAAGGACGAAAATTCAAGAGAT TTTCGTCCTTAATGTCGCTTTTTTgagct	Top strand for shPIM3.1 insert for TST30
30	**Oligo_shPIM3.1_B**	cAAAAAAGCGACATTAAGGACGAAAATCTCTTG AATTTTCGTCCTTAATGTCGCa	Bottom strand for shPIM3.1 insert for TST30
31	**Oligo_shPIM3.2_T**	gatctGCCGCCAACTCTGTTATTTATTCAAGAGAT AAATAACAGAGTTGGCGGTTTTTTgagct	Top strand for shPIM3.2 insert for TST30
32	**Oligo_shPIM3.2_B**	cAAAAAACCGCCAACTCTGTTATTTATCTCTTGA ATAAATAACAGAGTTGGCGGCa	Bottom strand for shPIM3.2 insert for TST30
33	**Oligo_shPIM3.3_T**	gatctGCTGTCAGAAGATGAACATGTTCAAGAGA CATGTTCATCTTCTGACAGTTTTTTgagct	Top strand for shPIM3.3 insert for TST30
34	**Oligo_shPIM3.3_B**	cAAAAAACTGTCAGAAGATGAACATGTCTCTTGA ACATGTTCATCTTCTGACAGCa	Bottom strand for shPIM3.3 insert for TST30
35	**Oligo_shPIM3.4_T**	gatctGCTGTGAAGCACGTGGTGAATTCAAGAGA TTCACCACGTGCTTCACAGTTTTTTgagct	Top strand for shPIM3.4 insert for TST30
36	**Oligo_shPIM3.4_B**	cAAAAAACTGTGAAGCACGTGGTGAATCTCTTGA ATTCACCACGTGCTTCACAGCa	Bottom strand for shPIM3.4 insert for TST30
37	**Oligo_shPIM3.5_T**	gatctGCAGGACCTCTTCGACTTTTTCAAGAGAAA AGTCGAAGAGGTCCTGCTTTTTTgagct	Top strand for shPIM3.5 insert for TST30

38	**Oligo_shPIM3.5_B**	cAAAAAAGCAGGACCTCTTCGACTTTTCTCTTGAA AAAGTCGAAGAGGTCCTGCa	Bottom strand for shPIM3.5 insert for TST30
39	**Oligo_shSCR_T**	gatctCCTAAGGTTAAGTCGCCCTCGCTCGAGCGA GGGCGACTTAACCTTAGGTTTTTTgagct	Top strand for shSCR insert for TST30
40	**Oligo_shSCR_B**	cAAAAAACCTAAGGTTAAGTCGCCCTCGCTCGAGC GAGGGCGACTTAACCTTAGGa	Bottom strand for shSCR insert for TST30

3.3.1.10 List of plasmids used in this work

Table 3.5 Plasmids used in this work

#	NAME	BACKBONE	DESCRIPTION	SOURCE
1	**TST-209**	pT2-CAG-puro-TetR	Sleeping Beauty system plasmid. Encodes tetracycline-repressor.	Kindly provided by Thorsten Stühmer (University of Würzburg)
2	**pCMV(CAT)T7-SB100**	pCMV	Sleeping Beauty system plasmid. Contains Sleeping Beauty transposase gene.	Kindly provided by Thorsten Stühmer (University of Würzburg)
3	**TST-30**	pSUSTER2	Sleeping Beauty system plasmid for doxycycline-induced expression. Contains H1 promoter followed by tet operator.	Kindly provided by Thorsten Stühmer (University of Würzburg)
4	**TST30-shPIM1.1**	TST30	TST30 plasmid for PIM1 silencing. shRNA target sequence: CCATCAAACACGTGGAGAA	This work
5	**TST30-shPIM1.2**	TST30	TST30 plasmid for PIM1 silencing. shRNA target sequence: GTGCAAGATCTCTTCGACT	This work
6	**TST30-shPIM1.3**	TST30	TST30 plasmid for PIM1 silencing. shRNA target sequence: GCAAGATCTCTTCGACTTC	This work
7	**TST30-shPIM1.4**	TST30	TST30 plasmid for PIM1 silencing. shRNA target sequence: GAGTGAACTGGTCTTCCTT	This work
8	**TST30-shPIM1.5**	TST30	TST30 plasmid for PIM1 silencing. shRNA target sequence: CCTGGAGGTCAATGTTATG	This work
9	**TST30-shPIM2.1**	TST30	TST30 plasmid for PIM2 silencing. shRNA target sequence: GCTTGACTGGTTTGAGACA	This work
10	**TST30-shPIM2.2**	TST30	TST30 plasmid for PIM2 silencing. shRNA target sequence: GCTTCATGATGAACCCTAC	This work
11	**TST30-shPIM2.3**	TST30	TST30 plasmid for PIM2 silencing. shRNA target sequence: AGGAGATTCTGGAAGCTGA	This work
12	**TST30-shPIM2.4**	TST30	TST30 plasmid for PIM2 silencing. shRNA target sequence: CCGGGACTCTTATTCTGAT	This work
13	**TST30-shPIM2.5**	TST30	TST30 plasmid for PIM2 silencing. shRNA target sequence: CCAGGATCTCTTTGACTAT	This work
14	**TST30-shPIM3.1**	TST30	TST30 plasmid for PIM3 silencing. shRNA target sequence: GCGACATTAAGGACGAAAA	This work
15	**TST30-shPIM3.2**	TST30	TST30 plasmid for PIM3 silencing. shRNA target sequence: CCGCCAACTCTGTTATTTA	This work

16	**TST30-shPIM3.3**	TST30	TST30 plasmid for PIM3 silencing. shRNA target sequence: CTGTCAGAAGATGAACATG	This work
17	**TST30-shPIM3.4**	TST30	TST30 plasmid for PIM3 silencing. shRNA target sequence: CTGTGAAGCACGTGGTGAA	This work
18	**TST30-shPIM3.5**	TST30	TST30 plasmid for PIM3 silencing. shRNA target sequence: GCAGGACCTCTTCGACTTT	This work
19	**TST30-SCR**	TST30	TST30 control plasmid with scrambled DNA. shSCR oligo sequence: gatctCCTAAGGTTAAGTCGCCCTC GCTCGAGCGAGGGCGACTTAACCTTAGGTTTTTT gagct	This work
20	**TST-201**	pT2/SVneo NB	Sleeping Beauty system plasmid for doxycycline-induced PIM silencing.	Kindly provided by Thorsten Stühmer (University of Würzburg)
21	**TST201-shPIM1.1**	TST201	TST-201 plasmid with shPIM1.1 sequence and H1 promoter.	This work
22	**TST201-shPIM1.2**	TST201	TST-201 plasmid with shPIM1.2 sequence and H1 promoter.	This work
23	**TST201-shPIM1.3**	TST201	TST-201 plasmid with shPIM1.3 sequence and H1 promoter.	This work
24	**TST201-shPIM1.4**	TST201	TST-201 plasmid with shPIM1.4 sequence and H1 promoter.	This work
25	**TST201-shPIM1.5**	TST201	TST-201 plasmid with shPIM1.5 sequence and H1 promoter.	This work
26	**TST201-shPIM2.1**	TST201	TST-201 plasmid with shPIM2.1 sequence and H1 promoter.	This work
27	**TST201-shPIM2.2**	TST201	TST-201 plasmid with shPIM2.2 sequence and H1 promoter.	This work
28	**TST201-shPIM2.3**	TST201	TST-201 plasmid with shPIM2.3 sequence and H1 promoter.	This work
29	**TST201-shPIM2.4**	TST201	TST-201 plasmid with shPIM2.4 sequence and H1 promoter.	This work
30	**TST201-shPIM2.5**	TST201	TST-201 plasmid with shPIM2.5 sequence and H1 promoter.	This work
31	**TST201-shPIM3.1**	TST201	TST-201 plasmid with shPIM3.1 sequence and H1 promoter.	This work
32	**TST201-shPIM3.2**	TST201	TST-201 plasmid with shPIM3.2 sequence and H1 promoter.	This work
33	**TST201-shPIM3.3**	TST201	TST-201 plasmid with shPIM3.3 sequence and H1 promoter.	This work
34	**TST201-shPIM3.4**	TST201	TST-201 plasmid with shPIM3.4 sequence and H1 promoter.	This work
35	**TST201-shPIM3.5**	TST201	TST-201 plasmid with shPIM3.5 sequence and H1 promoter.	This work
36	**TST201-SCR**	TST201	TST-201 plasmid with shSCR sequence and H1 promoter.	This work
37	**TST201-shTRIPLE**	TST201	TST-201 plasmid with shPIM1.5, shPIM2.4, shPIM3.4 sequence and H1 promoter.	This work
38	**pLV-SFFV-MCS-IRES-GFP**	pSSFV	Expression plasmid with strong, constitutive SFFV promoter.	Kindly provided by Magdalena Winiarska

				(Medical University of Warsaw)
39	**pcDNA3.1+/C-DYK-H3F3A**	pcDNA3.1+	pcDNA3.1+/C-DYK plasmid with the protein coding region of the H3-3A cDNA for cloning to pRetroX, (later cloned with Flag tag and S10A mutation into pSFFV-IRES-GFP)	Purchased from GenScript
40	**pSFFV-H3S10A**	pSFFV	pSFFV with Kozak sequence, and *H3F3A* cDNA sequence with point mutation T28>G, resulting in S10A protein mutation, tagged with FLAG at C terminus	This work
41	**pSFFV-H3wt**	pSFFV	pSFFV with Kozak sequence, and *H3F3A* cDNA sequence tagged with FLAG at C terminus	This work
42	**pTRIPZ-shPIM1**	pTRIPZ	TRIPZ lentiviral plasmid for doxycycline-inducible expression of human PIM1 shRNA	Purchased from Dharmacon; Clone Id: V2THS_170014
43	**pTRIPZ-shPIM2**	pTRIPZ	TRIPZ lentiviral plasmid for doxycycline-inducible expression of human PIM2 shRNA	Purchased from Dharmacon; Clone Id: V3THS_381052
44	**pTRIPZ-shPIM3**	pTRIPZ	TRIPZ lentiviral plasmid for doxycycline-inducible expression of human PIM3 shRNA	This work
45	**pTRIPZ-NTC**	pTRIPZ	TRIPZ lentiviral plasmid for doxycycline-inducible expression of non-targeting control shRNA	Kindly provided by Małgorzata Bajor (Medical University of Warsaw)
46	**pRetroX**	pBabe	Retroviral plasmid for inducible expression. Not used functionally in this work.	Purchased from Addgene
47	**pRetroX-H3wt**	pRetroX	pRetroX retroviral plasmid with *H3F3A* with Flag tag. The plasmid was obtained in the course of the described project, but not used for functional studies. Used for cloning of *H3F3A* to pSFFV.	This work
48	**pRetroX-H3S10A**	pRetroX	pRetroX retroviral plasmid with *H3F3A* gene with point mutation resulting in S10A aminoacid mutation. The plasmid was obtained in the course of the described project, but not used for functional studies. Used for cloning of *H3F3A* mutant to pSFFV.	This work

3.3.1.11 Generation of Sleeping Beauty Plasmids

Schematic plan of Sleeping Beauty experiment and used vectors is shown in Fig.3.3. Oligo sequence for Sleeping Beauty plasmids with shRNAs targeting PIM kinases were designed by Filip Garbicz, MD. 5 oligos with different shRNA for each PIM kinase and one scrambled RNA control (shSCR), i.e. 16 oligos in total, were ordered. The target sequences are listed in the "List of plasmids used in this work" section, by TST30 plasmids. The oligos were enzymatically phosphorylated by PNK and hybridised by heating and subsequent cooling. The inserts were then cloned into TST30 plasmids, previously digested with BglII and SacI, to place the shRNA sequence under doxycycline-inducible H1 promoter. Then, the promoter-shRNA cassette was digested out from TST30 plasmid with BstXI and SacI enzymes and ligated with TST201 plasmid, previously linearised with BstXI and dephosphorylated with FastAP, to flank the insert with transposase-reactive elements. Plasmid with shPIM1.1 was not obtained for technical reasons – despite numerous attempts, ligation with TST30 was not successful only in case of this insert. The other 15 obtained TST201-derivative plasmids were then electroporated to the Ly1-SB-209 cell line. Silencing efficiency was assessed by western blots for each of 16 generated cell lines. From 5 cell lines expressing different shRNA for each PIM, two that generated the deepest silencing were selected for functional experiments (shPIM1.4, shPIM1.5, shPIM2.1, shPIM2.4, shPIM3.2 and shPIM3.4), and for introduction to HBL1-SB-TST209 cell line. Finally, one of the two shRNAs for each PIM was selected for the construction of shTRIPLE, which expressed shPIM1.5, shPIM2.4 and shPIM3.4. In order to clone shTRIPLE plasmid, shRNA inserts were sequentially digested out from TST30 plasmid and cloned into TST201-shRNA. The shTRIPLE plasmid was electroporated to Ly1-SB-209 and HBL1-SB-209 cell lines with tetracycline repressor. In total, 34 plasmids, and 27 DLBCL cell lines were generated and inspected for inducible PIM kinase silencing in the Sleeping Beauty system.

3.3.2 Protein methods

3.3.2.1 Histone isolation

Histones were isolated using Histone Extraction Kit (Abcam; ab113476) according to the manufacturer's manual:

https://www.abcam.com/ps/products/113/ab113476/documents/ab113476%20Histone%20Extraction%20Kit%20v5c%20(website).pdf . Briefly, the procedure involves resuspension of the cell pellet in pre-lysis buffer, centrifugation, lysis of the pellet by resuspension in lysis buffer, and neutralisation. The composition of the buffers is not publicly available.

3.3.2.2 Total protein isolation

Cells were centrifuged (300 x g, 5 min), washed in PBS, and centrifuged again. The cell pellet was resuspended in RIPA buffer (50 mM Tris HCl, 150 mM NaCl, 1.0% (v/v) NP-40, 0.5% (w/v) Sodium Deoxycholate, 1.0 mM EDTA, 0.1% (w/v) SDS and 0.01% (w/v) sodium azide at a pH of 7.4.) supplemented with protease and phosphatase inhibitors, incubated on ice for 30 minutes, with vortexing every 10 minutes. RIPA buffer contains NP-40, sodium deoxycholate, and SDS, i.e. detergents that disrupt both cellular, and nucleolar membrane, resulting in whole-cell lysis. The suspension was then centrifuged for 10 min, at 12 000 g in 4°C to sediment non-soluble elements of the cell. The supernatant containing cytoplasmic and nuclear proteins was then transferred to a new tube and stored in -80°C.

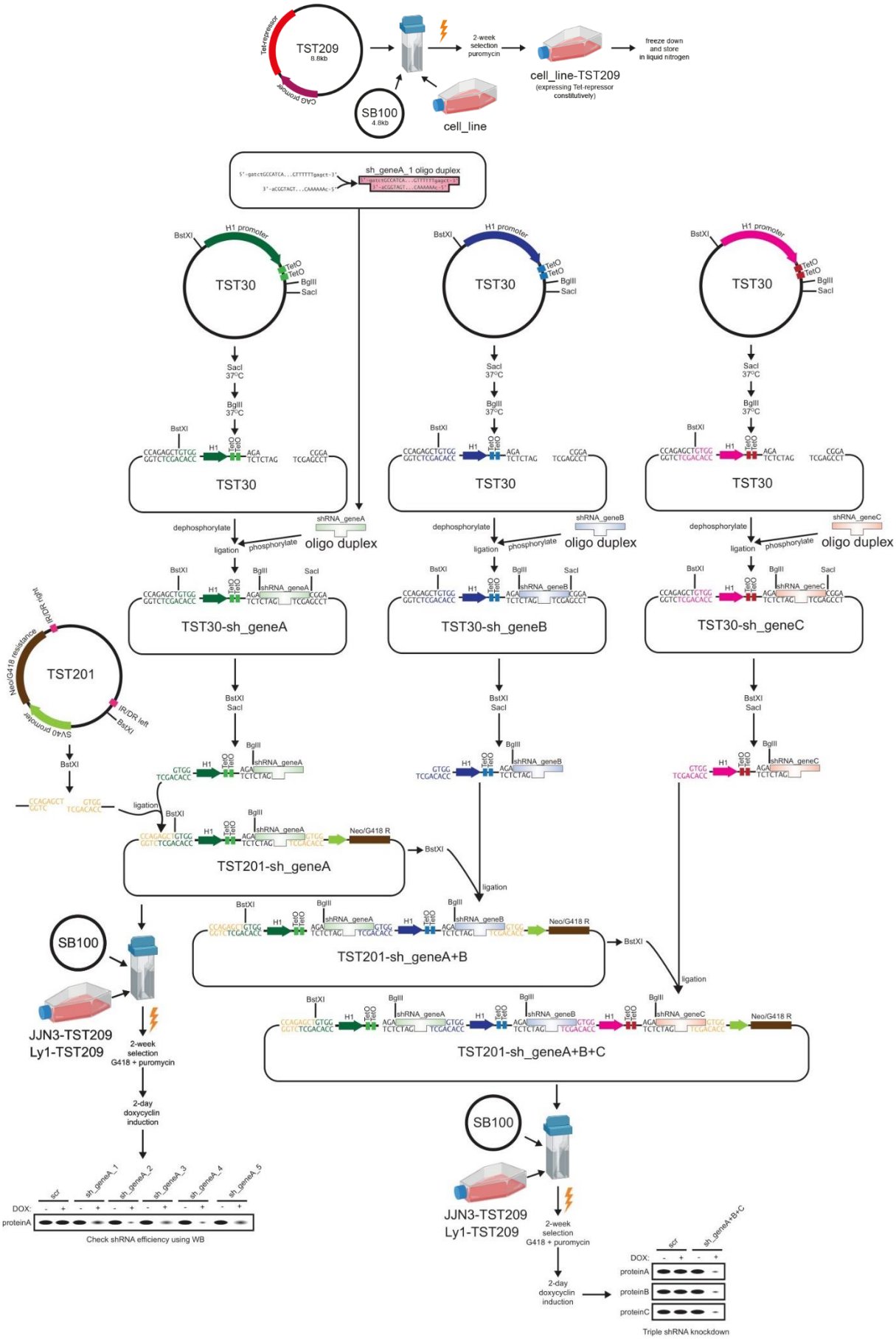

Figure 3.3 Diagram showing steps in preparation of Sleeping Beauty vectors and cell lines. Created in BioRender by Filip Garbicz.

3.3.2.3 Chromatin fractionation

Differential salt fractionation of nuclei was performed according to the protocol by Hermann et al., 2017 [159]. Nuclei were isolated with the sucrose cushion method (which proved to be superior to hypotonic isolation in the course of optimisation).

3.3.2.4 Protein concentration measurement – BCA method

The concentration of proteins in whole cell lysate, and histone isolate samples was determined with Pierce™ BCA Protein Assay Kit (Thermo Fisher, 23225), according to the manufacturer's protocol for microplate procedure: https://assets.thermofisher.com/TFS-Assets/LSG/manuals/MAN0011430_Pierce_BCA_Protein_Asy_UG.pdf. The method uses the biuret reaction, e.g. reduction of Cu^{+2} to Cu^{+1} by protein in an alkaline medium, and the sensitive and selective detection of the cuprous cation (Cu^{+1}) using a reagent containing bicinchoninic acid, BCA. Chelation of two BCA molecules with one Cu^{+1} ion results in a purple product, detected in 562 nm wavelength, proportional to the protein concentration in the sample.

3.3.2.5 Western blots and densitometry

20-40 µg of protein from whole cell lysate, or 1-5 µg of histone lysate was used per sample. The required amount of sample was mixed with loading buffer and filled with water to the total volume of 20 µl. The samples were boiled at 95°C for 10 min.

Protein samples were resolved by SDS-PAGE. For histone samples, Bolt™ 4 to 12%, Bis-Tris gels (Invitrogen; NW00082BOX) and MES buffer (Invitrogen; B0002) were used. Whole-cell lysates were developed in manually casted gels (polyacrylamide percentage depended on the molecular weight of the protein of interest, for PIM proteins - 10%), in TRIS/Glycine/SDS running buffer. Protein size was assessed by comparison to PageRuler Prestained Protein Ladder (Thermo Scientific; 26617). The samples were subsequently transferred from the gel to PVDF membrane (Thermo Fisher, 88518) in TRIS/Glycine/Methanol transfer buffer for 1h at a constant current of 400mA. Transfer efficacy was assessed by Ponceau staining. Washed

membrane was then blocked with 5% solution of BSA in TBS for 1 hour, and incubated overnight with primary antibody. The following day, membranes were thoroughly washed with TBST, by three 10-minute incubations, and incubated with secondary antibody conjugated with horseradish peroxidase diluted in 5% milk in TBST (1:5000 for anti-rabbit, and 1:50000 for anti-mouse antibodies) for 40 min. All incubations were made with rocking. The membranes were then washed again in the same conditions, drained, and incubated with ECL reagent (Perkin Elmer; NEL120E001EA). Chemiluminescence was acquired as a digital image (G-Box, Syngene).

To reprobe with another antibody, the membrane was incubated with a SDS/HCl/ß-mercaptoethanol stripping buffer at 50°C for 30 min with shaking, followed by a thorough wash with TBST and 1-hour blocking with 5% BSA. Quantification of band intensities (densitometry) was done with Fiji software (ImageJ).

3.3.2.6 Antibodies used for western blot

Primary antibodies are listed in Table 3.5. For rabbit antibodies, secondary Anti-Rabbit IgG-Peroxidase produced in goat (Sigma Aldrich, A0545) was used. For mouse antibodies, secondary Anti-Mouse IgG (whole molecule)-Peroxidase antibody produced in rabbit was used (Sigma Aldrich, A9044).

Table 3.6 Primary western blot antibodies used in this work.

#	ANTIGEN	ANTIBODY NAME	MANUFACTURER, CATALOGUE NUMBER
		ANTI-HISTONE ANTIBODIES	
1	H3S10ph	Phospho-Histone H3 (Ser10) (D2C8) XP® Rabbit mAb	Cell Signaling Technology, 3377
2	H3K9acK14ac	Anti-Histone H3 (acetyl K9 + K14) antibody	Abcam, ab232952
3	H3K4me3	Histone H3K4me3 antibody (pAb)	Active Motif, 39159
4	H4K16ac	Anti-acetyl-Histone H4 (Lys16) Antibody	Merck, 07-329
5	H4panAc	Histone H4ac (pan-acetyl) antibody (pAb)	Active Motif, 39026
6	H3K27me3	Histone H3K27me3 antibody (pAb)	Active Motif, 39155
7	γH2AX	Phospho-Histone H2A.X (Ser139) (D7T2V) Mouse mAb	Cell Signaling Technology, 80312
8	H3	Histone H3 (96C10) Mouse mAb	Cell Signaling Technology, 3638
9	H4	Histone H4 (L64C1) Mouse mAb	Cell Signaling Technology, 2935
		ANTI-PIM ANTIBODIES	
10	PIM1	Pim-1 (D8D7Y) Rabbit mAb	Cell Signaling Technology, 54523

11	PIM2	Pim-2 (D1D2) Rabbit mAb	Cell Signaling Technology, 4730
12	PIM3	Pim-3 (D17C9) Rabbit mAb	Cell Signaling Technology, 4165
ANTI-RNA POLYMERASE II ANTIBODIES			
13	RNAPII CTD pSer2	Phospho-Rpb1 CTD (Ser2) (E1Z3G) Rabbit mAb	Cell Signaling Technology, 13499
14	RNAPII CTD pSer5	Phospho-Rpb1 CTD (Ser5) (D9N5I) Rabbit mAb	Cell Signaling Technology, 13523
15	RNAPII	RNA pol II antibody (mAb)	Active Motif, 39097
OTHER ANTIBODIES			
16	BRD4	BRD4 antibody (pAb)	Active Motif, 39010
17	EZH2	Ezh2 (AC22) Mouse mAb	Cell Signaling Technology, 3147
18	FLAG tag	ANTI-FLAG ® antibody produced in rabbit	Sigma Aldrich, F7425
19	GAPDH	Ms X GAPDH	MAB374
20	HMGB1	HMGB1 (D3E5) Rabbit mAb	Cell Signaling Technology, 6893
21	Tubulin	Anti-alpha-Tubulin Mouse mAb (DM1A)	Merck, CP06
22	Lamin B	Lamin B1 (D4Q4Z) Rabbit mAb	Cell Signaling Technology, 12586

3.3.3 High-throughput methods

3.3.3.1 Gene expression profiling with microarrays

DHL4, HBL1 and U2932 cells were treated with DMSO or SEL24/MEN1703 for 24h and subject to gene expression profiling on GeneChip Human Gene 1.0 ST Array (Affymetrix, 901085). The experiment was performed by Maciej Szydłowski. The bioinformatic analysis of the RNA-Seq results was performed by Przemysław Juszczyński and Sonia Dębek.

3.3.3.2 RNA Sequencing - Ly1, DHL4, HBL1 and TMD8

LY1, DHL4, HBL1 and TMD8 cell lines were seeded out at 0.5×10^6 cells/ml 24h before the experiment in full medium, to allow cell cycle synchronisation. On the day of the experiment, cells were counted and seed out at 0.5×10^6 cells/ml in fresh medium with either 1.5 µM SEL24/MEN1703 or DMSO for 3 h and 24 h. 1-2 $\times10^6$ of cells were collected at each timepoint. The experiment was performed in 3 biological replicates.

RNA was extracted using GeneMATRIX Universal RNA Purification Kit (EurX, E3599). In order to minimise bias in RNA Sequencing, RNA samples were digested with DNAse (New England Biolabs, M0303) for 30 min in 37°C, in the dedicated DNAse reaction buffer (New

England Biolabs, B0303). The samples were then purified using GeneMATRIX Universal RNA/miRNA Purification Kit (EurX, E3599), according to the manufacturer's manual: https://eurx.com.pl/docs/manuals/pl/e3599.pdf, Section "Dodatek II: Oczyszczanie RNA/miRNA po reakcjach enzymatycznych".

Sample quality was assessed with TapeStation with RNA ScreenTape Analysis kit. mRNA enrichment, library preparation and sequencing of samples from Ly1, DHL4, HBL1 and TMD8 cell lines treated with 1.5 µM SEL24/MEN1703 or DMSO for 3h or 24h was ordered at CeGaT, GmbH in Tübingen, Germany.

The bioinformatic analysis of the RNA-Seq results was performed by Sonia Dębek and Przemysław Juszczyński.

3.3.3.3 RNA Sequencing – Ly1 time course

LY1 cell line were seeded out at 0.5×10^6 cells/ml 24h before the experiment in 10% FBS IMDM medium, to allow cell cycle synchronisation. On the day of the experiment, cells were counted and seed out at 0.5×10^6 cells/ml in fresh medium. Untreated cells were collected as time 0h, and the rest were then treated with 1.5 mM SEL24/MEN1703 for 3, 6, 12 and 24h. 2 mln cells were collected at each timepoint. The experiment was performed in 5 biological replicates. DMSO treatment for 24h was used as a control. RNA was extracted using GeneMATRIX Universal RNA Purification Kit, digested with DNAse I, and purified with GeneMATRIX Universal RNA Purification Kit (analogously to the procedure described in 3.3.3.2).

Libraries were prepared by Dorota Komar, using mRNA enrichment kit: NEBNext® Poly(A) mRNA Magnetic Isolation Module (New England Biolabs; E7490) and NEBNext Ultra II Directional RNA Library Prep Kit for Illumina (New England Biolabs, E7760) according to the manufacturer's manual.

Libraries size distribution have been checked by TapeStation with Agilent High Sensitivity D1000 ScreenTape System, concentrations were quantified using KAPA Library Quantification Kit Complete Kit and Qubit dsDNA HS Assay Kit.

The libraries were sequenced on Illumina NextSeq 500 at the Insititute of Haematology and Transfusion Medicine by Magdalena Skrzypczak and Sylwia Radomska.

The bioinformatic analysis of the RNA-Seq results was performed by Sonia Dębek, Przemysław Juszczyński and Michał Pawlak.

3.3.3.4 Chromatin immunoprecipitation and sequencing (ChIP-Seq)

Samples and libraries for ChIP-Seq were prepared by Dorota Komar, PhD. They were sequenced on Illumina NovaSeq 6000 at Centre of New Technologies (CeNT), University of Warsaw. The results were processed and analysed by Michał Pawlak, Przemysław Juszczyński and Sonia Dębek.

3.3.3.5 RNA quantification and quality assessment for RNA-Seq - Qubit™ and Tape Station

Before RNA-Seq library preparation, sample concentrations were quantified with Qubit™ 4 Fluorometer (Invitrogen; Q33226), using dedicated reagents: Qubit™ RNA BR Assay Kit (Invitrogen; Q10211), and Qubit™ Assay Tubes (Invitrogen; Q32856).

Sample integrity was assessed with automated electrophoresis device, 4200 TapeStation (Agilent; G2991BA) with dedicated RNA ScreenTapes (Agilent; 5067-5576), RNA ScreenTape Sample Buffer (Agilent; 5067-5577) and RNA ScreenTape Ladder (Agilent; 5067-5578), or, if the RNA quantity was below 25 ng/ul in Qubit quantification, RNA High Sensitivity screen tapes (Agilent; 5067-5579), High Sensitivity RNA ScreenTape Sample Buffer (Agilent; 5067-5580) and High Sensitivity RNA ScreenTape Ladder (5067-5581), according to the manufacturer's manuals: https://www.agilent.com/cs/library/usermanuals/public/4200-TapeStation_RNA_QG.pdf (RNA ScreenTape) or https://www.agilent.com/cs/library/usermanuals/public/4200-TapeStation_HS-RNA_QG.pdf (High Sensitivity Screen RNA Tape). High-quality samples with RIN>8 were used for further handling.

3.3.3.6 Library quality assessment for RNA-Seq - Tape Station

Fragment size distribution was assessed with automated electrophoresis device, 4200 TapeStation (Agilent; G2991BA) with dedicated DNA D1000 ScreenTapes (Agilent; 5067-5582), DNA D1000 ScreenTape Sample Buffer (Agilent; 5067-5602) and DNA D1000 ScreenTape Ladder (Agilent; 5067-5586), according to the manufacturer's instructions: https://www.agilent.com/cs/library/usermanuals/public/D1000_QuickGuide.pdf. 300bp fragments were expected. If a peak of adapters at ~150bp was detected, the sample was purified again with magnetic beads.

3.3.3.7 Library concentration measurement – KAPA Library Quantification Kit Complete Kit and Qubit dsDNA HS Assay Kit

Quantification of library concentration was done with KAPA Library Quantification Kit Complete Kit according to manufacturer's manual: https://rochesequencingstore.com/wp-content/uploads/2022/07/KAPA-Library-Quantification-Kit-Technical-Data-Sheet.pdf and with Qubit dsDNA HS Assay Kit according to the manufacturer's manual: https://www.thermofisher.com/document-connect/document-connect.html?url=https://assets.thermofisher.com/TFS-Assets%2FLSG%2Fmanuals%2FQubit_dsDNA_HS_Assay_UG.pdf.

3.4 Bioinformatic methods

3.4.1 Demultiplexing and Nexflow pipeline

Demultiplexing of RNA-Seq results was performed with bcl2fastq (v2.20.0.422) with default settings. The FASTQ files are stored on the IHIT-NGS server. The FASTQ files were then processed with nextflow (nf-core/rnaseq v1.4.2) RNA-seq pipeline. Reads were aligned with STAR algorithm to the Genome Reference Consortium Human Build 37 (GRCh37) in RNA-Seq, and to the Genome Reference Consortium Human Build 38 (GRCh38) in ChIP-Seq. The script is stored in IHIT-ZHE GitHub: https://github.com/zhe-lab-ihit/.

3.4.2 Differential gene expression

For analysis of microarray expression data from DHL4, HBL1 and U2932 cell lines were pooled, filtered using GenePattern [156] (the ComparativeMarkerSelection module) and analysed using Gene Set Enrichment Analysis (GSEA) in GSEA Software [157]. The deregulated pathways identified with GSEA were then compared with deregulated pathways from Chapuy *et al.* 2013 (Gene Expression Omnibus accession number: GSE45630) [158]. Expression of the top deregulated genes after SEL24/MEN1703 treatment was then assessed in expression data from Chapuy *et al.*, 2013 using GSEA.

For RNA-Seq experiments, differential gene expression was assessed with DeSeq2 in R Studio ("DEseq2" package [159]) and GSEA. Each cell line was analysed separately. Read counts from SEL24/MEN1703-treated samples were compared with DMSO control samples from the same time point in case of the experiment with 3h and 24h treatment, or with the 0h time point in case of Ly1 time course analysis.

3.4.3 Identification of SE-encoded lncRNA

Deregulated lncRNAs with their coordinates were selected from all deregulated transcripts (identified with DeSeq2) in R Studio, with "biomaRt" package [160,161]. Then, lncRNA coordinates were intersected with the SE coordinates from Chapuy *et al.*, 2013 [158] using BEDtools suite [162].

3.4.4 Visualisation of results

Heatmaps and dot plots were prepared in R studio using "ggplot2" [163] and "gage" [164] packages in R Studio. Volcano plots were visualised with "Volcano plot" module, heatmap of Z-scores of deregulated genes of HBL1 line after PIM inhibition was done in "heatmap2" - both tools in Galaxy (www.usegalaxy.org,[165]).

3.5 Statistical methods

Statistical analyses were performed with GraphPad Prism 9 software (GraphPad Software Inc.) or R software package (version 4.0.4). The used tests are indicated in figures. Multiple comparisons were made with regard to the control cell line. P value < 0.05 was considered statistically significant. The p values were marked with the asterisks on the charts (* = P < 0.05; ** = P < 0.01; *** = P < 0.001; *** = P < 0.0001).

4. Results

4.1 Inhibition of PIM kinases has a profound effect on transcription

One of the canonical functions of PIM kinases is regulation of TFs, such as MYC or NF-κB. In our previous studies, we have initially characterised the consequences of PIM inhibition by SEL24/MEN1703 in DLBCL and demonstrated that the inhibitor blocked MYC-driven transcriptional program [74]. However, gene expression profiling suggested that PIMs' effect on transcription is wider than solely through regulation of MYC. For example, we found that PIM inhibition blocked numerous key lymphoma pathways, such as Toll-like receptor signalling, antigen processing and presentation, cell cycle and G1-S/G2-M phase transition, aminoacyl-tRNA biosynthesis and pyrimidine metabolism, as well as MYC/E2F1-dependent transcription (Figure 4.1A). The list of pathways deregulated by the PIM inhibitor resembled, at least partially, those deregulated by a BRD4 inhibitor JQ1 [158] : of 33 pathways altered by JQ1, 8 were also modulated by MEN1703 (Figure 4.1B). To formally assess these similarities, we selected the top 100 most significantly downregulated genes in PIM-inhibitor-treated cell lines, and investigated the expression of this gene set in JQ1-treated cell lines (Figure 4.1C). We found that PIM-inhibitor-downregulated genes exhibited reduced expression also after BRD4 inhibition. Taken together, these data indicate that activity of BRD4 and PIM at least partially overlap.

Since wide deregulation of transcription is frequently associated with global epigenetic changes, we referred to the available literature to search if PIM kinases have a documented epigenetic function. Two published studies reported a detailed mechanism of phosphorylation of serine 10 at histone 3 (H3S10ph) by PIM1 at MYC targets in endothelial cells [69,70]. This epigenetic activation included the recruitment of BRD4, which further facilitated transcriptional machinery assembly. BRD4 is an established epigenetic regulator of transcription (reviewed in ref. 166). Given the potential cooperation between PIM1 and BRD4, we investigated if PIM inhibition influences total RNA levels. Moreover, previous reports from our group highlighted decreased MYC abundance following PIM inhibition and disruption of MYC-associated transcriptional program in DLBCL cells treated with SEL24/MEN1703 [37]. Since MYC amplifies transcriptional output of active genes, increasing cellular RNA content [167], we measured total RNA amount in six DLBCL cell lines treated with PIM inhibitor. We noted

universal decrease in RNA levels in comparison to control cells (Figure 4.1D), indicating that PIM kinases appear to have a universal role in control of RNA biosynthesis and/or stability.

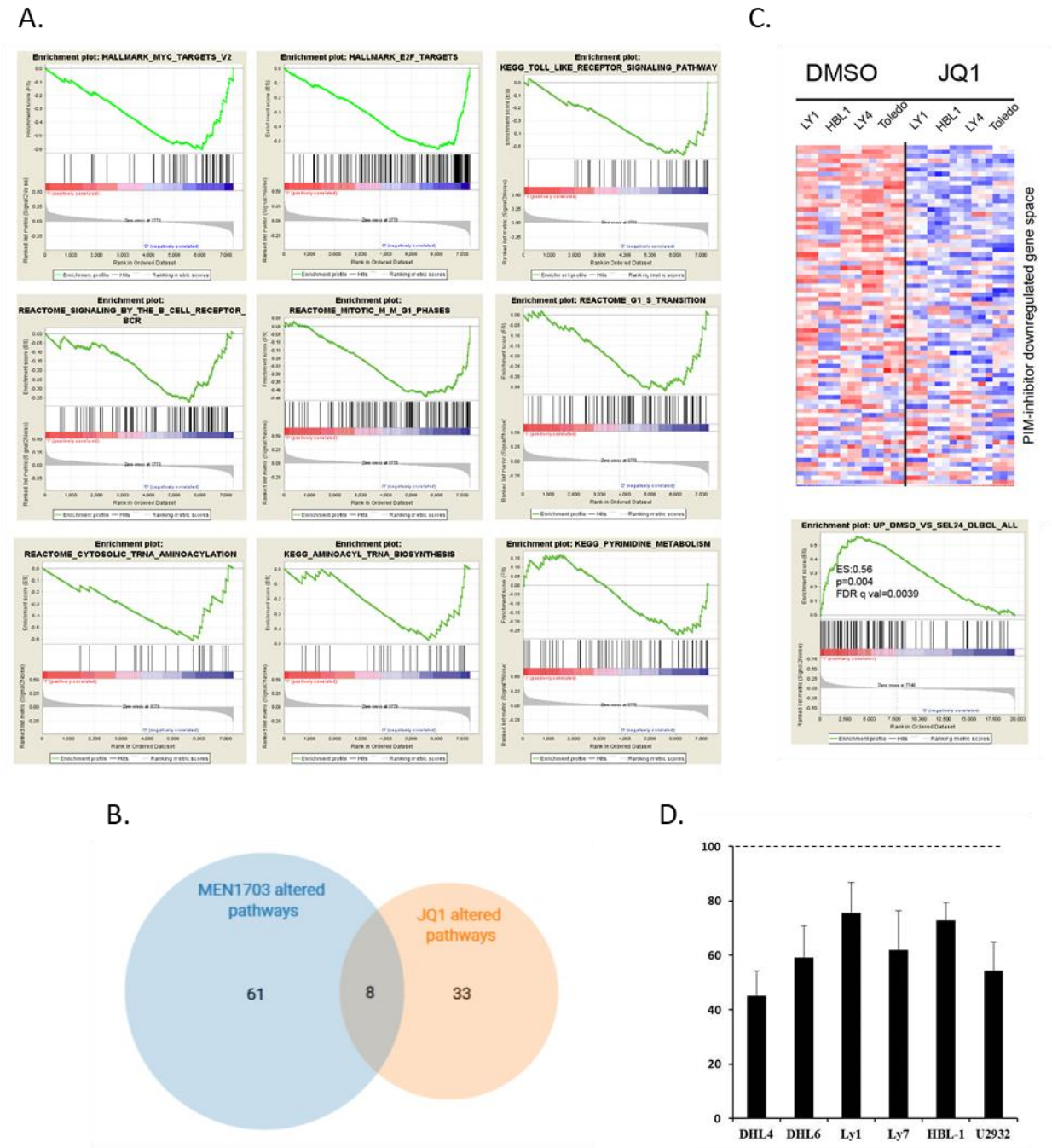

Figure 4.1. Transcriptional outcomes of PIM inhibition resemble inhibition of BRD4

A. Enrichment plots of gene set expression analysis (GSEA) of pathways deregulated in DHL4, HBL1 and U2932 after PIM inhibition with SEL24/MEN1703
B. Heatmap and GSEA enrichment plot showing expression and enrichment of top deregulated genes after PIM inhibition in the geneset of deregulated genes after BRD4 inhibition with JQ1
C. Venn diagram presenting the overlap of pathways deregulated after PIM inhibitor and BRD4 inhibitor
D. RNA levels after 24-hour treatment with SEL24/MEN1703 compared to cellst treated with DMSO (=100%)

4.2 PIM1 is a H3S10 kinase in DLBCL

4.2.1 PIM as H3S10ph kinase(s): results of chemical inhibition and genetic silencing

Since PIM1 has already been described as a histone writer in endothelial cells [70], we investigated whether it plays epigenetic role also in DLBCL. In order to assess the scope of PIM's activity in epigenetic patterns, selected post-translational histone modification levels: H3S10ph, and H4K16ac or H4panAc, were assessed after 24-hour treatment with three different pan-PIM inhibitors that have reached clinical trials. We used: SEL24/MEN1703, PIM447, and a first-generation PIM inhibitor SGI-1776. All compounds effectively diminished the levels of H3S10ph and H4 acetylation (Figure 4.2A). The changes were seen on the global level, confirming an important role of PIM in maintaining the abundance of H3S10ph. The reduction of histone modification levels was the strongest for SEL24/MEN1703 and for PIM447, while the weakest effect was achieved with SGI-1776. For this reason, only SEL24/MEN1703 and PIM447 were used in further experiments.

4.2.2 PIM subcellular localisation

PIM localisation differs in cell types and differentiation stages [47–51]. Moreover, to-date, epigenetic function has been described only for PIM1, but since the three family members are largely homologous, it is possible that other PIMs are also histone writers, provided they localise in the nucleus. To address these issues, we performed subcellular fractionation followed by western blot to determine whether PIMs are present in the nuclei of DLBCL cells (Figure 4.2B). The localisation of PIM kinases was universal for all cell lines. PIM1 and PIM3 have mixed, cytoplasmic-nuclear localisation, with a preference for the cytoplasm, while PIM2 is exclusively cytoplasmic. Therefore, the nuclear PIM1 and PIM3 could potentially interact with chromatin in DLBCL.

To investigate this hypothesis further, chromatin fractionation was performed: nuclei of Ly1 cell line were gently permeabilised with a detergent, and washed with increasing amounts of salt to separate nuclear proteins according to their strength of interaction with chromatin.

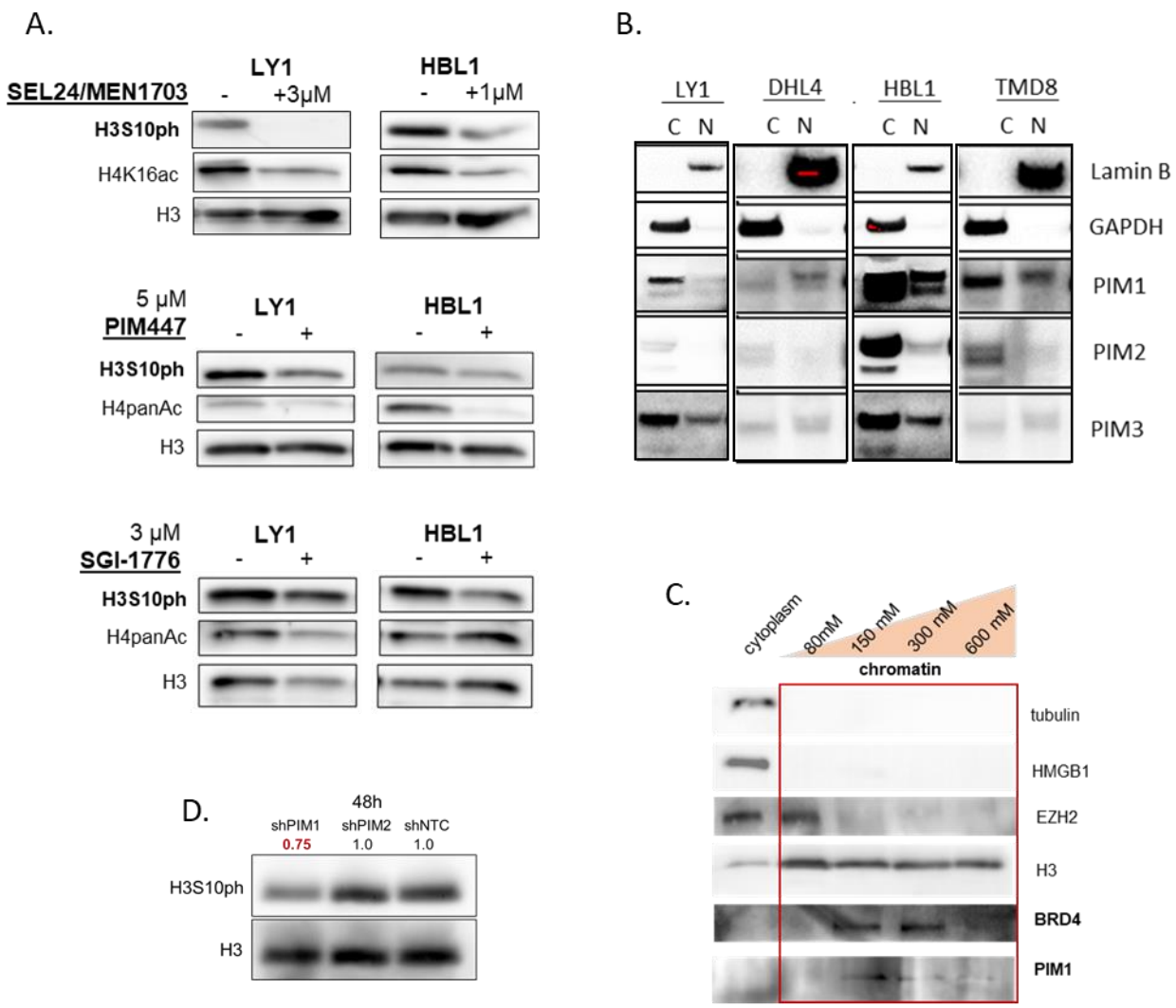

Figure 4.2. PIM kinases localise in the nucleus, and their inhibition decreases H3S10ph

A. Western blots with samples from DLBCL cell lines treated with different small-molecule pan-PIM inhibitors: SEL24/MEN1703, PIM447 and SGI-1776 for 24h with doses indicated in the figure.
B. Western blot analysis of PIM localisation in subcellular fractions. Lamin B and GAPDH were used for verification of the fractions cleannes (i.e. lack of other subcellular contamination), for nuclear (N) and cytoplasmic (C) fractions respectively.
C. Chromatin fractionation followed by western blot indicates that PIM1 interacts with chromatin, and co-occurs in the same fraction as BRD4.
D. Genetic silencing of PIM kinases confirms epigenetic function of cytoplasmic-nuclear PIM1, but not cytoplasmic PIM2.

PIM1 was found to enrich the same fraction as BRD4, and interact relatively strongly with the chromatin (Figure 4.2C). The interaction was stronger than in case of the highly mobile chromatin protein HMGB1 (which was eluted even before the salt washes), or even another histone modifier, a H3K27-methyltransferase EZH2. Despite numerous attempts, PIM3 levels

were undetectable in this experiment, most likely due to the low abundance of PIM3 isoform, and “troublesome” antibodies. Thus, we confirmed that PIM1 interacts with the chromatin in DLBCL cells. Perhaps, it could also form complexes with other epigenetic proteins, but this hypothesis requires further, comprehensive studies.

4.2.3 Genetic knock down of PIM1 reduces levels of H3S10ph

Chemical inhibition of PIMs showed downregulation of histone modifications (Figure 4.2A). However, small molecule drugs have been shown to bind on average to at least 6-11 distinct off-targets [168,169]. To rule out the possibility that the H3S10ph decrease in DLBCL cell lines is attributable to off-target effects, I investigated the impact of PIM KD on H3S10ph levels. Lentiviral vector pTRIPZ for effective, inducible expression of microRNA-adapted shRNA targeting PIM1 or PIM2 was immediately available for purchase and ready to use. Therefore, this system was chosen for initial analyses with PIM genetic silencing. Ly1 cells were transfected with pTRIPZ-PIM1, -PIM2, and –NTC (non-targeting control). The cells were then selected with puromycin, and their ability to silence PIM1 or PIM2 was confirmed with western blots. Finally, levels of H3S10ph were assessed, which showed that KD of the cytoplasmic-nuclear PIM1**,** but not cytoplasmic PIM2**,** was followed by global H3S10ph reduction (Figure 4.2D). The plasmid containing shPIM3 was not available for purchase, and an attempt was made to design and clone it in-house. Cloning was successful and the correct plasmid sequence was confirmed. However, PIM3 was not reliably silenced in DLBCL cells with the developed plasmid. Taken together, these observations confirmed that the decrease in H3S10ph was specifically due to inhibition of at least PIM1.

4.3 Depletion of single PIM kinase induces compensatory upregulation of other family member(s)

Since PIM3 KD in pTRIPZ system was unsuccessful, I generated cell lines with doxycycline-inducible KD of PIM1, PIM2, and PIM3 in another system, the Sleeping Beauty transposon system. The experiment was designed and performed in collaboration with a PhD

candidate from our group, Filip Garbicz, MD, who performed parallel PIM KD experiments in plasma cell myeloma. Moreover, the system allows for combination of multiple shRNAs in one plasmid, so we also used it for the construction of triple PIM KD.

Previous reports showed that PIM depletion can be compensated in certain contexts [37,54–56]. In order to investigate possible compensation, which could distort the outcomes of single PIM KDs, stable Ly1 cells with Sleeping Beauty plasmids for single silencing of either PIM1, 2, or 3 were treated with doxycycline to induce the expression of shRNAs. The cells were collected at three time points of doxycycline treatment (24h, 48h, 72h), subject to whole cell lysis, and the levels of all PIM proteins were assessed with western blot.

PIM levels changed throughout the silencing (Figure 4.3A). In the case of PIM1, the most striking observation was an acute upregulation of PIM3, which consequently faded in time. Likewise, PIM1 also seemed to correlate with PIM3 abundance – its levels were reciprocal to those of PIM3. Therefore, PIM1 and PIM3 seem to compensate for their diminished levels. Silencing of PIM2 induced compensation by both other PIMs from 72h on, even though the silencing was becoming increasingly ineffective.

Since PIMs compensate for the loss of one another, and the epigenetic function of PIM3 remains unknown, we generated cell lines with triple PIM KD for studying the role of PIM-induced H3S10ph. As the Sleeping Beauty system allows for inducible, simultaneous expression of several shRNA from the same promoter, the most efficient shRNAs (one for each PIM) were combined in a single plasmid for inducible triple PIM KD.

The KD level was modest, but sufficient to reduce the levels of H3S10ph and H4panAc (Figure 4.3B), similarly to PIM inhibitor treatment. The triple KD cells were also subject to proliferation assay (Figure 4.3C). Cells with induced expression of shTRIPLE showed universal slower proliferation than their PIM-sufficient counterparts. Although the difference is minute (~0.9 times slower proliferation than that without the silencing), this trend is consistent, regardless of number of splits, or cell line, and statistically significant for both cell lines (p value = 0.0022 for Ly1, and 0.0003 for HBL1; Mann-Whitney test). It is likely that the small difference in proliferation is connected to the insufficient level of KD.

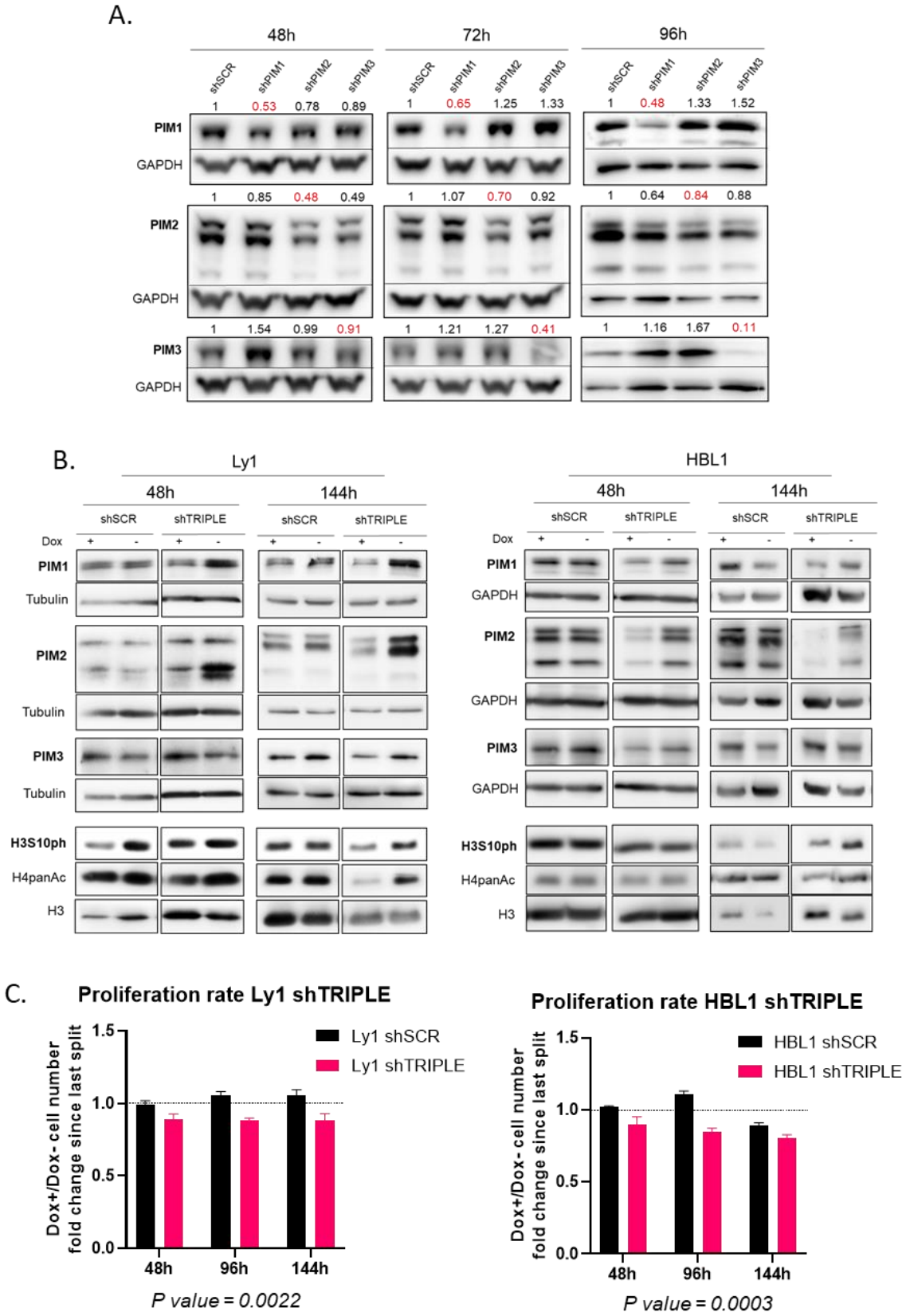

Figure 4.3 PIM kinases compensate for the loss of one another

A. Western blot analysis of PIM kinases levels in single PIM KD.

B. Western blot analysis of PIM kinases levels, and selected histone modification levels in samples with triple KD of PIMs.

C. Proliferation rate of cells with triple PIM knock down. Cells were split every 48h; before and after the split the cells were counted. Fold change of cell numer was calculated for Dox+ and Dox- samples (Dox- = 100%) at each time point. The Dox+/Dox- ratios are shown of the graph. Statistical significance of the difference between „SCR" and „TRIPLE" ratios was calculated with Mann-Whitney test.

In conclusion, PIM1 and PIM3 compensate for the loss of each other, while the knock down of PIM2 induces mild upregulation of PIM1 and PIM3. Moreover, KD of all three PIMs reduces DLBCL proliferation. Therefore, targeting all three PIMs is recommended to achieve a stable effect for functional studies, and for this reason we focused on triple PIM inhibition with the most effective small-molecules SEL24/MEN1703, and PIM447.

4.4 Pan-PIM inhibition reduces interphase, i.e transcription-associated, H3S10ph

In the previous experiment, we observed that chemical inhibition as well as genetic silencing of PIMs reduces global H3S10ph level. Since H3S10ph is especially enriched in mitotic cells [131], the observed reduction of H3S10ph after inhibition or silencing could have been the reflection of PIM-induced G1/S phase arrest [37]. In order to rule out this scenario, DLBCL cell lines DHL4 and HBL1 were treated with thymidine, which blocks cell cycle progression at the G1/S phase checkpoint, followed by a wash with fresh medium, and treated with pan-PIM inhibitors for 2 hours (Figure 4.4A). The compounds declined the level of interphase H3S10ph, which was especially visible for SEL24/MEN1703.

Additionally, H3S10ph abundance was measured in each phase of cell cycle in Ly1 cell line after 6-hour treatment with SEL24/MEN1703 (Figure 4.4B). The results show decrease of overall H3S10ph in cells, as the median intensity of fluorescent signal is generally lower in all cell cycle phases, including G1/S. Therefore, PIMs are responsible for phosphorylation of H3S10 in interphase. In this phase, transcription is the most robust, thus PIMs' epigenetic activity might regulate transcription.

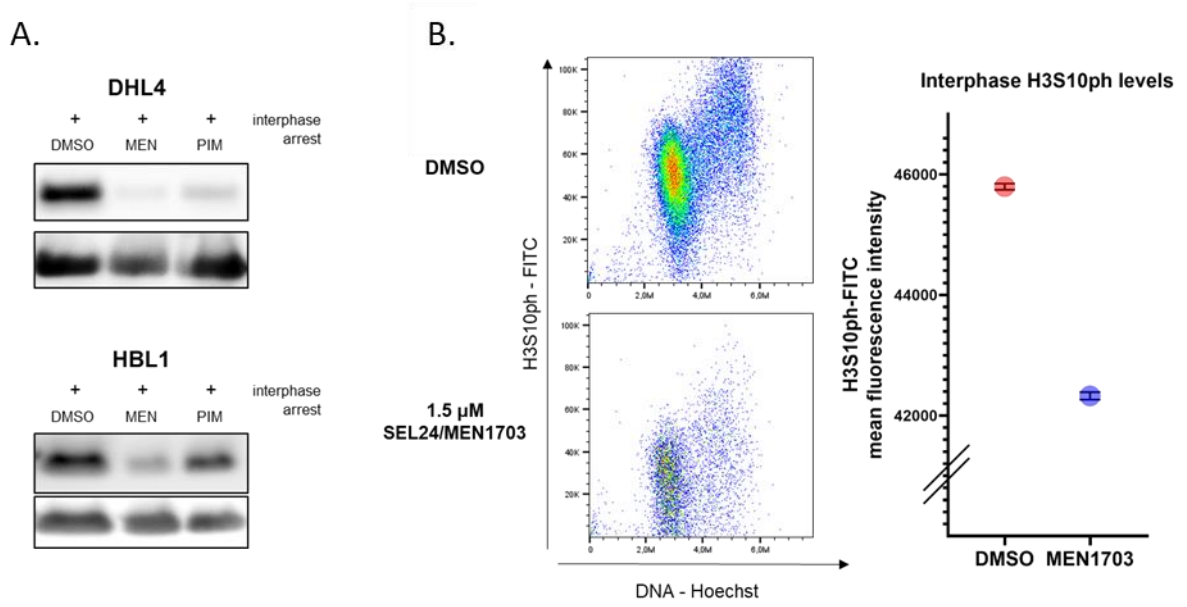

Figure 4.4 Inhibition of PIM causes decrease of interphase H3S10ph levels.
A. Western blot assessment of H3S10ph levels in histones isolated from cultures arrested in G1/S phase by thimidine, and treated with PIM inhibitors for 2 h. MEN=1.5µM SEL24/MEN1703, PIM=7µM PIM447.
B. Assessment of the impact of 6-hour PIM inhibition on H3S10ph levels in cell cyle phases by flow cytometry. Treatment with 1.5µM SEL24/MEN1703 decreases global levels of H3S10ph in all cell cycles phases, including interphase. The graph presents mean fluorescence intensity in the interphase. Error bars represent SEM (standard error of the mean).

4.5 Transcriptional H3S10ph plays a role in cell proliferation and viability

The role of H3S10ph for cell function has not been fully clarified (reviewed in ref. 131). In order to better characterise the significance of H3S10ph in DLBCL biology, I studied the outcomes of introduction of H3S10A mutation, where serine 10 of histone H3 has been substituted with non-phosphorylatable alanine. I first obtained histone H3.3 gene (*H3F3A*) with a FLAG tag, and *H3F3A* with a FLAG tag and S10A mutation introduced through directional mutagenesis in pRetroX plasmid. Histone H3.3 was chosen for this experiment, since it is the most common non-centromeric variant of histone H3, taking part in transcription [170]. The two variants (wild type and the mutant) were cloned into pSFFV, a plasmid with strong SFFV promoter that has been shown to yield particularly high level of expression in haematopoietic cells [171]. Having confirmed plasmid sequences, DHL4 and HBL1 cell lines were infected with pSFFV-*H3F3A*_WT, pSFFV-*H3F3A*_S10A, or empty pSFFV lentiviruses and flow-cytometry-

sorted. The correctness of the sorted populations was then confirmed with flow cytometry and with western blot.

Stable cell lines were then functionally tested. Before the experiment, the cells were synchronised in cell cycle: with thymidine, or by serum starvation. pSFFV-transfected DHL4 (GCB subtype) reacted particularly strongly to the overnight thymidine treatment, which resulted in poor viability. Therefore, this cell line was blocked in cell cycle by overnight starvation, i.e. FBS deprivation. Thymidine treatment of pSFFV-transfected HBL1 (ABC subtype) cells did not show any adverse effects. In turn, this resilient cell line responded too weakly to FBS starvation. Therefore, experimental conditions were adjusted to each cell line.

Proliferation rate was measured with cell counting using flow cytometry every 24 hours after overnight exposure to the cell-cycle-arresting method. Additionally, the cells were stained with 7-aminoactinomycin D (7AAD) to determine the number of live cells. For both cell lines, viable cells with the H3S10A mutation grew significantly slower (Figure 4.5), confirming the important role of H3S10ph in DLBCL proliferation.

Since cells with wild type H3.3 proliferated rapidly, and the proliferation or viability was affected only in the case of H3S10A mutants, these results indicate that H3S10ph deprivation induces changes that impair basic cell functions, resulting in decreased proliferation.

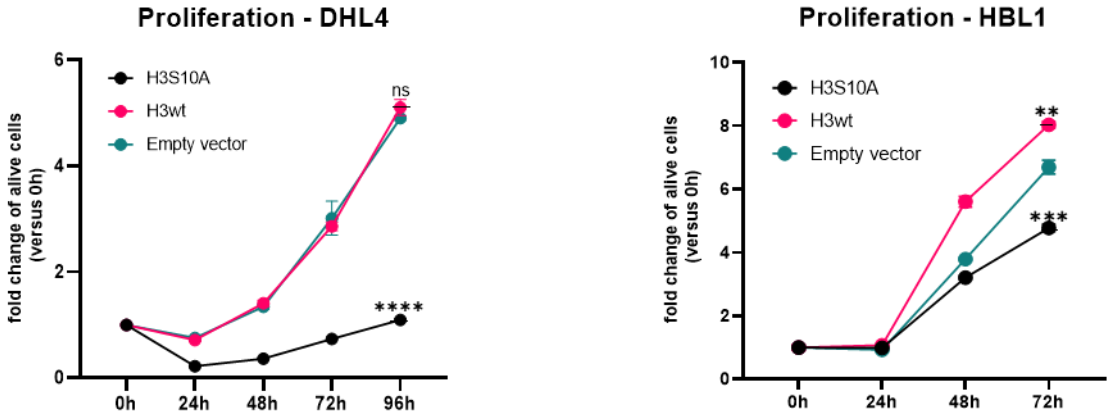

Figure 4.5 DLBCL cell lines expressing non-phosphorylatable histone H3S10A mutant exhibit slower proliferation. Proliferation rate of generated cell lines is expressed as a fold change of number of live cells for each cell line at each time point, versus their respective 0h. Statictical significance was calculated with two-way ANOVA. Comparisons were made with the control „Empty vector" cell lines.

4.6 Pan-PIM inhibition changes global epigenetic landscape and RNAPII phosphorylation status in DLBCL cell lines

We have identified that PIM kinases regulate levels of H3S10ph in the interphase, and that this modification is important for DLBCL proliferation. Histone modifications often operate in combinations and are hierarchical (i.e. one modification entails subsequent ones, forming together so-called "histone code" [172]). H3S10ph's function in epigenetics appears to be particularly convoluted, since it is highly context-dependent [131]. Previous studies demonstrated that at the *FOS1L* promote*r,* H3S10ph cooperates with H3K9ac14ac in 14-3-3 recruitment, which facilitates promoter-tethering of MOF acetyltransferase, acetylating H4K16, leading to subsequent BRD4 engagement, and transcriptional elongation [69]. Since our studies indicate that transcriptional consequences of PIM inhibition partially resemble JQ1 inhibition, we hypothesized that this scenario might be a mechanistic basis of this similarity. For this reason, we assessed the changes in the epigenetic landscape following PIM inhibition. Six cell lines representing GCB and ABC subtypes of DLBCL were treated with different doses of SEL24/MEN1703 for 3h, or 24h, and examined for the abundance of H3S10ph, active chromatin markers: H4panAc, H4K16ac, H3K9acK14 and H3K4me3, and transcription repressive marker – H3K27me3 (Figure 4.6A). The H3K27me3 was used as a control to verify that the effect is specific to active chromatin regions, and not all histone modifications. It is worth noting that the analysis focused on global levels of the modifications, therefore, the distribution at specific *loci* might show greater, or milder changes. Nevertheless, I assume that global alteration in modification levels translates to general epigenetic changes. Moreover, the genomic distribution of selected marks in HBL1 was later assessed by ChIP-Seq.

In most cell lines, pan-PIM inhibition was followed by dose-dependent H3S10ph reduction observable already at 3h, and further reduced at 24h. Other histone modifications did not show evident deregulation at 3h. However, their levels were severely disrupted at 24h, and the changes followed the dose-dependent manner, suggesting that the deficiency of activating modifications is the consequence of H3S10ph downregulation.

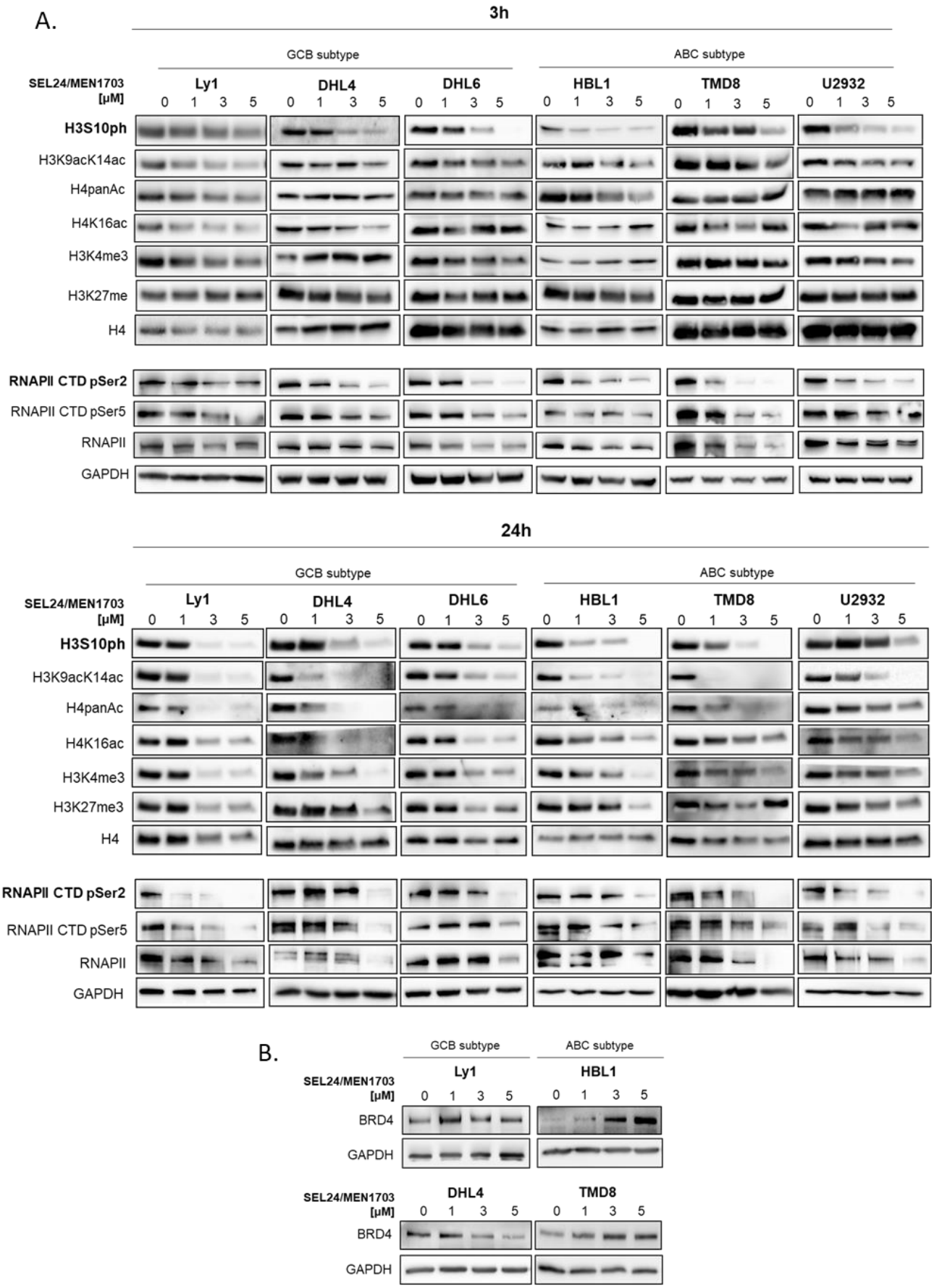

Figure 4.6 Inhibition of PIM changes epigenetic landscape and RNA levels in the cell.

A. Global levels of selected histone modifications and RNAPII CTD phosphorylation status after treatment with SEL24/MEN1703 change in dose-dependent manner.

B. BRD4 levels after 3-hour inhibition of PIM.

Interestingly, RNAPII CTD phosphorylation of Ser2, i.e. the elongation-enabling modification, showed lower levels as soon as at 3h of treatment, which are partially regained at 24h. The only exception is Ly1 cell line, which exhibits dramatic loss of Ser2-ph only at 24h. Phosphorylation of Ser5 remained at similar levels throughout the experiment.

The epigenetic screening identified reduction in acetylated histones, which form a binding platform for BRD4. Given our hypothesis that PIMs induce transcription at least in part *via* BRD4, levels of this protein were assessed after PIM inhibition (Figure 4.6B) to confirm that the observed effect could be attributed to interactions between the proteins, and not the downregulation of BRD4. For GCB subtype cell lines, BRD4 expression remained virtually stable at all doses at 3h. Interestingly, PIM inhibition upregulates BRD4 expression in ABC cell lines, suggesting a likely compensatory mechanism in response to PIM- blocked transcription.

4.7 Pan-PIM inhibition causes reduction in H3K27ac levels at enhancers, and reduction in H3K9ac at transcription start sites (TSS), leading to transcriptional downregulation

4.7.1 Inhibition of PIM reduces the density of activating epigenetic marks at regulatory regions

Given the profound and early decrease of H3S10ph in HBL1 cells, this line was used to perform ChIP-Seq to identify genomic regions that change their histone modification abundance after 3-hour PIM inhibition with 1.5 μM SEL24/MEN1703. We focused on the identification of the active chromatin mark H3K27ac at enhancers (including SEs), and the active promoter mark H3K9ac in the proximity of transcription start sites (TSS).

After 3h of treatment, there was a general decrease in H3K27ac levels at enhancers (Figures 4.7A and 4.7B). Since PIM kinases potentially cooperate with BRD4 - the key protein of SEs, we identified SEs in our control DMSO dataset using the ROSE (Rank Ordering of Super-Enhancers) algorithm for SE detection [139], based on the abundance of H3K27ac (Figure 4.7C). 582 regions were rendered as SEs, including the enhancers of proteins like DAD1 (Defender Against cell Death 1), DLL3 (Delta Like Canonical Notch Ligand 3), BCL9L (B-cell CLL/lymphoma

9 Like) or CXCR5 (C-X-C chemokine receptor type 5, also known as Burkitt lymphoma receptor 1). We then investigated how H3K27ac abundance changes specifically at the SEs in response to SEL24/MEN1703 (Figure 4.7D). PIM inhibition caused a generally modest, but significant decrease in H3K27ac level in these regions. Apparently, there are SEs that drastically reduce their H3K27ac load, while some SEs are not affected by PIM inhibition. When scrutinising the genomic distribution of the mark (Figure 4.7E), we noticed that the locations of the marks were usually similar for treated (SEL24/MEN1703, red tracks) and untreated (DMSO, blue tracks) samples, but the coverage was decidedly lower for the former.

We also characterised the level of H3K9ac at promoters (near TSS; Figure 4.7F, 4.7G). Noteworthy, acetylation of H3K9 at promoters has been described as a switch from transcription initiation to elongation phase [173], which is exactly the process that we hypothesise PIMs regulate - according to the literature, but also to the results of RNAPII CTD phosphorylation screening presented earlier in this work (Figure 4.6A). In line with this hypothesis, we noted a significant decrease of H3K9ac at TSS (Figure 4.7E).

4.7.2 Epigenetic changes induced by PIM inhibition influence gene expression

Collectively, weaker acetylation at promoters and enhancers following PIM inhibition likely translates to decreased gene expression. To formally test this hypothesis, we performed RNA sequencing (RNA-Seq) in HBL1 cell line and juxtaposed the results with the ChIP-Seq results.

The cells were treated with 1.5 µM SEL24/MEN1703, or DMSO, for 3h. Deregulated genes were identified between PIM inhibitor-treated and DMSO-treated samples. The analysis showed over 11 times more downregulated than upregulated genes, precisely: 854 downregulated, and 75 upregulated genes (Figure 4.8A). This observation confirms that PIMs play a major role in active transcription. We also evaluated if genes controlled by TEs or SEs are differently affected. Although SE-regulated genes exhibited universal downregulation, the effect was even stronger in the case of genes regulated by TEs (Figure 4.8B). For this reason, we did not separate the SE-regulated group in the integrative analysis. Extended analysis of the RNA-Seq results is presented in chapter 4.8.

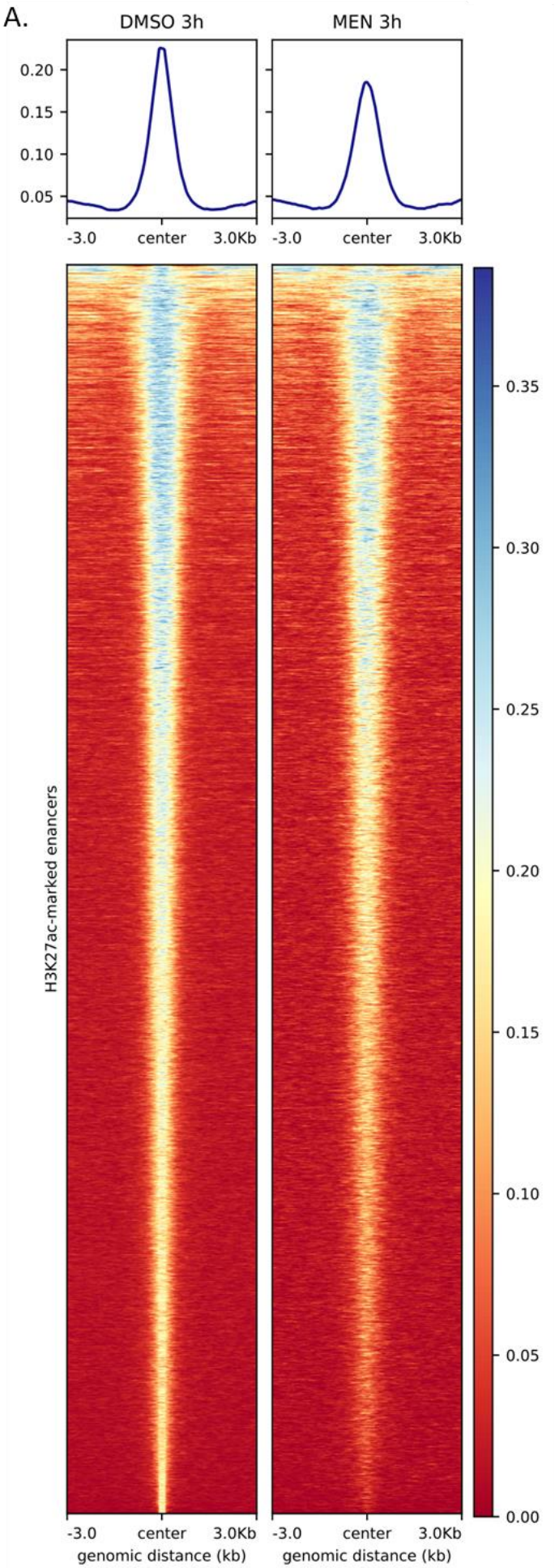
A.
DMSO 3h
MEN 3h
0.20
0.15
0.10
0.05
-3.0
center
3.0Kb
H3K27ac-marked enancers
0.35
0.30
0.25
0.20
0.15
0.10
0.05
0.00
genomic distance (kb)

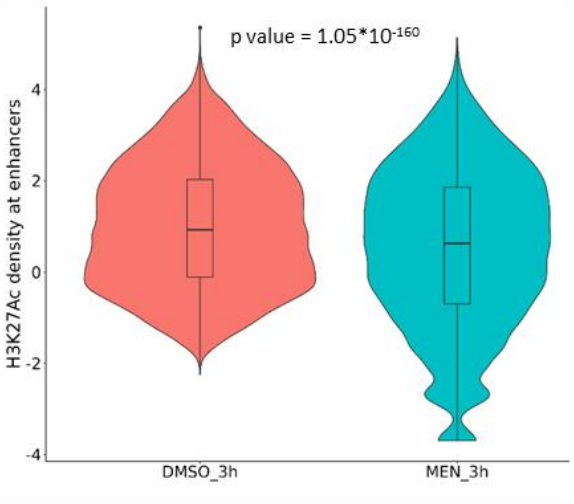
B.
p value = 1.05*10-160
H3K27Ac density at enhancers
4
2
0
-2
-4
DMSO_3h
MEN_3h

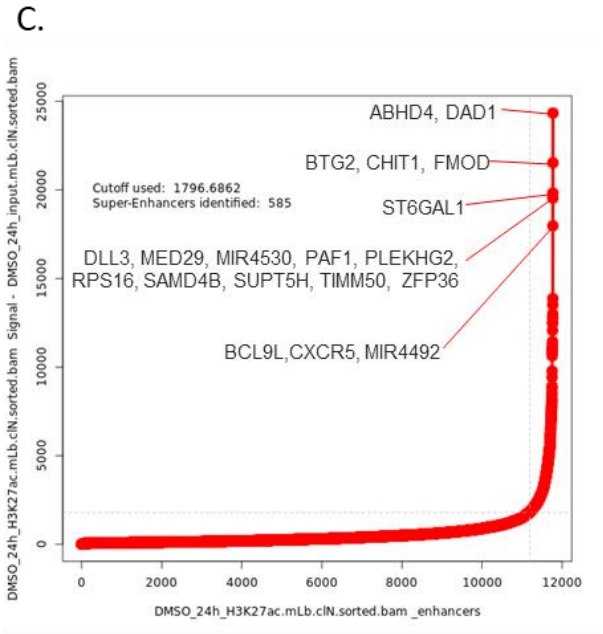
C.
ABHD4, DAD1
BTG2, CHIT1, FMOD
Cutoff used: 1796.6862
Super-Enhancers identified: 585
ST6GAL1
DLL3, MED29, MIR4530, PAF1, PLEKHG2,
RPS16, SAMD4B, SUPT5H, TIMM50, ZFP36
BCL9L,CXCR5, MIR4492
DMSO_24h_H3K27ac.mLb.clN.sorted.bam Signal - DMSO_24h_input.mLb.clN.sorted.bam
25000
20000
15000
10000
5000
0
0
2000
4000
6000
8000
10000
12000
DMSO_24h_H3K27ac.mLb.clN.sorted.bam _enhancers

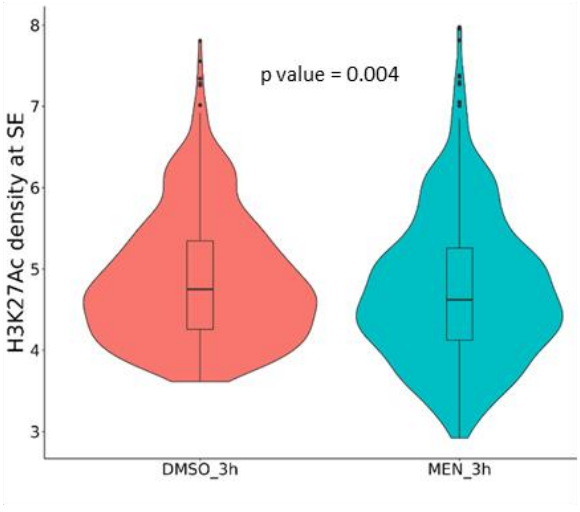
D.
p value = 0.004
H3K27Ac density at SE
8
7
6
5
4
3
DMSO_3h
MEN_3h

E.

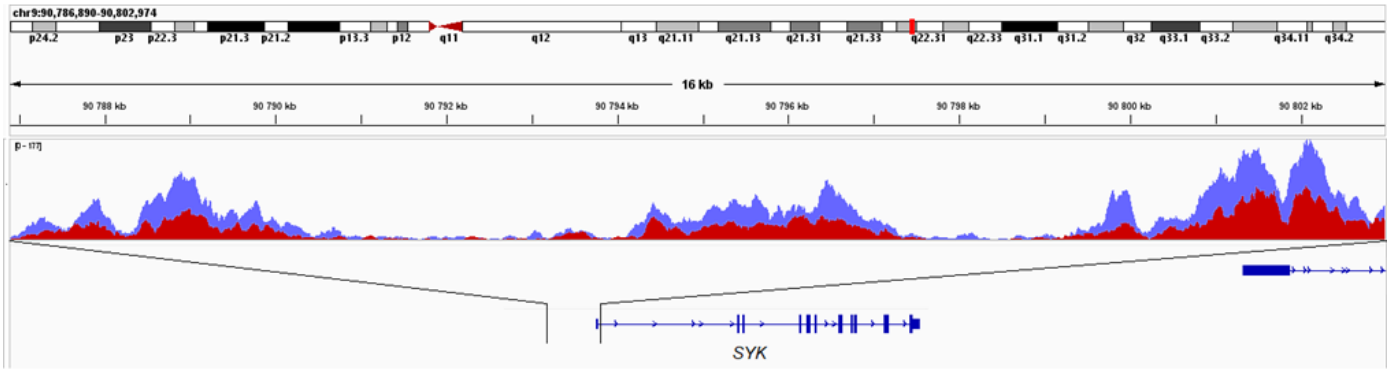
chr9:90,786,890-90,802,974
16 kb
SYK

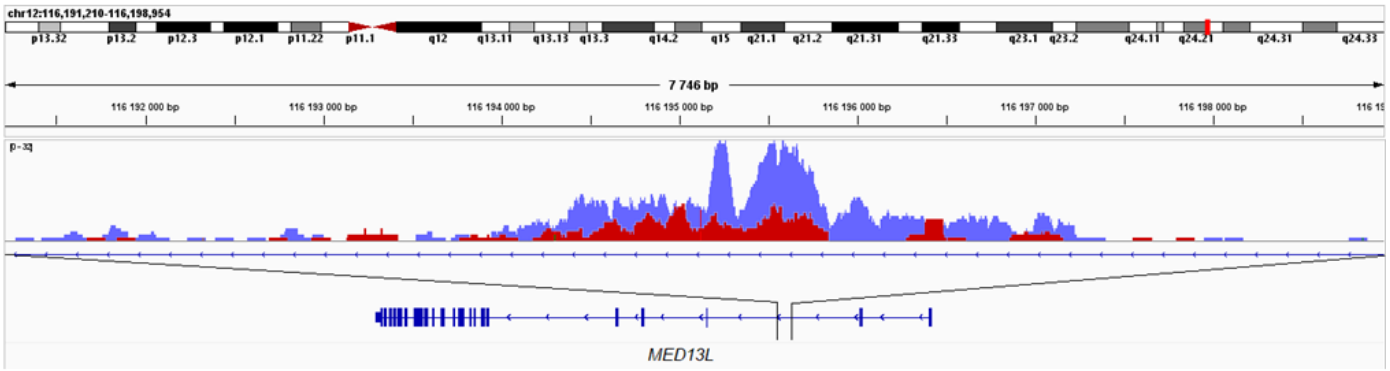
chr12:116,191,210-116,198,954
7 746 bp
MED13L

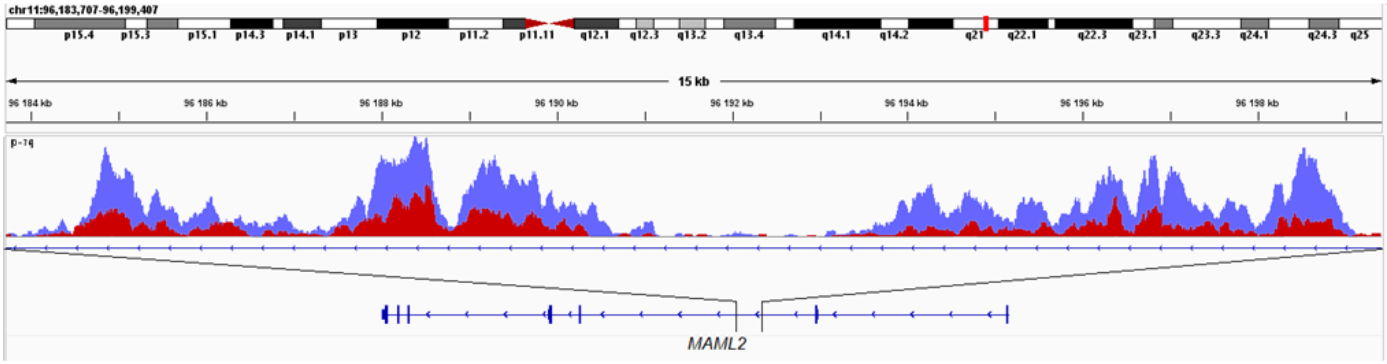
chr11:96,183,707-96,199,407
15 kb
MAML2

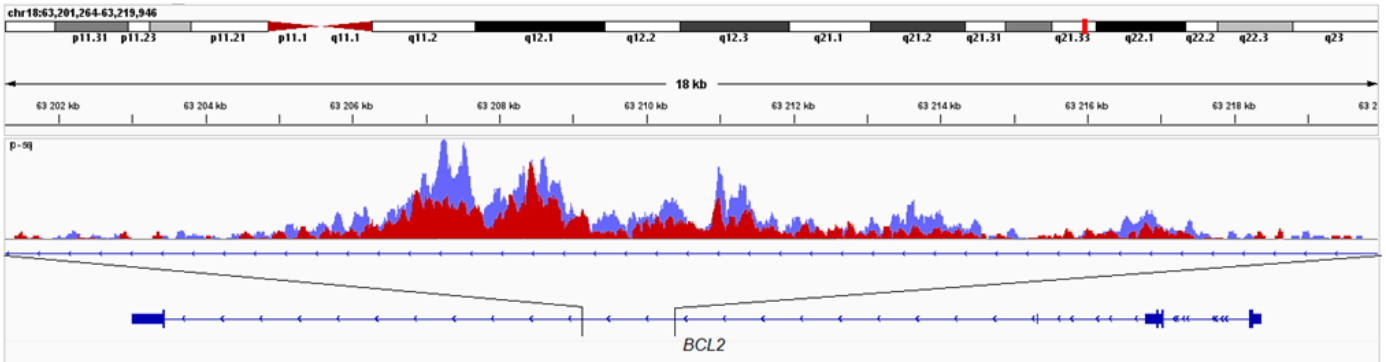
chr18:63,201,264-63,219,946
18 kb
BCL2

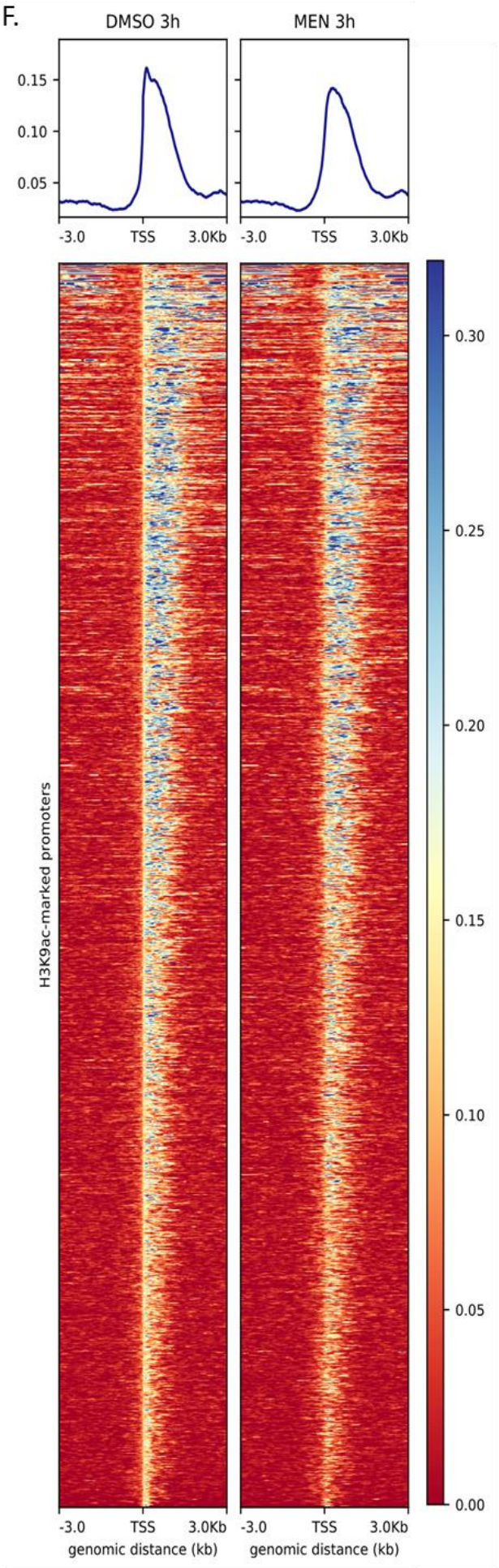

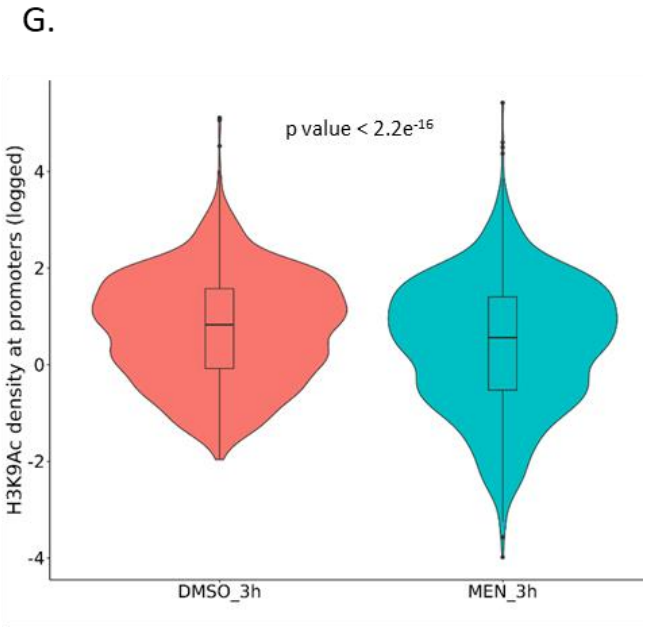

Figure 4.7. 3-hour inhibition of PIM with 1.5 µM SEL24/MEN1703 decreases H3K27ac at enhancers and SEs, and H3K9ac at TSS.

A. Heatmap of H3K27ac coverage of enhnacers.
B. Violin plots showing H3K27ac density at all enahncers in control cells (DMSO) and PIM-inhibitor-treated cells (MEN = SEL24/MEN1703).
C. Diagram showing the result of ROSE identification of SEs in HBL1. Genes in proximity of the top 5 SEs are listed.
D. Violin plots showing H3K27ac density at SE only in control and PIM-inhibitor-treated cells.
E. Representative genome browser overlay tracks of read coverage profiles of H3K27ac. Blue tracks = DMSO, red tracks = SEL24/MEN1703.
F. Heatmap of H3K9ac at promoters.
G. Violin plot showing H3K9ac density at promoters.

Finally, we integrated the epigenetic and transcriptional data. Changes in H3K27ac load at enhancers (both SEs and TEs) after SEL24/MEN1703 treatment were juxtaposed with transcriptional changes (Figure 4.8C). As expected, the majority of genes exhibited lower expression and weaker H3K27ac density at enhancers. We analysed enriched pathways among the genes with downregulated expression and poorer epigenetic activation (Figure 4.8D). Interestingly, many pathways were associated with RNA metabolism or TF binding, suggesting that PIM regulate transcription on multiple levels: not only through the canonical modification of TFs, but also the modulation of RNAPII CTD phosphorylation, and, finally, epigenetic regulation of expression of genes involved in RNA synthesis. Other largely represented groups of genes were associated with chromatin, regulation of apoptosis, or DNA damage. Given that PIMs are known to interact with multiple TFs, we additionally assessed whether the downregulated genes are orchestrated by a common TF (Figure 4.8E). Among the top results there were MYC and MYC-MAX, for which the mechanism of PIM-dependent epigenetic activation of target genes was previously described [37,69]. However, the analysis identified more TFs, including the ones known to interact with PIM, but without any known epigenetic mechanism, such as Hif-1 [174]. Other examples include TFs from the E2F family, which participate in DNA damage response pathway [175]. Interestingly, YY1 binding sites also showed weaker epigenetic activation. YY1 occupies active promoters and enhancers, including SEs, and facilitates their interactions through formation of loops [176,177]. We can therefore conjecture that PIMs potentially regulate chromatin conformation by activation of sites recognised by chromatin modellers, like YY1. This hypothetical mechanism might be another mode of regulation of expression SE-dependent genes.

These results may indicate that there are more TFs (other than MYC-MAX) that recruit PIM to the chromatin to phosphorylate H3S10 for epigenetic activation at enhancers. Since PIMs do not have a DNA-binding domain (PROSITE [178]), it is probable that the formation of complexes with TFs is the main mode of PIM recruitment to the chromatin.

We also examined which genes were the most affected by epigenetic changes in response to PIM inhibition (Figure 4.8F). The analysis identified numerous genes such as: *BCL2, BCL6, AICDA* (AID), *CCND2, MDM2, FANCC, FANCF,* as well as genes coding epigenetic proteins: *KDM2A, KDM2B, KDM6A, KDM8, KAT5* (Tip60), *PRMT6* and numerous TFs. Interestingly, many of these genes encode proteins that interact with PIMs (e.g. MDM2, RUNX2, SMAD3, CDC25A),

therefore, not only do PIMs regulate their activity, but also their expression, and thus control cell function.

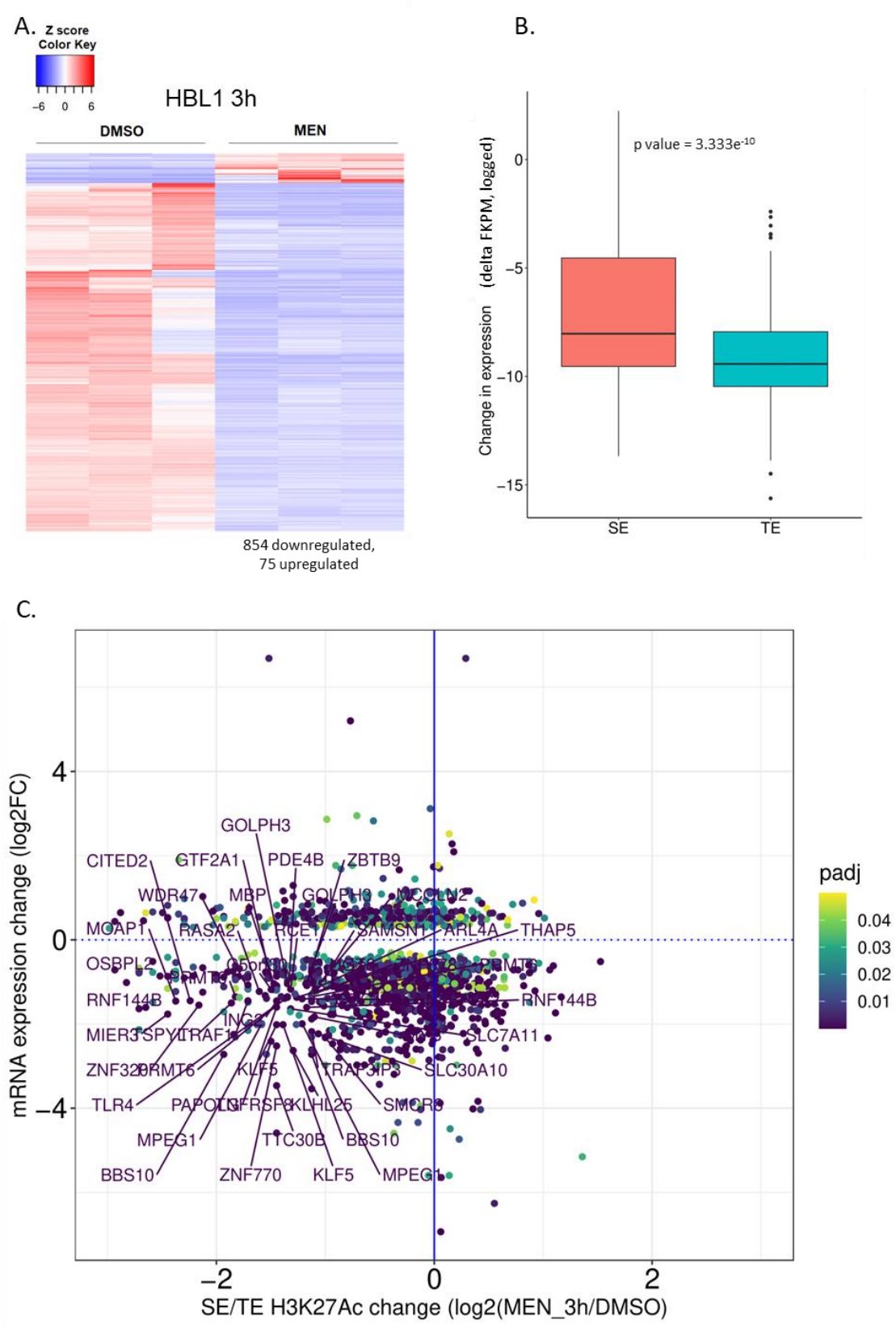

D.

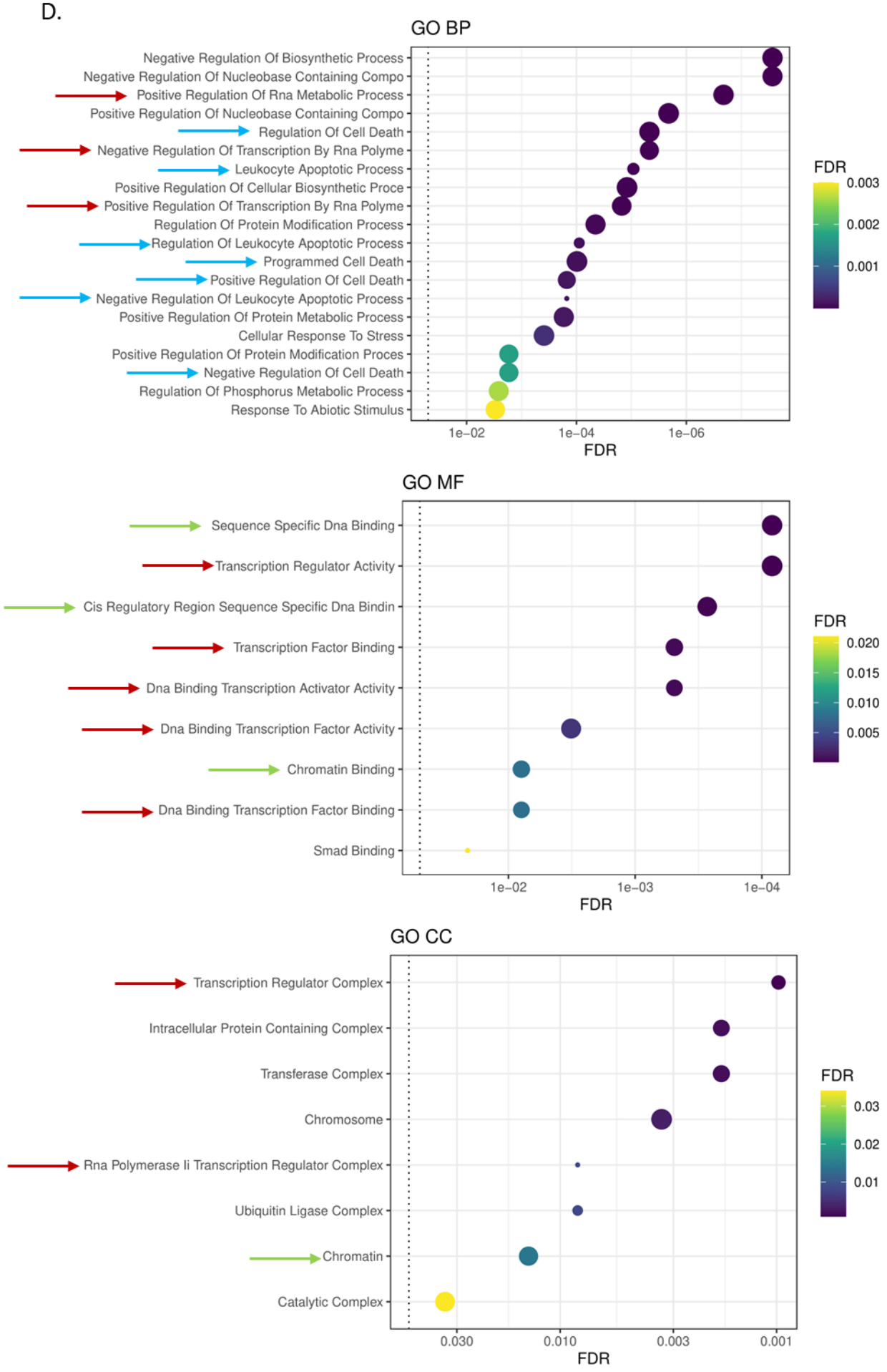
GO BP
Negative Regulation Of Biosynthetic Process
Negative Regulation Of Nucleobase Containing Compo
Positive Regulation Of Rna Metabolic Process
Positive Regulation Of Nucleobase Containing Compo
Regulation Of Cell Death
Negative Regulation Of Transcription By Rna Polyme
Leukocyte Apoptotic Process
Positive Regulation Of Cellular Biosynthetic Proce
Positive Regulation Of Transcription By Rna Polyme
Regulation Of Protein Modification Process
Regulation Of Leukocyte Apoptotic Process
Programmed Cell Death
Positive Regulation Of Cell Death
Negative Regulation Of Leukocyte Apoptotic Process
Positive Regulation Of Protein Metabolic Process
Cellular Response To Stress
Positive Regulation Of Protein Modification Proces
Negative Regulation Of Cell Death
Regulation Of Phosphorus Metabolic Process
Response To Abiotic Stimulus
1e−02
1e−04
1e−06
FDR
FDR
0.003
0.002
0.001
GO MF
Sequence Specific Dna Binding
Transcription Regulator Activity
Cis Regulatory Region Sequence Specific Dna Bindin
Transcription Factor Binding
Dna Binding Transcription Activator Activity
Dna Binding Transcription Factor Activity
Chromatin Binding
Dna Binding Transcription Factor Binding
Smad Binding
1e−02
1e−03
1e−04
FDR
FDR
0.020
0.015
0.010
0.005
GO CC
Transcription Regulator Complex
Intracellular Protein Containing Complex
Transferase Complex
Chromosome
Rna Polymerase Ii Transcription Regulator Complex
Ubiquitin Ligase Complex
Chromatin
Catalytic Complex
0.030
0.010
0.003
0.001
FDR
FDR
0.03
0.02
0.01

D. *continued*

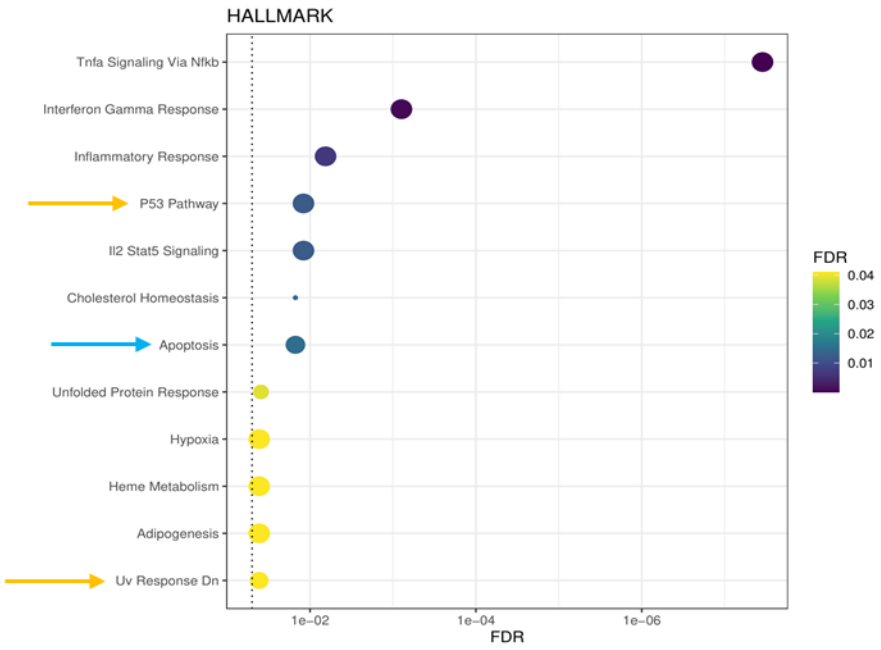

E.

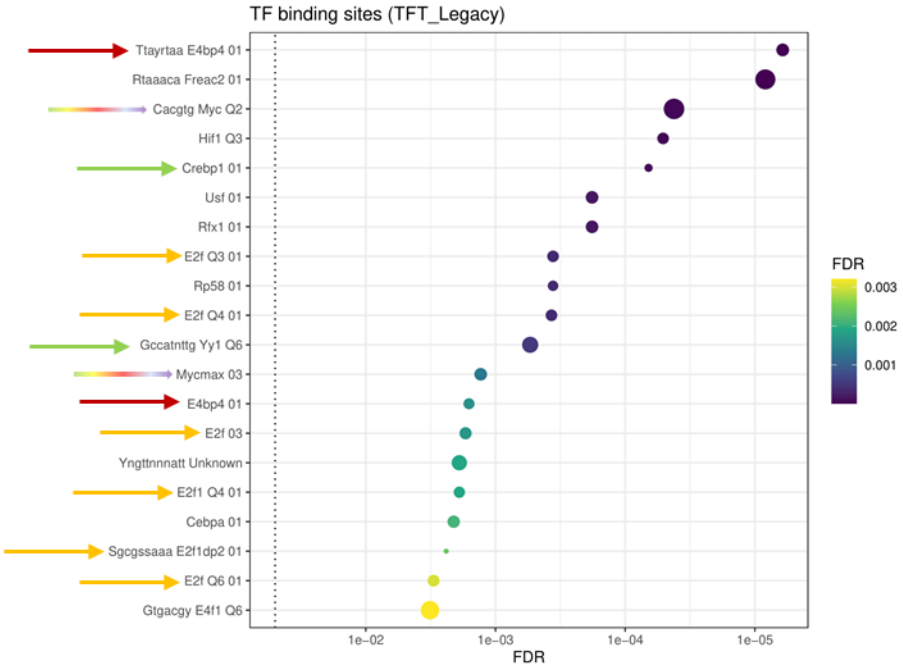

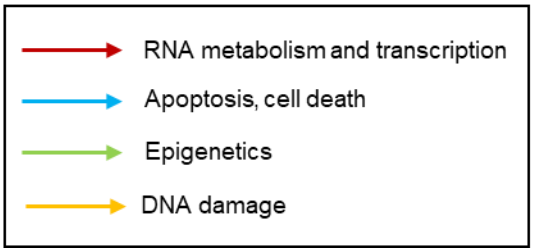

F.

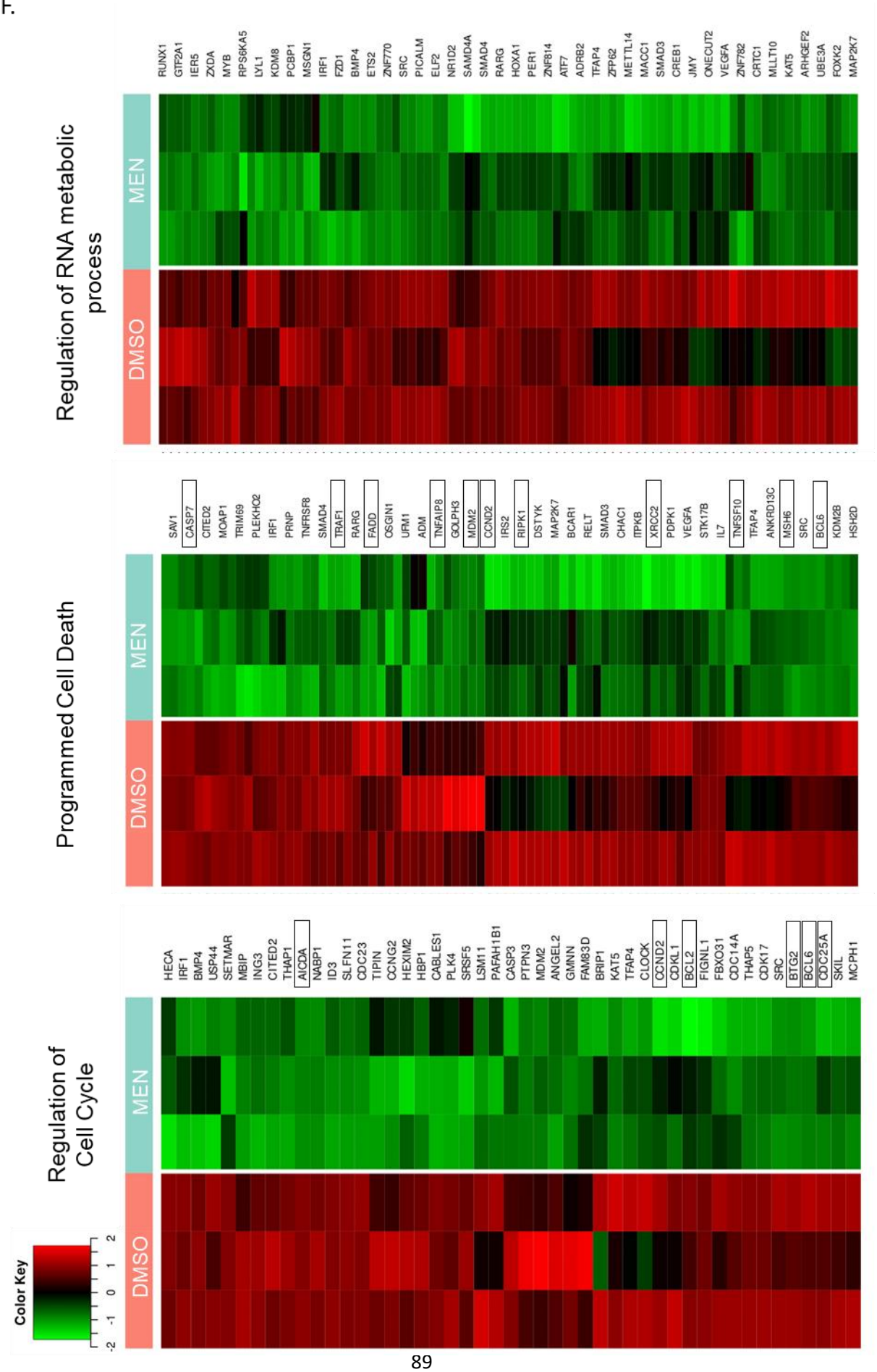
Color Key
-2 -1 0 1 2
Regulation of Cell Cycle
DMSO
MEN
HECA
IRF1
BMP4
USP44
SETMAR
MBIP
ING3
CITED2
THAP1
AICDA
NABP1
ID3
SLFN11
CDC23
TIPIN
CCNG2
HEXIM2
HBP1
CABLES1
PLK4
SRSF5
LSM11
PAFAH1B1
CASP3
PTPN3
MDM2
ANGEL2
GMNN
FAM83D
BRIP1
KAT5
TFAP4
CLOCK
CCND2
CDKL1
BCL2
FIGNL1
FBXO31
CDC14A
THAP5
CDK17
SRC
BTG2
BCL6
CDC25A
SKIL
MCPH1
Programmed Cell Death
DMSO
MEN
SAV1
CASP7
CITED2
MOAP1
TRIM69
PLEKHO2
IRF1
PRNP
TNFRSF8
SMAD4
TRAF1
RARG
FADD
OSGIN1
URM1
ADM
TNFAIP8
GOLPH3
MDM2
CCND2
IRS2
RIPK1
DSTYK
MAP2K7
BCAR1
RELT
SMAD3
CHAC1
ITPKB
XRCC2
PDPK1
VEGFA
STK17B
IL7
TNFSF10
TFAP4
ANKRD13C
MSH6
SRC
BCL6
KDM2B
HSH2D
Regulation of RNA metabolic process
DMSO
MEN
RUNX1
GTF2A1
IER5
ZXDA
MYB
RPS6KA5
LYL1
KDM8
PCBP1
MSGN1
IRF1
FZD1
BMP4
ETS2
ZNF770
SRC
PICALM
ELF2
NR1D2
SAMD4A
SMAD4
RARG
HOXA1
PER1
ZNF814
ATF7
ADRB2
TFAP4
ZFP62
METTL14
MACC1
SMAD3
CREB1
JMY
ONECUT2
VEGFA
ZNF782
CRTC1
MLLT10
KAT5
ARHGEF2
UBE3A
FOXK2
MAP2K7

F. *continued*

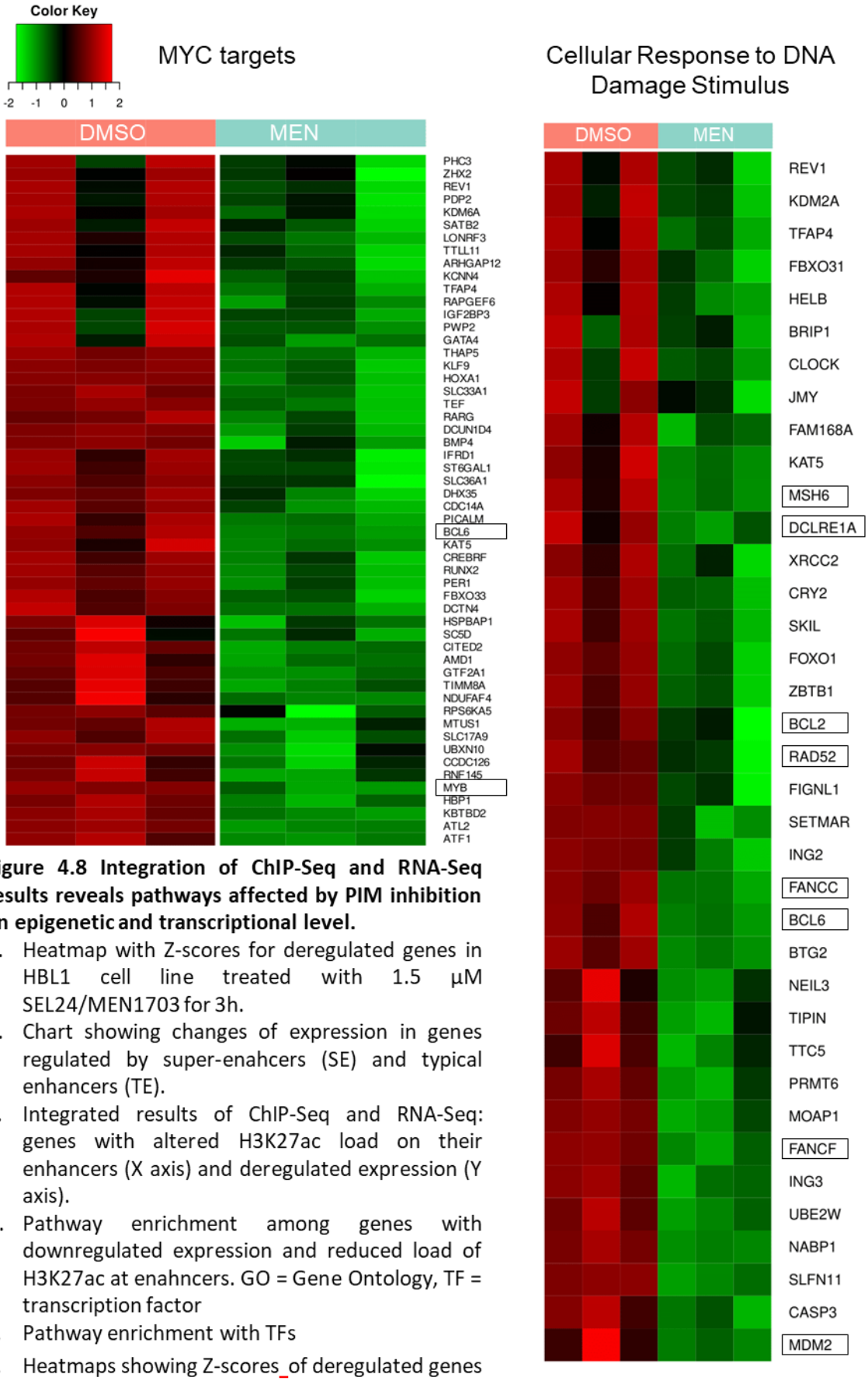

Figure 4.8 Integration of ChIP-Seq and RNA-Seq results reveals pathways affected by PIM inhibition on epigenetic and transcriptional level.

A. Heatmap with Z-scores for deregulated genes in HBL1 cell line treated with 1.5 µM SEL24/MEN1703 for 3h.
B. Chart showing changes of expression in genes regulated by super-enahcers (SE) and typical enhancers (TE).
C. Integrated results of ChIP-Seq and RNA-Seq: genes with altered H3K27ac load on their enhancers (X axis) and deregulated expression (Y axis).
D. Pathway enrichment among genes with downregulated expression and reduced load of H3K27ac at enahncers. GO = Gene Ontology, TF = transcription factor
E. Pathway enrichment with TFs
F. Heatmaps showing Z-scores of deregulated genes within selected pathways identified in GO pathway enrichment. Selected genes important for the given function are framed.

4.8 Transcriptional analysis of PIM-inhibitor-treated DLBCL cells confirms PIM's involvement is vast regulation of transcription

4.8.1 Transcriptional analysis of four DLBCL cell lines reveals common pathways deregulated by PIM inhibition

Integration of ChIP-Seq and RNA-Seq data confirmed that PIM inhibition induces epigenetic changes that are coupled with impaired expression of the related genes. In order to examine the extent of transcriptional changes in other DLBCL cell lines, we performed RNA-Seq with additional DLBCL cell lines: Ly1 and DHL4 of the GCB subtype, and TMD8 of the ABC subtype, treated with 1.5 µM SEL24/MEN1703 for 3h.

Deregulated genes were identified among PIM inhibitor-treated and DMSO-treated pairs for each cell line. At 3h, majority of genes were downregulated for all cell lines (Figure 4.9A); respectively downregulated and upregulated: 1870 and 389 for Ly1, 2292 and 239 for DHL4, 854 and 75 for HBL1, and 1733 and 317 for TMD8. The fact that all of the studied cell lines show prevailing downregulation of expression is in perfect agreement with the hypothesis that PIMs play a major role in transcription activation.

In order to investigate which pathways were the most affected by PIM inhibition at each stage of treatment, we performed Gene Ontology (GO) term enrichment. Similarly to the previously obtained results for HBL1, at 3h, the majority of the deregulated pathways in all cell lines affected RNA metabolism (Figure 4.9B and C). Remarkably, PIM inhibition affects the expression of genes involved in biogenesis and processing of not only mRNA, but also non-coding RNA (ncRNA), as well as tRNA, rRNA, and mitochondrial RNA.

DNA damage response was identified as PIM-dependent in the previous epigenetic screen in HBL1. We therefore investigated if pathways connected with this process were affected also in other DLBCL cell lines (Figure 4.9D). The analysis confirmed that genes involved in DNA repair were deregulated upon PIM inhibition in all studied cell lines. Moreover, genes associated with double-strand break repair were particularly enriched, suggesting that PIM kinases participate in response to this kind of DNA damage.

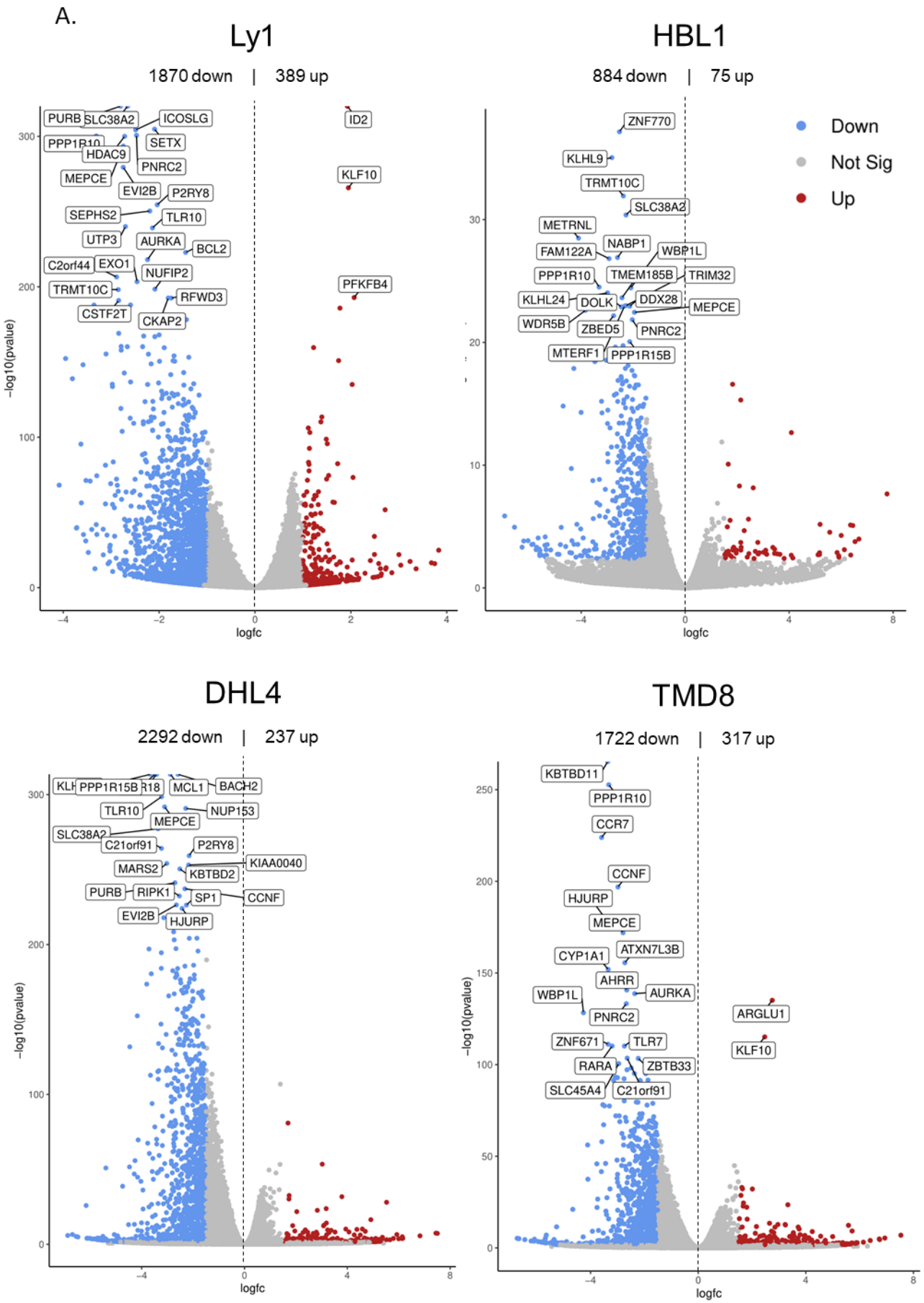
A.
Ly1
1870 down | 389 up
HBL1
884 down | 75 up
DHL4
2292 down | 237 up
TMD8
1722 down | 317 up
Down
Not Sig
Up
−log10(pvalue)
logfc
PURB
SLC38A2
ICOSLG
PPP1R10
SETX
HDAC9
PNRC2
MEPCE
EVI2B
P2RY8
SEPHS2
TLR10
UTP3
AURKA
BCL2
C2orf44
EXO1
NUFIP2
TRMT10C
RFWD3
CSTF2T
CKAP2
ID2
KLF10
PFKFB4
ZNF770
KLHL9
TRMT10C
SLC38A2
METRNL
NABP1
WBP1L
FAM122A
PPP1R10
TMEM185B
TRIM32
KLHL24
DOLK
DDX28
MEPCE
WDR5B
ZBED5
PNRC2
MTERF1
PPP1R15B
MCL1
BACH2
TLR10
NUP153
MEPCE
SLC38A2
C21orf91
P2RY8
MARS2
KBTBD2
KIAA0040
PURB
RIPK1
SP1
CCNF
EVI2B
HJURP
KBTBD11
PPP1R10
CCR7
CCNF
HJURP
MEPCE
ATXN7L3B
CYP1A1
AHRR
WBP1L
AURKA
PNRC2
ARGLU1
ZNF671
TLR7
KLF10
RARA
ZBTB33
SLC45A4
C21orf91

B.

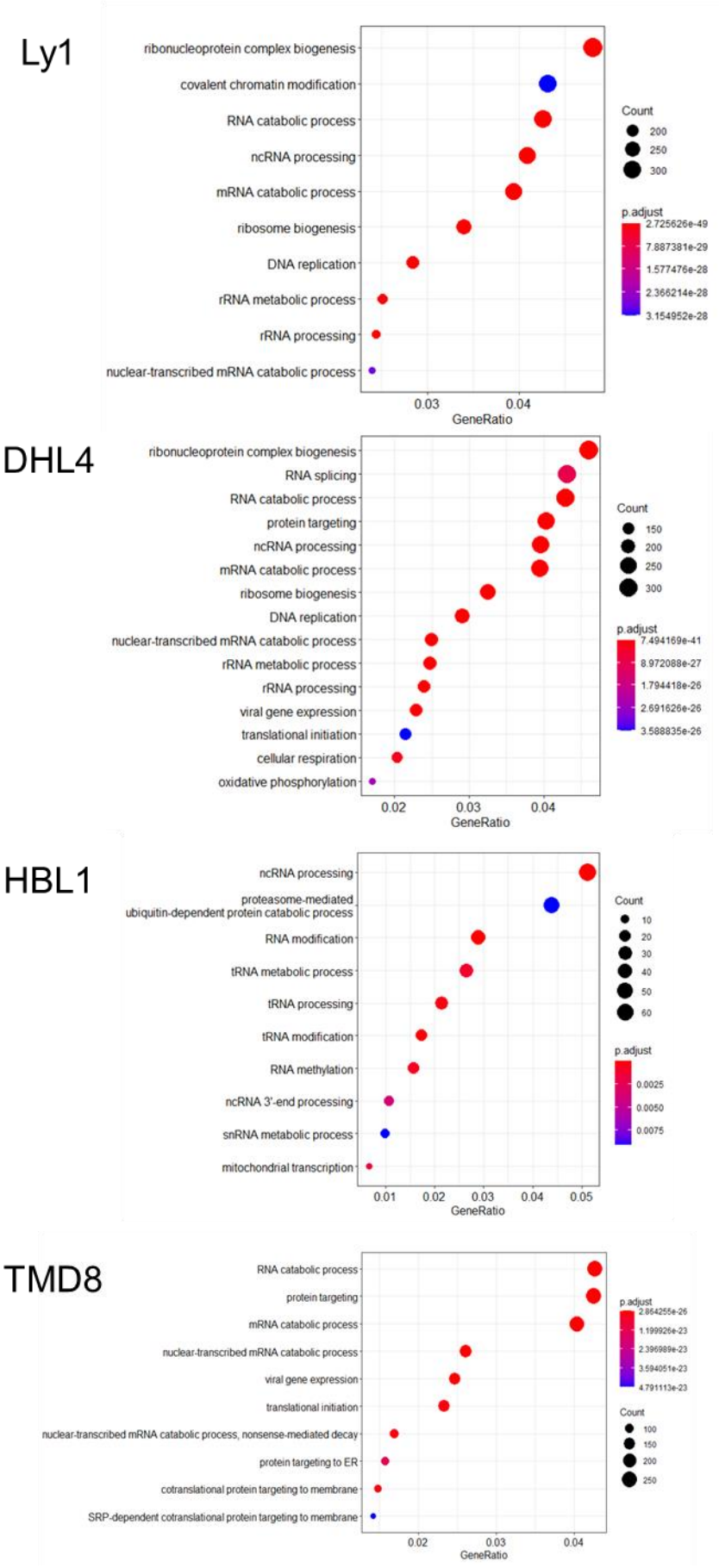
Ly1
ribonucleoprotein complex biogenesis
covalent chromatin modification
RNA catabolic process
ncRNA processing
mRNA catabolic process
ribosome biogenesis
DNA replication
rRNA metabolic process
rRNA processing
nuclear-transcribed mRNA catabolic process
0.03
0.04
GeneRatio
Count
200
250
300
p.adjust
2.725626e-49
7.887381e-29
1.577476e-28
2.366214e-28
3.154952e-28
DHL4
ribonucleoprotein complex biogenesis
RNA splicing
RNA catabolic process
protein targeting
ncRNA processing
mRNA catabolic process
ribosome biogenesis
DNA replication
nuclear-transcribed mRNA catabolic process
rRNA metabolic process
rRNA processing
viral gene expression
translational initiation
cellular respiration
oxidative phosphorylation
0.02
0.03
0.04
GeneRatio
Count
150
200
250
300
p.adjust
7.494169e-41
8.972088e-27
1.794418e-26
2.691626e-26
3.588835e-26
HBL1
ncRNA processing
proteasome-mediated ubiquitin-dependent protein catabolic process
RNA modification
tRNA metabolic process
tRNA processing
tRNA modification
RNA methylation
ncRNA 3'-end processing
snRNA metabolic process
mitochondrial transcription
0.01
0.02
0.03
0.04
0.05
GeneRatio
Count
10
20
30
40
50
60
p.adjust
0.0025
0.0050
0.0075
TMD8
RNA catabolic process
protein targeting
mRNA catabolic process
nuclear-transcribed mRNA catabolic process
viral gene expression
translational initiation
nuclear-transcribed mRNA catabolic process, nonsense-mediated decay
protein targeting to ER
cotranslational protein targeting to membrane
SRP-dependent cotranslational protein targeting to membrane
0.02
0.03
0.04
GeneRatio
p.adjust
2.864255e-26
1.199926e-23
2.396989e-23
3.594051e-23
4.791113e-23
Count
100
150
200
250

C.

Ly1

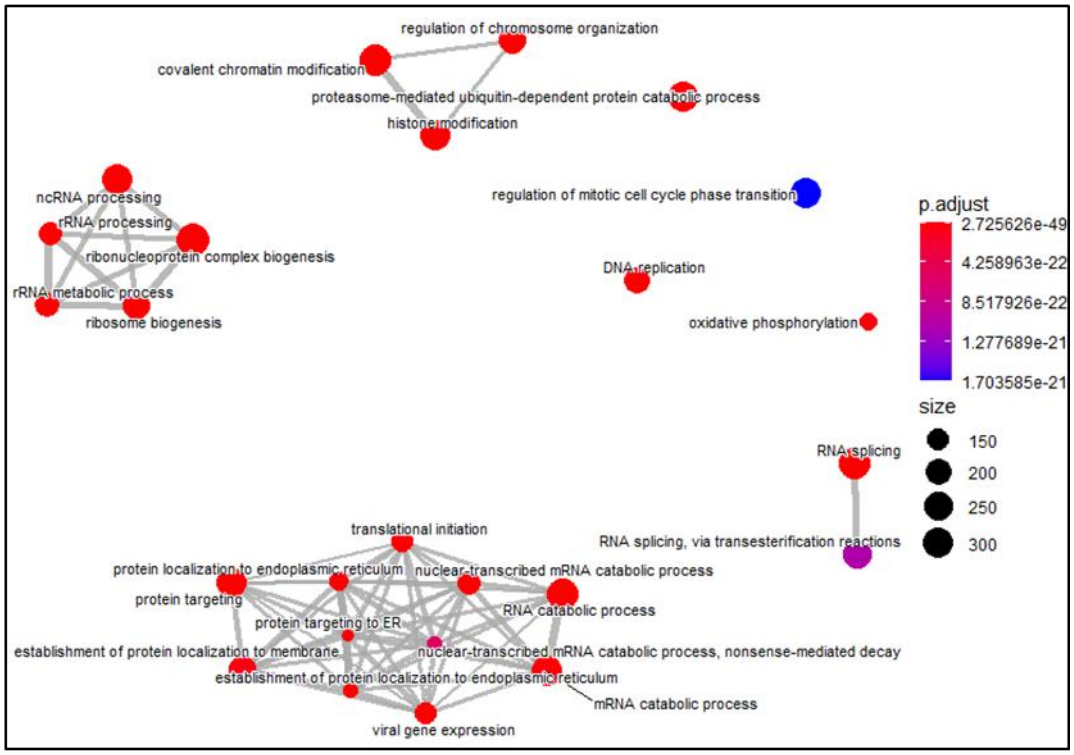
regulation of chromosome organization
covalent chromatin modification
proteasome-mediated ubiquitin-dependent protein catabolic process
histone modification
ncRNA processing
rRNA processing
ribonucleoprotein complex biogenesis
rRNA metabolic process
ribosome biogenesis
regulation of mitotic cell cycle phase transition
DNA replication
oxidative phosphorylation
RNA splicing
RNA splicing, via transesterification reactions
translational initiation
protein localization to endoplasmic reticulum
nuclear-transcribed mRNA catabolic process
protein targeting
RNA catabolic process
protein targeting to ER
establishment of protein localization to membrane
nuclear-transcribed mRNA catabolic process, nonsense-mediated decay
establishment of protein localization to endoplasmic reticulum
mRNA catabolic process
viral gene expression
p.adjust
2.725626e-49
4.258963e-22
8.517926e-22
1.277689e-21
1.703585e-21
size
150
200
250
300

DHL4

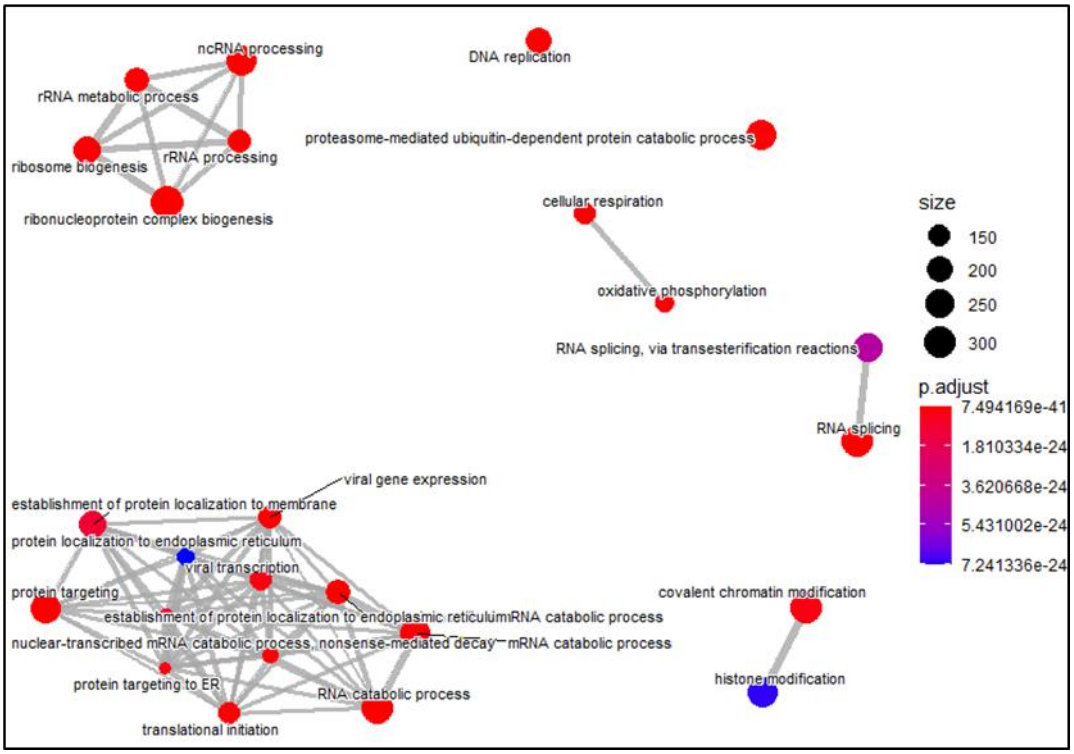
ncRNA processing
DNA replication
rRNA metabolic process
proteasome-mediated ubiquitin-dependent protein catabolic process
ribosome biogenesis
rRNA processing
ribonucleoprotein complex biogenesis
cellular respiration
oxidative phosphorylation
RNA splicing, via transesterification reactions
RNA splicing
viral gene expression
establishment of protein localization to membrane
protein localization to endoplasmic reticulum
viral transcription
protein targeting
establishment of protein localization to endoplasmic reticulumRNA catabolic process
nuclear-transcribed mRNA catabolic process, nonsense-mediated decay
mRNA catabolic process
covalent chromatin modification
protein targeting to ER
RNA catabolic process
histone modification
translational initiation
size
150
200
250
300
p.adjust
7.494169e-41
1.810334e-24
3.620668e-24
5.431002e-24
7.241336e-24

C. *continued*

HBL1

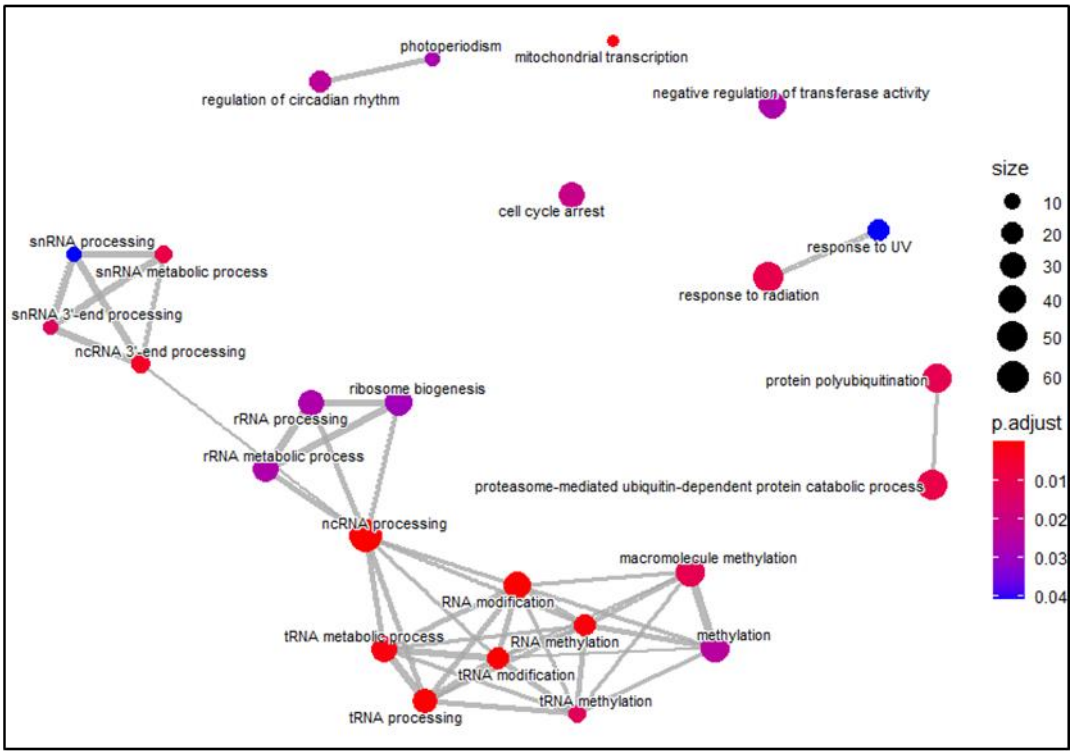

TMD8

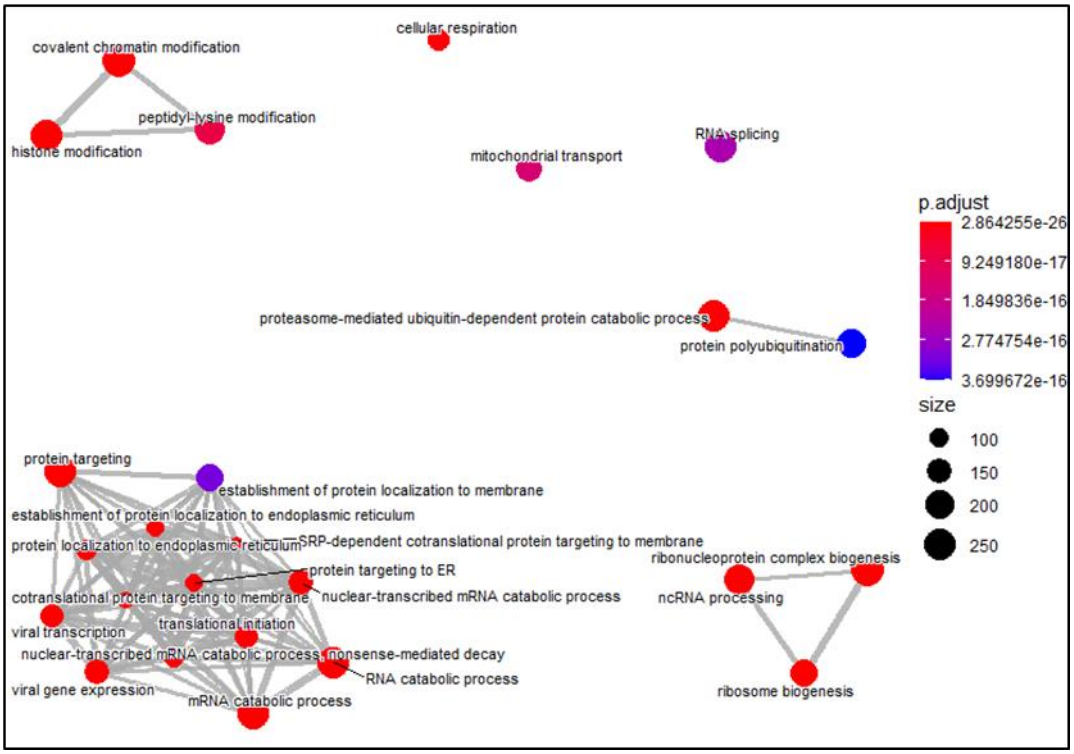

D.

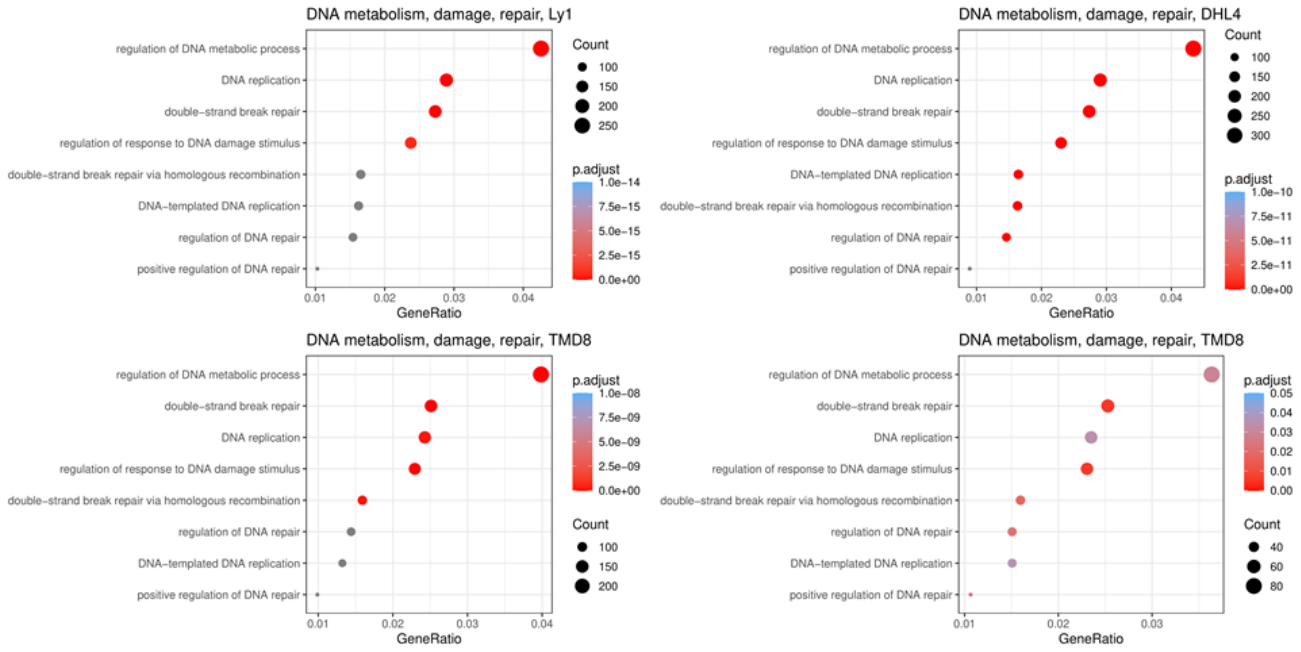

Figure 4.9 RNA-Seq of four DLBCL cell lines detects strong downregulation of gene expression, including genes involved in RNA metabolism

A. Volcano plots showing deregulated genes after 3-hour treatment with 1.5 µM SEL24/MEN1703. Top significant genes are labeled.

B and C. Pathway enrichment dot plots and maps of deregulated genes in each of the cell lines.

D. Deregulated pathways related to DNA metabolism, damage and repair in each cell line.

4.8.3 Inhibition of PIM diminishes expression of SE-regulated genes in DLBCL cell lines

The ChIP-Seq experiment documented reduction of active chromatin marks at SEs. We therefore examined the expression of SE-regulated genes by GSEA. We tested several different DLBCL SE gene sets: one was defined previously in this work, while the others were publicly available, defined by Chapuy *et al*. in several DLBCL cell lines and in normal, reactive lymphoid tissue (tonsils) [158]. The analysis confirmed enrichment of SE-regulated genes among the downregulated genes after PIM inhibition (Figure 4.10A). SE gene sets were universally downregulated, regardless of the tested DLBCL SE gene set, which confirms the impact of PIM inhibition on DLBCL SE expression.

Moreover, we have recently performed another RNA-Seq experiment using Ly1 cell line, treated with SEL24/MEN1703 for 0h, 3h, 6h, 12h and 24h and by GSEA, we assessed the expression of SE-regulated genes as defined by Chapuy *et al.*[158] in the time course of PIM inhibition (Figure 4.10B). The compound markedly downregulated the expression of transcripts controlled by SE, regardless of the DLBCL cell line in which they were defined - but usually the most downregulated for Ly1 SE-dependent gene set, which additionally confirms the specificity of the effect. Importantly, the normalised enrichment score was decreasing with every time point, suggesting that PIMs' activity in SE function is not easily compensated.

Furthermore, recent studies demonstrated robust transcription from SE regions (not of SE-regulated genes, but from the SE regions *per se*) as a marker of active SE [142,179]. SE RNAs are usually capped and polyadenylated [180] and since the library of the Ly1 time course experiment was enriched for polyadenylated mRNA, a pool of long non-coding RNAs (lncRNA) was included in the experiment. The lncRNAs genes were extracted from the RNA-Seq results, and their genomic *loci* were juxtaposed to SE coordinates from the work by Chapuy *et al.*, 2013, thus identifying SE-encoded lncRNAs. The preliminary *in silico* analysis showed a rapid deregulation of approximately 300 polyadenylated lncRNAs per time point – of which almost all lncRNAs encoded within SEs were downregulated at all time points (Figure 4.10C). These observations suggest a general mechanism for regulation of lncRNAs, and diminished SE function after PIM inhibition.

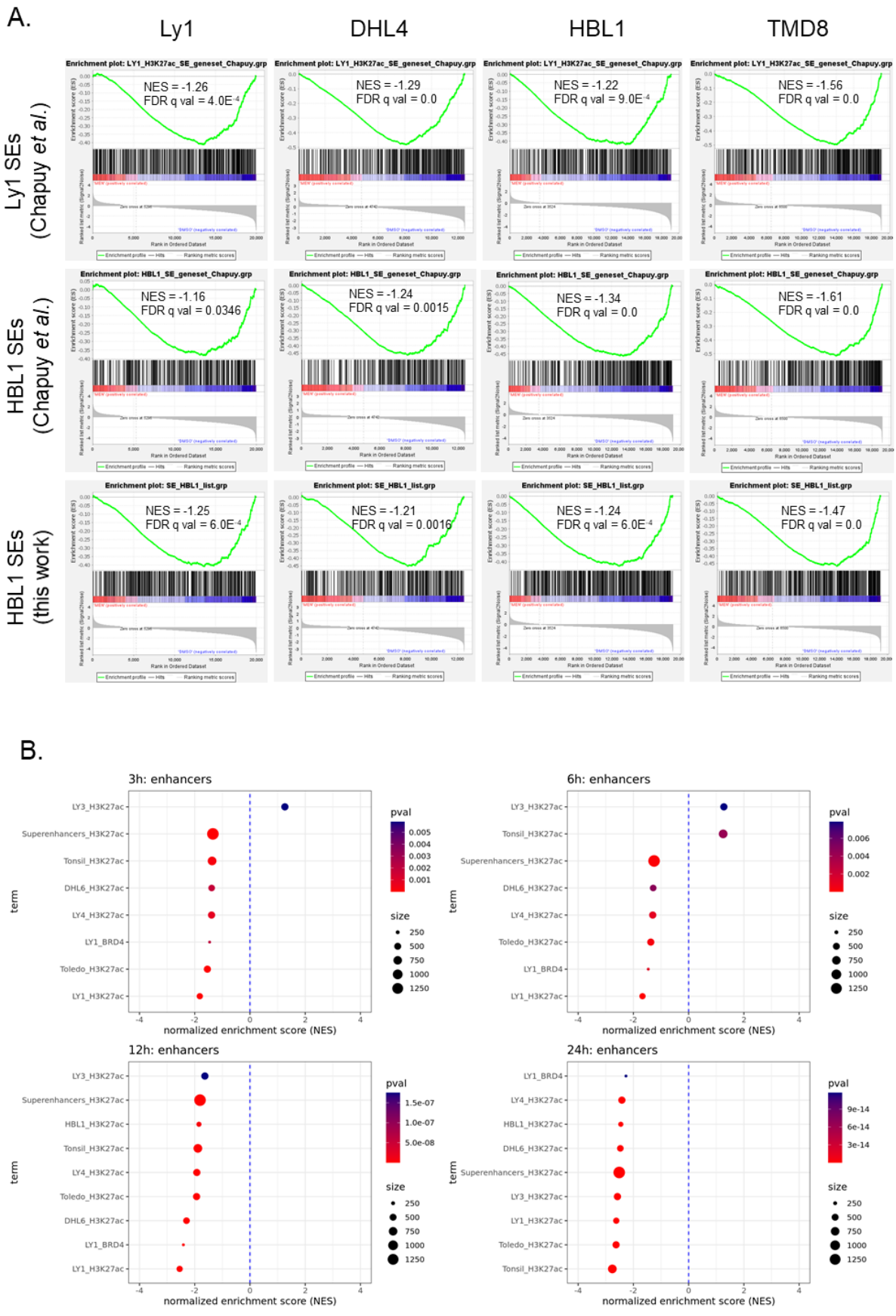
A.
Ly1
DHL4
HBL1
TMD8
Ly1 SEs (Chapuy et al.)
HBL1 SEs (Chapuy et al.)
HBL1 SEs (this work)
Enrichment plot: LY1_H3K27ac_SE_geneset_Chapuy.grp
NES = -1.26
FDR q val = 4.0E-4
NES = -1.29
FDR q val = 0.0
NES = -1.22
FDR q val = 9.0E-4
NES = -1.56
FDR q val = 0.0
Enrichment plot: HBL1_SE_geneset_Chapuy.grp
NES = -1.16
FDR q val = 0.0346
NES = -1.24
FDR q val = 0.0015
NES = -1.34
FDR q val = 0.0
NES = -1.61
FDR q val = 0.0
Enrichment plot: SE_HBL1_list.grp
NES = -1.25
FDR q val = 6.0E-4
NES = -1.21
FDR q val = 0.0016
NES = -1.24
FDR q val = 6.0E-4
NES = -1.47
FDR q val = 0.0
B.
3h: enhancers
6h: enhancers
12h: enhancers
24h: enhancers
term
normalized enrichment score (NES)
pval
size
LY3_H3K27ac
Superenhancers_H3K27ac
Tonsil_H3K27ac
DHL6_H3K27ac
LY4_H3K27ac
LY1_BRD4
Toledo_H3K27ac
LY1_H3K27ac
HBL1_H3K27ac

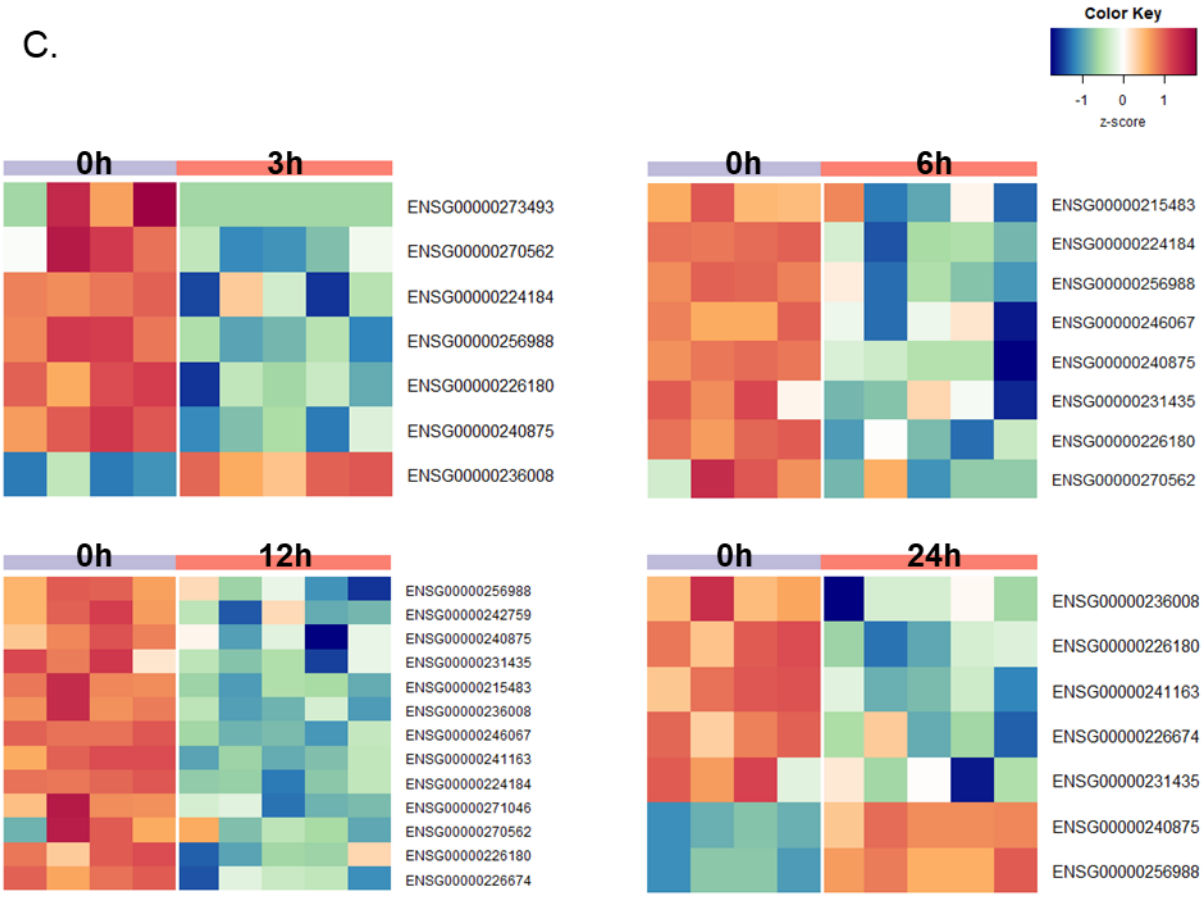

Figure 4.10 Inhibition of PIM downregulates super-enhancer-dependent genes.
A. GSEA of SE-regulated gene sets (defined by Chapuy et al., 2013, or within this work) at 3h of treatment with SEL24/MEN1704 of four DLBCL cell lines. Used gene set is indicated on the chart.
B. Overview of normalised enrichments scores (from GSEA) for SE gene sets defined by Chapuy *et al.*, 2013., analysed in Ly1 cell line at 4 times of treatment with SEL24/MEN1703.
C. Heatmaps presenting Z-scores of expression of long non-coding RNAs encoded in SE regions, analysed in Ly1 cell line at 4 times of treatment with SEL24/MEN1703.

4.9 DNA damage, identified through transcriptional and epigenetic analyses, is confirmed as an outcome of PIM inhibition

One of the repetitive results in the analyses of pathways affected by PIM inhibition was DNA damage response. We investigated if these transcriptional and epigenetic changes are reflected in cell function by assessing the level of γH2AX - i.e. phosphorylated histone H2AX, which participates in early cellular response to the induction of DNA double-strand breaks [181]. In agreement with our previous analyses, the level of γH2AX was markedly increased in different DLBCL cell lines treated with the PIM inhibitor, in a dose-dependent

manner (Figure 4.11). Therefore, through transcriptional and epigenetic screening we identified and confirmed a potential novel mode of cytotoxicity of PIM inhibition in DLBCL.

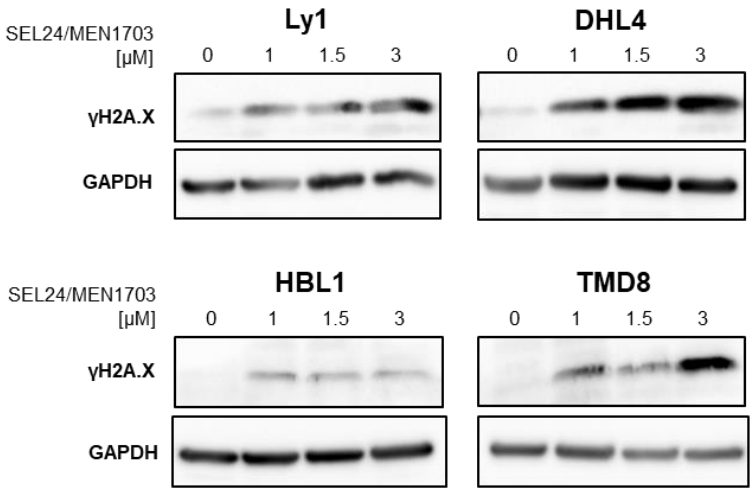

Figure 4.11 PIM inhibition induces DNA damage and/or undermines DNA repair. Western blots showing the level of histone γH2A.X, a marker of DNA damage, in cells treated with SEL24/MEN1703 for 24h.

5. Discussion

Even though new therapeutic vulnerabilities in DLBCL are constantly identified, heterogeneity, aggressive nature, and the frequent development of resistance and/or relapse after treatment with standard chemotherapy raise the need for new, more effective treatments. PIM kinases have long been considered a potential therapeutic target in numerous solid and haematological malignancies. They are overexpressed in DLBCL, while *PIM1* is among the most frequently mutated genes in this disease, which suggests an important function in DLBCL. Our group's previous studies demonstrated that the expression of PIM in DLBCL is associated with more aggressive disease, while its inhibition is toxic for the cells. Importantly, PIMs regulate crucial lymphoma oncogenes, including MYC, and these two proteins regulate their levels in a feed-forward mechanism [37]. Other crucial, and fairly characterised oncogenic functions include: protein translation, transcription, cell metabolism, cell cycle, and apoptosis. Beyond these canonical functions, epigenetic role of PIM kinases has been identified, but very poorly characterised. To date, PIM's epigenetic role has been shown for a single *locus* [69,70]. Therefore, exploration of its poorly described activity might reveal another pathogenic role of PIM kinases in DLBCL and identify novel mechanisms of activity of PIM inhibitors, contributing to design of more effective DLBCL therapies. This work addressed the role of PIM kinases in genome-wide epigenetic regulation of transcription through phosphorylation of H3S10 in DLBCL cell lines. The findings bring vital conclusions for understanding not only PIM biology, but also DLBCL pathogenesis and vulnerabilities, as well as the role of H3S10ph for executing cell function and SE regulation.

5.1 PIM kinases regulate epigenetic patterns in DLBCL

The analysis of global levels of epigenetic marks in response to SEL24/MEN1703 showed persistent, dose-dependent impact on histone modification landscape (Figure 4.6A), similar among all tested cell lines. Even though DLBCL is highly heterogeneous, GCB and ABC subtypes did not present striking differences to SEL24/MEN1703 treatment in terms of histone modification changes and RNAPII phosphorylation status. Therefore, PIM-related epigenetic

mechanisms work in a similar way, independently of a cell's molecular phenotype. This, in turn, proves that PIM's involvement in epigenetic regulation is its primary, direct function.

At 3h, changes at the global level were seen only for H3S10ph (Figure 4.6A). However, ChIP-Seq showed that the load of H3K27ac and H3K9ac changed locally after 3h of PIM inhibition (Figure 4.7), which supports the specific role of PIM for proper function of enhancers and promoters. At 24h, all examined chromatin activating marks showed significant downregulation globally. For example, levels of BRD4-recruiting H4K16ac and H4panAc were reduced after PIM inhibition, in accordance with the mechanism suggested by Zippo *et al* [69,70]. Another modification, H3K9acK14ac was also very strongly reduced, even more than H4panAc. The co-occurrence of H3K9acS10phK14ac was shown to enhance 14-3-3 binding, and positively regulate further H3 acetylation [182,183]. This mechanism was also operating in our DLBCL cells, as H3S10ph depletion prevented histone acetylation and/or promoted deacetylation (Figure 4.6A). Moreover, in ChIP-Seq, we observed that the level, but not the distribution of H3K27ac changed after PIM inhibition (Figure 4.7). This suggests that PIM's epigenetic function stabilises deposited H3K27ac in active enhancers, rather than promoting activation of new regions. This observation is in agreement with previously proposed mechanisms, where H3S10ph is deposited at pre-acetylated histones [69]. At promoters, H3S10ph likely stabilises active regions marked with H3K9acK14ac. In fact, H3S10ph has been described as an epigenetic switch, blocking the access of silencing histone methyltransferases to H3K9 [130], and our ChIP-Seq experiments confirmed that H3K9ac level is diminished at promoters after PIM inhibition (Figure 4.7).

Surprisingly, inhibition of the PIM family appears sufficient to substantially erase H3S10ph (Figure 4.2A, Figure 4.6A), which suggests that this is the main H3S10 kinase in DLBCL. Despite notorious unspecific activity of many small-molecule drugs, this effect cannot be attributed to SEL24/MEN1703 off-targets as other PIM inhibitors have similar impact on H3S10ph (Figure 3C). Moreover, kinome analysis of cells treated with SEL24/MEN1703 did not detect inhibition of any other known H3S10 writer [174]. Since genetic silencing of PIM additionally confirmed that PIM KD indeed translates to H3S10ph decrease, we can conclude that PIMs play a vital role in maintaining the global levels of H3S10ph, which in turn impacts other epigenetic changes.

However, there are certain limitations to these studies that must be acknowledged. Examination of H3S10ph and PIM1 chromatin distribution after PIM inhibition in ChIP-Seq, which would ultimately confirm the role of PIM-induced H3S10ph on enhancer and/or promoter epigenetic patterns is missing (but have already become the subject of studies by another member of the team). Our attempt to assess the level and genomic distribution of H3S10ph in ChIP-Seq were inconclusive, as this is a ubiquitous mark, that did not form distinctive peaks, and this experiment requires further optimisation. Moreover, PIM1 ChIP-Seq was also unsuccessful. One reason was technical issues with PIM1 antibodies – and we are currently working on a ChIP-Seq with PIM1 tagged with HA tag, where we will use anti-HA antibody. Secondly, the mechanism of PIM1´s recruitment to chromatin likely render ChIP especially challenging. PIM1 does not have a DNA-binding domain (PROSITE [178]), thus it needs to be recruited to the chromatin in an indirect way, by interacting with other proteins. The role for MYC-MAX complex in this recruitment has been described [69,70], but since PIM1 interacts with multiple TF, it is highly probable that PIM1 is present on the chromatin as a member of many different complexes, acting as a kinase, not always in the H3S10ph-context. This makes immunoprecipitation of PIM1-protein complexes-DNA particularly technically challenging.

5.2 PIM kinases control transcription *via* epigenetic mechanisms, and regulation of genes involved in RNA biosynthesis and processing

Although the canonical function of PIM kinases in transcription is performed through phosphorylation of TFs, PIM1's activity as an epigenetic writer suggests that this kinase, and perhaps also other PIMs, has a more direct role in regulation of gene expression. Firstly, we confirmed that PIM inhibition reduces the global level of RNA, which reinforces PIM's role in maintaining cellular amounts of RNA.

This work is the first to identify that pan-PIM inhibition impacts global RNAPII phosphorylation status (Figure 4.6), induces changes in global epigenetic landscape (Figure 4.6), decreases chromatin activating marks: H3K9ac at TSS and H3K27ac at enhancers (Figure 4.7), which is collectively translated to vast deregulation of gene expression (Figure 4.8, Figure 4.9), supporting PIM as one of the epigenetic regulators of transcription in DLBCL. Especially,

PIM's activity seems to be directly crucial for transcript elongation, and to much lesser extent for transcription initiation, given the differences in Ser2 and Ser5 phosphorylation. Thus, soon after PIM inhibition, RNAPII is likely arrested in the transcription initiation phase. It is worth mentioning that, encouraged by these results, another lab member recently commenced another ChIP-Seq experiment with RNAPII to verify this hypothesis.

The phosphorylated Ser2 levels at CTD are partially restored at 24h, signifying a re-boot of elongation at 24h (Figure 4.6A). Therefore, a back-up mechanism guarding RNAPII function must be operating in the cells. In turn, the epigenetic landscape is progressively deficient in activating modifications in the course of PIM inhibition, showing that PIMs' epigenetic function is irreplaceable.

Moreover, genes involved in RNA metabolism are characterised with particularly deregulated expression following PIM inhibition. At 3h, such enrichment is similar among all the examined cell lines, regardless of their subtype, which implies that PIMs are universally involved in the regulation of genes responsible for RNA transcription and processing. Intriguingly, this deregulation of expression is coupled with epigenetic changes at the related enhancers, at least in HBL1 cell line (Figure 4.8). Hence, RNA biogenesis is regulated by PIM in multiple mechanisms, including epigenetic activation of chromatin, epigenetic control of RNAPII phosphorylation, but also the expression of genes that encode effector proteins involved in RNA metabolism, and the canonical modifications of TFs. Taken together, this versatile role in transcription renders PIM an new, important transcriptional regulator in DLBCL, whose novel functions discovered in this work decidedly exceed the previously defined roles.

5.3 PIM kinases are involved in SE regulation

Inhibition of PIM shows similar transcriptional outcomes to the inhibition of key SE protein - BRD4 (Figure 4.1). Given that PIM1 has been documented to participate in transcriptional activation of *FOSL1* gene *via* BRD4 [69,70], we repeatedly examined whether a similar mechanism operates in DLBCL on a global level, possibly at all SEs. Gene Set Enrichment Analysis (GSEA) confirmed that PIMs are generally involved in the expression of

SE-dependent genes in DLBCL (Figure 4.10A). Since SE-controlled genes often establish pro-survival circuitry, targeting these regulatory mechanisms is an attractive therapeutic strategy. In fact, several compounds targeting SE constituents are currently tested in clinical trials for various hematologic diseases (reviewed in ref. 155) Thus, deregulation of SE-dependent expression is another advantage of prospective PIM-targeted therapy in DLBCL. This discovery also constitutes a starting point for characterisation of the mechanism of PIM-SE interactions. We confirmed that inhibition of PIM does not diminish cellular BRD4 levels at 3h (Figure 4.6B). Therefore, the observed SE disruption is not a consequence of BRD4 depletion, but rather an outcome of altered chromatin interactions.

In addition, we noted a universal downregulation of multiple lncRNA transcribed from SE regions after PIM kinase inhibition (Figure 4.9C). Given the recent studies highlighting the regulatory role of seRNA and their involvement in the assembly of regulatory/transcriptional complexes [147,184–188], these observations might constitute an additional layer of PIM-related transcriptional complexity in DLBCL cells. Moreover, one (and the only, at the moment) publication linking PIMs and ncRNA reports that PIM1 indeed regulates the level of H19 lncRNA, and thus regulates the expression of pluripotency genes and tumour growth in T-cell acute lymphoblastic leukaemia and prostate cancer [173]. Hence – PIM1 is functionally capable of regulating a ncRNA, and our preliminary results show that this could be not an isolated case, but a more general mechanism. The experiment presented in this work analysed only selected lncRNA. The function of PIM inhibition on all ncRNA expression and its role in transcription regulation is further studied in my National Science Centre grant Preludium 20. Within the ongoing grant, I started by comprehensive characterisation of the ncRNA landscape in DLBCL cells. Through RNA-Seq, I currently identify seRNAs with the use of BRD4 inhibitor, JQ1, and PIM-dependent ncRNAs (including seRNAs) with PIM inhibitors SEL24/MEN1703 and PIM447. I will further identify the associations between changes in ncRNA levels, particularly seRNA, and changes in expression of respective, SE-controlled genes. Finally, I plan to functionally verify the findings by KD of the identified, crucial seRNA using shRNA and evaluation of expression of the paired protein–coding oncogenes using RT-PCR and/or western blot analysis. Should a major decrease in the oncogene expression be identified, I will follow with proliferation and viability assays. The project started in January 2022, and is envisioned until January 2025 (#2021/41/N/NZ5/04244, PI: Sonia Dębek).

Finally, an interesting fact has been identified by the integrated ChIP-Seq and RNA-Seq results, namely, that PIM inhibition diminishes the expression of YY1-regulated genes. YY1 is a versatile protein that plays several functions in the chromatin – it is a canonical TF that can be found in the promoters and enhancers (generally abundant at SEs regions [176]), but it also regulates 3D genome organisation by long-distance interactions, and cooperation with chromatin remodellers, and insulators, such as cohesin, or CTCF [189]. Therefore, the decline in YY1-regulated genes after PIM inhibition likely signifies detachment of YY1 from the chromatin, and disruption of 3D chromatin organisation. In fact, chromatin conformation in DLBCL after PIM inhibition or depletion will be the subject of my 6-month scientific internship at prof. Ari Melnick's lab at Weill Cornell Medical College in New York (starting August 2023). Therefore, this upcoming project should provide a multitude of valuable information about PIMs' role in genome organisation.

5.4 PIM-induced H3S10ph is involved in DLBCL interphase cell function

H3S10ph is a marker of mitosis, therefore, decrease of the levels of this marker upon PIM inhibition might result from fewer cells in mitosis due to cell cycle arrest. We, however, disproved this hypothesis by showing that PIMs reduce interphase levels of HS10ph (Figure 4.4), and diminish H3S10ph as soon as 3h of treatment (Figure 4.6). Thus, H3S10 phosphorylation is a *bona fide* function of PIM, which promotes normal cell proliferation.

PIMs are versatile kinases that participate in multiple cellular processes, hence, it is challenging to extract only the role of the epigenetic aspect of their activity on cell function. Therefore, results of different experiments have to be analysed together. In order to investigate the role of PIM-induced H3S10ph, we confirmed that PIM phosphorylate H3S10 (Figure 4.2A, 4.6A), analysed cell proliferation and H3S10ph levels in the context of triple PIM KD (Figure 4.3), and studied the role of lower levels of H3S10ph with H3S10A, a non-phosphorylatable mutant of H3S10, in cell proliferation and viability (Figure 4.5). Pan-PIM inhibition with SEL24/MEN1703 virtually erases H3S10ph (Figure 4.6) suggesting that this is the main H3S10 kinase in DLBCL. Since H3S10A mutants showed slower cell divisions, we can conclude that a similar mechanism operates when PIM is silenced or inhibited. However, it

has to be remembered that the epigenetic mechanism of cell cycle progression by PIM kinases is not isolated and works in cooperation with the canonical regulation of cell cycle proteins. For this reason, inhibition or silencing of PIM should result in a profound cell cycle arrest. This effect has been observed previously in our group [37]. The triple KD of PIM generated in this work also impaired proliferation, however, to much lesser extent than expected, i.e. the effect on both H3S10ph levels and proliferation was much milder than what was previously observed with chemical inhibition. The gentle result was probably caused by insufficient downregulation of PIMs (Figure 4.3B). Also for this reason, the impact of PIM KD on cell function has been evaluated in proliferation rather than apoptosis. In the future, we might enhance Sleeping Beauty KD by addition of another set of other shRNA targeting all three PIMs to a cell line, or study the effect of acute PIM deletion by generation of inducible "triple" CRISPR/Cas9 KO.

5.5 PIM regulate DNA damage response pathway through epigenetic activation of expression of related genes

PIM2 has been previously associated with DNA damage response, albeit with little information about the mechanism of this interaction. One study reported that PIM2 regulated UV damage response upstream of E2F TF in osteosarcoma [190], but this deregulation was dependent on stabilisation of MYC or activation of ATM by PIM2. Another group revealed that deregulation of E2F and MYC targets was an outcome of combined JAK1/2, pan-PIM, and CDK4/6 inhibition [191]. In this work, we show that E2F target genes are characterised by weakened activation at enhancers, and lower expression after 3 h of PIM inhibition (Figure 4.8D) in HBL1 cell line. Therefore, regulation of E2F genes is regulated on an epigenetic level by PIM, in addition to the indirect regulation by MYC and ATM documented in the previous reports. Deregulation of pathways inflicted with DNA damage response was identified also in RNA sequencing of another three DLBCL cell lines (Figure 4.9), confirmed by functional analysis which showed that PIM inhibition increases DNA damage marker, γH2AX (Figure 4.10). Taken together, this study identifies a new role for PIM kinases in DNA damage response. Moreover, unrepaired DNA damage is a potential new cytotoxic mechanism of PIM inhibition in DLBCL. This observation is particularly vital for therapy design. For example, it likely explains why PIM

inhibition sensitises cells to radiotherapy and cisplatin [25,102,192,193], and further supports the combination of PIM inhibition and DNA-damaging agents.

Another prevalent process affected by PIM inhibition was RNA metabolism. This observation prompted us to coin an alternative hypothesis about the mechanism of DNA damage consequential to PIM inhibition. H3S10ph abundance is associated with formation of "R-loops", i.e. regulatory regions composed of hybridised nascent RNA with template DNA strand, and non-template DNA strand [131]. R-loops play a role in stimulation or inhibition transcription, while mechanistically, their formation exposes the single-stranded non-template DNA to damage, and halts replication fork progression. This, in turn, causes replication stress and frequent mutations. H3S10ph leads to chromatin compaction and heterochromatin formation at R-loops, and deregulation of this mark leads to increased genomic instability [131]. In this work, one of the pathways affected by PIM inhibition identified by RNA-Seq was nonsense mediated decay (NMD). Therefore, in addition to transcriptional pausing, PIM inhibition likely leads to faulty transcription. Before the RNA would be degraded, it can lead to enhanced formation of R-loops and DNA damage. Another argument in favour of the hypothesis is that R-loops effectively form at double-strand breaks [194], which were identified as a prevailing form of DNA damage after PIM inhibition. Therefore, it is possible that the observed DNA damage is the result of accumulation of R-loops.

5.6 Epigenetic role of other PIM kinases, and another epigenetic role of PIM1

The first step in examining the histone-modifying function of PIM kinases was the confirmation that PIM localise in the nucleus of DLBCL cells. The subcellular fractionation followed by western blot revealed that in DLBCL, PIM1 and PIM3 are localised in the nucleus as well as in the cytoplasm, while PIM2 is a cytoplasmic protein (Figure 4.2B). To-date, epigenetic activity in cells has been described for PIM1. Given the localisation, we were especially interested in the potential epigenetic function of PIM3. Interestingly, early studies of PIM3 showed that this protein is able to phosphorylate histone H1 *in vitro* [181,182], but these discoveries were not developed further. The question of PIM3's epigenetic function was subsequently addressed in this work, however, these experiments were particularly

challenging. Neither characterisation of interactions with chromatin (chromatin fractionation), nor impact on H3S10ph of deep KD of PIM3 (pTRIPZ-shPIM3) succeeded for technical reasons, despite multiple attempts. However, several isolated observations collectively suggest that this protein might also have novel epigenetic function, namely: PIM3's nuclear localisation (Figure 4.2B), its apparent ability to compensate PIM1's loss (Figure 4.3A) as well as the aforementioned phosphorylation of H1 in vitro [181,182], and the computational prediction that PIM3 is able to phosphorylate H3S10 (Figure 1.3). Further studies would decidedly be beneficial for comprehensive verification of PIM3's epigenetic function.

An interesting idea vaguely suggested by chromatin fractionation studies (Figure 4.2C) is that PIM1 also has an architectural function on the chromatin, in addition to histone phosphorylation. Based on the results, PIM1 binds rather strongly to the chromatin, similarly to BRD4 - a protein which forms chromatin complexes, and interacts with the Mediator complex, which folds DNA to link gene enhancers and promoters. In fact, the work by Zippo *et al*., which characterised the molecular mechanism of epigenetic activation by PIM1 for *FOSL1* gene also reported that PIM1 was necessary for looping between promoter and enhancer at this locus. It will therefore be especially interesting to examine chromatin conformation after PIM inhibition, or characterise the phenotype of PIM kinase-dead K67M mutant. As mentioned earlier, PIMs' role in chromatin conformation will be studied during my scientific internship at Weill Cornell Medical College in the winter semester 2023/2024.

5.7 Clinical implications

The described work proves SEL24/MEN1703's efficacy in DLBCL, as was previously observed in pre-clinical studies performed by our group [65]. Currently, PIM inhibitors are not studied as a treatment option in DLBCL. However, there are ongoing studies in various hematologic malignancies at phase I or II. Considering the new results provided by the described work, and other observations about PIMs' role in DLBCL made by other lab members (e.g. recently published PIM-MYC cooperation in DLBCL [37]), as well as manageable safety profile in AML patients, SEL24/MEN1703 could be considered for clinical trials in DLBCL. Given SEL24/MEN1703's favourable safety profile in the AML clinical trial, and high efficacy in pre-

clinical studies, selectivity towards cancer cells, synergy with anti-CD20 antibodies and other drugs, as well as the fact that it is easy to administer orally, the compound could be implemented in a first-line therapy. However, the patients would first have to be tested for PIM expression, since PIMs are expressed in majority, but not all DLBCLs [37].

This work presents a novel, epigenetic function of PIM. In recent years, epigenetics has garnered attention as a driving force for DLBCL carcinogenesis. Thus, targeting epigenetic pathways in DLBCL treatment is a promising approach. Several epigenetic drugs have been developed and tested in clinical trials for DLBCL, including EZH2 inhibitors (trials NCT02889523, NCT02220842) and histone deacetylase inhibitors (NCT04231448, NCT03373019, NCT03939182). Moreover, combination therapies that target both epigenetic and conventional chemotherapy mechanisms have demonstrated a synergistic effect in DLBCL treatment. There are numerous examples of such synergy from pre-clinical trials in various mechanisms, such as: sensitisation of DLBCL cells [195–197], enhanced CD19 expression on lymphoma cells, recognised by CAR-T [198], or re-juvenation of exhausted T-cells in PD-1 blockade treatment [199]. There are also preliminary results of early phase clinical trials [200,201] (they are not yet focused, however, on the efficacy), or case reports [202]. Therefore, targeting epigenetic pathways in DLBCL treatment can be a potential strategy to improve patient outcomes and warrants further investigation. It has to be noted, however, that not all studies investigating the addition of epigenetic drugs to standard therapy have shown improved outcomes. Therefore, the use of epigenetic drugs in DLBCL should be considered on a case-by-case basis, taking into account the patient's individual characteristics and treatment history.

H3S10 kinases and phosphatases have been known as oncogenic factors for a long time [203–206]. Recent research suggests that their abnormal activity can lead to fundamental changes in chromatin structure (reviewed in ref. [131]), which is an important aspect of epigenetic regulation. This epigenetic memory ensures that the effects of these enzymes' activity are maintained long-term, even after initial developmental and environmental stimuli have been removed. Thus, it is important to account for chromatin changes in the development of therapeutic compounds, and drugs that target H3S10 modifiers appear appropriate for this task. Further research into links between chromatin remodelling and signalling pathways can also help develop more precise therapeutic strategies.

Moreover, through integrated epigenetic and transcriptomic screening we identified and functionally examined a novel mode of toxicity after PIM inhibition, namely - DNA damage. Accumulated and unrepaired DNA damage can lead to cell death or senescence, providing a therapeutic ground for cancer treatment. Moreover, DNA damage can activate the immune system, triggering an immune response against cancer cells [207]. Additionally, targeting DNA repair pathways in cancer cells can increase their sensitivity to other treatments, such as radiation therapy and chemotherapy - which was shown in published reports [25,102,192,193]. Thus, the accumulation of DNA damage after PIM inhibition offers a broad range of treatment options with potential synergistic effects.

Finally, since PIM compensates for the loss of one another, it is very likely that only pan-PIM inhibition, and not single PIM inhibition, would achieve clinical effect. To date, all of the clinical-stage PIM inhibitors are capable of targeting all three proteins, however, sometimes the specificity depends on the dose – e.g. PIM447 targets only PIM1 in lower doses, and PIM1, 2 and 3 at higher doses. Actually, such dose-dependent selectivity could have been the reason why the drugs did not show efficacy in clinical trials, while the highly potent SEL24/MEN1703 is so far the most clinically developed drug of the PIM inhibitors. Therefore, scrutinising drug's specificity and pharmacodynamics should be especially important in the design and dose selection of PIM inhibitors.

6. Conclusion

In the described work, I characterised epigenetic alterations that accompany PIM inhibition, linked them to transcriptional changes, and functionally verified one of the findings. This dissertation is the first to report a vast role of PIM-induced H3S10ph in epigenetic regulation of transcription not only in DLBCL, but in any type of cell.

In the course of the project, I managed to prove that PIM inhibition results in the erasure of H3S10ph, which is followed by further alteration of the epigenetic landscape, accompanied by massive deregulation of transcription, which is likely a factor in the final outcome: in case of treatment with SEL24/MEN1703, the cells succumb to apoptosis, but depending on the scale and dynamics of depletion, PIM deprivation can also lead to proliferation impairment and cell cycle arrest. Moreover, I found that depletion of one PIM induces compensatory upregulation of other PIMs, therefore inhibition of all three PIMs should be necessary for achieving therapeutic effect. Furthermore, one of our scientific questions was whether PIMs are involved in SE function. We found out that PIM inhibition indeed decreased the crucial active chromatin mark H3K27ac at SE, which was reflected in universal downregulation of SE-regulated genes. The function was, however, not specific to SE, and even more visible in case of TE. I verified the findings with chemical inhibition and genetic silencing of PIM kinases, as well as by overexpression of non-phosphortylatable H3S10A.

The main findings can be concluded as follows:

1. PIM kinases are involved in the regulation of epigenetic patterns in DLBCL, including the cellular level of H3S10ph and, consequently, chromatin-activating histone modifications: H3K27ac, H3K9ac, H3K4me3, or H4 acetylation.
2. PIM kinases are involved in the regulation of transcription by modulation of the load of epigenetic activating signals for transcription, i.e. H3K9ac at promoters and H3K27ac at enhancers; of RNAPII phosphorylation status, and of genes involved in RNA metabolism. This novel function, in addition to the canonical regulation of transcription through TFs, renders PIM kinases as important regulators of transcription in DLBCL.

3. PIM kinases considerably influence SE activity, however are not their main regulators.
4. H3S10ph participates in DLBCL cell survival and proliferation.

Bibliography

1. Chapuy, B. *et al.* Molecular Subtypes of Diffuse Large B Cell Lymphoma Are Associated WIth Distinct Pathogenic Mechanisms and Outcomes. *Nat. Med.* (2018).
2. Ollila, T. A. & Olszewski, A. J. Extranodal Diffuse Large B Cell Lymphoma: Molecular Features, Prognosis, and Risk of Central Nervous System Recurrence. *Curr. Treat. Options Oncol.* **19**, (2018).
3. Bakhshi, T. J. & Georgel, P. T. Genetic and epigenetic determinants of diffuse large B-cell lymphoma. *Blood Cancer J.* **10**, (2020).
4. Wu, S., Yin, Y. & Wang, X. The epigenetic regulation of the germinal center response. *Biochim. Biophys. Acta - Gene Regul. Mech.* **1865**, 194828 (2022).
5. Talluri, S. *et al.* Apobec Family of Proteins Mediate Genomic Changes in Multiple Myeloma By Inducing DNA Damage and C>T Mutations. *Blood* **130**, (2017).
6. Pasqualucci, L. *et al.* Hypermutation of multiple proto-oncogenes in B-cell diffuse large-cell lymphomas. *Nature* **412**, 341–346 (2001).
7. Alizadeh, A. A. *et al.* Distinct types of diffuse large B-cell lymphoma identified by gene expression profiling. *Nature* **403**, 503–511 (2000).
8. Monti, S. *et al.* Molecular profiling of diffuse large B-cell lymphoma identifies robust subtypes including one characterized by host inflammatory response. *Blood* **105**, 1851–1861 (2005).
9. Alaggio, R. *et al.* The 5th edition of the World Health Organization Classification of Haematolymphoid Tumours: Lymphoid Neoplasms. *Leukemia* **36**, 1720–1748 (2022).
10. Wright, G. W. *et al.* A Probabilistic Classification Tool for Genetic Subtypes of Diffuse Large B Cell Lymphoma with Therapeutic Implications. *Cancer Cell* **37**, 551-568.e14 (2020).
11. Schmitz, R. *et al.* Genetics and Pathogenesis of Diffuse Large B-Cell Lymphoma. *N. Engl. J. Med.* **378**, 1396–1407 (2018).
12. Warzocha, K. & Puła, B. Rozpoznawanie i leczenie chorych na chłoniaka rozlanego z duzych komórek B. *Hematologia* **8**, 113–131 (2017).
13. Coiffier, B. & Sarkozy, C. Diffuse large B-cell lymphoma : R-CHOP failure — what to do ? *Hematol. Am Soc Hematol Educ Progr.* **1**, 366–378 (2016).
14. Tomita, N. *et al.* R-CHOP therapy alone in limited stage diffuse large B-cell lymphoma. *Br. J. Haematol.* **161**, 383–388 (2013).
15. Denlinger, N., Bond, D. & Jaglowski, S. CAR T-Cell Therapy for B-Cell Lymphoma. *Curr Probl Cancer* **26**, 597–601 (2022).
16. Sermer, D. *et al.* Outcomes in patients with DLBCL treated with commercial CAR T cells compared with alternate therapies. *Blood Adv.* **4**, 4669–4678 (2020).
17. Shadman, M. *et al.* Autologous transplant vs chimeric antigen receptor T-cell therapy for relapsed DLBCL in partial remission. *Blood* **139**, 1330–1339 (2022).
18. Hamadani, M. *et al.* Allogeneic transplant and CAR-T therapy after autologous transplant failure in DLBCL: A noncomparative cohort analysis. *Blood Adv.* **6**, 486–494 (2022).

19. Dreger, P. *et al.* CAR T cells or allogeneic transplantation as standard of care for advanced large B-cell lymphoma: An intent-to-treat comparison. *Blood Adv.* **4**, 6157–6168 (2020).

20. Cuypers, T. *et al.* Murine leukemia virus-induced T-cell lymphomagenesis: Integration of proviruses in a distinct chromosomal region. *Cell* **37**, 141–150 (1984).

21. Bellon, M. & Nicot, C. Targeting Pim kinases in hematological cancers : molecular and clinical review. *Mol. Cancer* 1–25 (2023). doi:10.1186/s12943-023-01721-1

22. Amson, R. *et al.* The human protooncogene product p33pim is expressed during fetal hematopoiesis and in diverse leukemias. *Proc. Natl. Acad. Sci. U. S. A.* **86**, 8857–8861 (1989).

23. Eichmann, A., Yuan, L., Bréant, C., Alitalo, K. & Koskinen, P. J. Developmental expression of Pim kinases suggests functions also outside of the hematopoietic system. *Oncogene* **19**, 1215–1224 (2000).

24. Te Riele, H., Maandag, E. R., Clarke, A., Hooper, M. & Berns, A. Consecutive inactivation of both alleles of the pim-1 proto-oncogene by homologous recombination in embryonic stem cells. *Nature* **348**, 649–651 (1990).

25. Singh, N. *et al.* PIM protein kinases regulate the level of the long noncoding RNA H19 to control stem cell gene transcription and modulate tumor growth. *Mol. Oncol.* **14**, 974–990 (2020).

26. Allen, J. D., Verhoeven, E., Domen, J., Van Der Valk, M. & Berns, A. Pim-2 transgene induces lymphoid tumors, exhibiting potent synergy with c-myc. *Oncogene* **15**, 1133–1141 (1997).

27. Dautry, F., Weil, D., Yu, J. & Dautry-Varsat, A. Regulation of pim and myb mRNA accumulation by interleukin 2 and interleukin 3 in murine hematopoietic cell lines. *J. Biol. Chem.* **263**, 17615–17620 (1988).

28. Temple, R. *et al.* Microarray analysis of eosinophils reveals a number of candidate survival and apoptosis genes. *Am. J. Respir. Cell Mol. Biol.* **25**, 425–433 (2001).

29. Domen, J. *et al.* Pim-1 levels determine the size of early B lymphoid compartments in bone marrow. *J. Exp. Med.* **178**, 1665–1673 (1993).

30. Matikainen, S. *et al.* Interferon-α activates multiple STAT proteins and upregulates proliferation-associated IL-2Rα, c-myc, and pim-1 genes in human T cells. *Blood* **93**, 1980–1991 (1999).

31. Yip-Schneider, M. T., Horie, M. & Broxmeyer, H. E. Transcriptional induction of pim-1 protein kinase gene expression by interferon γ and posttranscriptional effects on costimulation with steel factor. *Blood* **85**, 3494–3502 (1995).

32. Miura, O. *et al.* Induction of tyrosine phosphorylation of Vav and expression of Pim-1 correlates with Jak2-mediated growth signaling from the erythropoietin receptor. *Blood* **84**, 4135–4141 (1994).

33. Borg, K. E. *et al.* Prolactin regulation of pim-1 expression: Positive and negative promoter elements. *Endocrinology* **140**, 5659–5668 (1999).

34. Guo, S. *et al.* Overexpression of Pim-1 in bladder cancer. *J. Exp. Clin. Cancer Res.* **29**, 1–7 (2010).

35. Valdman, A., Fang, X., Pang, S. T., Ekman, P. & Egevad, L. Pim-I expression in prostatic intraepithelial neoplasia and human prostate cancer. *Prostate* **60**, 367–371 (2004).

36. Brasó-Maristany, F. *et al.* PIM1 kinase regulates cell death, tumor growth and chemotherapy

response in triple-negative breast cancer. *Nat. Med.* **22**, 1303–1313 (2016).

37. Szydłowski, M. *et al.* Inhibition of PIM Kinases in DLBCL Targets MYC Transcriptional Program and Augments the Efficacy of Anti-CD20 Antibodies. *Cancer Res.* **81**, 6029–6043 (2021).

38. Mikkers, H. *et al.* Mice Deficient for All PIM Kinases Display Reduced Body Size and Impaired Responses to Hematopoietic Growth Factors. *Mol. Cell. Biol.* **24**, 6104–6115 (2004).

39. De Benedetti, A. & Graff, J. R. eIF-4E expression and its role in malignancies and metastases. *Oncogene* **23**, 3189–3199 (2004).

40. Thomas, M. *et al.* The proto-oncogene Pim-1 is a target of miR-33a. *Oncogene* **31**, 918–928 (2012).

41. Wang, W. *et al.* Long Noncoding RNA KCNQ1OT1 Confers Gliomas Resistance to Temozolomide and Enhances Cell Growth by Retrieving PIM1 From miR-761. *Cell. Mol. Neurobiol.* **42**, 695–708 (2022).

42. Saris, C. J. M., Domen, J. & Berns, A. The pim-1 oncogene encodes two related protein-serine/threonine s by alternative initiation at AUG and CUG. *EMBO J.* **10**, 655–664 (1991).

43. Mondello, P., Cuzzocrea, S. & Mian, M. PIM kinases in hematological malignancies: Where are we now and where are we going? *J. Hematol. Oncol.* **7**, 1–9 (2014).

44. Julson, J. R., Marayati, R., Beierle, E. A. & Stafman, L. L. The Role of PIM Kinases in Pediatric Solid Tumors. *Cancers (Basel).* **14**, 1–18 (2022).

45. Mizuno, K. *et al.* Regulation of Pim-1 by Hsp90. *Biochem. Biophys. Res. Commun.* **281**, 663–669 (2001).

46. Iyer, R. S., Chatham, L., Sleigh, R. & Meek, D. W. A functional SUMO-motif in the active site of PIM1 promotes its degradation via RNF4, and stimulates protein kinase activity. *Sci. Rep.* **7**, 1–14 (2017).

47. Ionov, Y. *et al.* Pim-1 protein kinase is nuclear in Burkitt's lymphoma: nuclear localization is necessary for its biologic effects. *Anticancer Res.* **23**, 167–178 (2003).

48. Brault, L. *et al.* PIM kinases are progression markers and emerging therapeutic targets in diffuse large B-cell lymphoma. *Br. J. Cancer* **107**, 491–500 (2012).

49. Xie, Y. *et al.* The 44kDa Pim-1 kinase directly interacts with tyrosine kinase Etk/BMX and protects human prostate cancer cells from apoptosis induced by chemotherapeutic drugs. *Oncogene* **25**, 70–78 (2006).

50. Liu, Y. *et al.* Pim1 kinase positively regulates myoblast behaviors and skeletal muscle regeneration. *Cell Death Dis.* **10**, (2019).

51. Samse, K. *et al.* Functional effect of Pim1 depends upon intracellular localization in human cardiac progenitor cells. *J. Biol. Chem.* **290**, 13935–13947 (2015).

52. Baytel, D., Shalom, S., Madgar, I., Weissenberg, R. & Don, J. The human Pim-2 proto-oncogene and its testicular expression. *Biochim. Biophys. Acta - Gene Struct. Expr.* **1442**, 274–285 (1998).

53. Bullock, A. N., Debreczeni, J., Amos, A. L., Knapp, S. & Turk, B. E. Structure and substrate specificity of the Pim-1 kinase. *J. Biol. Chem.* **280**, 41675–41682 (2005).

54. Van Der Lugt, N. M. T. *et al.* Proviral tagging in Eμ-myc transgenic mice lacking the Pim-1 proto-oncogene leads to compensatory activation of Pim-2. *EMBO J.* **14**, 2536–2544 (1995).

55. Mikkers, H. *et al.* High-throughput retroviral tagging to identify components of specific signaling pathways in cancer. *Nat. Genet.* **32**, 153–159 (2002).

56. Spirli, A. *et al.* The serine-threonine kinase PIM3 is an aldosterone-regulated protein in the distal nephron. *Physiol. Rep.* **7**, 1–14 (2019).

57. Green, A. S. *et al.* Pim kinases modulate resistance to FLT3 tyrosine kinase inhibitors in FLT3-ITD acute myeloid leukemia. *Sci. Adv.* **1**, 1–14 (2015).

58. Wang, J. *et al.* Pim1 kinase is required to maintain tumorigenicity in MYC-expressing prostate cancer cells. *Oncogene* **31**, 1794–1803 (2012).

59. An, N., Kraft, A. S. & Kang, Y. Abnormal hematopoietic phenotypes in Pim kinase triple knockout mice. *J. Hematol. Oncol.* **6**, 1–10 (2013).

60. Möröy, T., Grzeschiczek, A., Petzold, S. & Hartmann, K. U. Expression of a Pim-1 transgene accelerates lymphoproliferation and inhibits apoptosis in lpr/lpr mice. *Proc. Natl. Acad. Sci. U. S. A.* **90**, 10734–10738 (1993).

61. Verbeek, S. *et al.* Mice Bearing the Ep.-myc and E,u-pim-l Transgenes Develop Pre-B-Cell Leukemia Prenatally. *Mol. Cell. Biol.* **11**, 1176–1179 (1991).

62. van Lohuizen, M. *et al.* Predisposition to lymphomagenesis in pim-1 transgenic mice: Cooperation with c-myc and N-myc in murine leukemia virus-induced tumors. *Cell* **56**, 673–682 (1989).

63. Liso, A. *et al.* Aberrant somatic hypermutation in tumor cells of nodular-lymphocyte-predominant and classic Hodgkin lymphoma. *Blood* **108**, 1013–1020 (2006).

64. Pasqualucci, L. Molecular pathogenesis of germinal center-derived B cell lymphomas. *Immunol. Rev.* **288**, 240–261 (2019).

65. Traverse-Glehen, A. *et al.* Analysis of BCL-6, CD95, PIM1, RHO/TTF and PAX5 mutations in splenic and nodal marginal zone B-cell lymphomas suggests a particular B-cell origin [3]. *Leukemia* **21**, 1821–1824 (2007).

66. Wang, W. *et al.* Cell-Free DNA in Cerebrospinal Fluid Complements the Monitoring Value of Interleukin-10 in Newly Diagnosed Primary Central Nervous System Lymphoma. *J. Oncol.* **2023**, (2023).

67. Kumar, A. *et al.* Crystal structures of proto-oncogene kinase Pim1: A target of aberrant somatic hypermutations in diffuse large cell lymphoma. *J. Mol. Biol.* **348**, 183–193 (2005).

68. Zhang, Y., Wang, Z., Li, X. & Magnuson, N. S. Pim kinase-dependent inhibition of c-Myc degradation. *Oncogene* **27**, 4809–4819 (2008).

69. Zippo, A. *et al.* Histone Crosstalk between H3S10ph and H4K16ac Generates a Histone Code that Mediates Transcription Elongation. *Cell* **138**, 1122–1136 (2009).

70. Zippo, A., Robertis, A. De, Serafini, R. & Oliviero, S. PIM1-dependent phosphorylation of histone H3 at serine 10 is required for MYC-dependent transcriptional activation and oncogenic transformation. *Nat. Cell Biol.* **9**, 932–944 (2007).

71. Choi, P. S. *et al.* Lymphomas that recur after MYC suppression continue to exhibit oncogene addiction. *Proc. Natl. Acad. Sci. U. S. A.* **108**, 17432–17437 (2011).

72. Sewastianik, T., Prochorec-Sobieszek, M., Chapuy, B. & Juszczyński, P. MYC deregulation in lymphoid tumors: Molecular mechanisms, clinical consequences and therapeutic implications. *Biochim. Biophys. Acta - Rev. Cancer* **1846**, (2014).

73. Nihira, K. *et al.* Pim-1 controls NF-B signalling by stabilizing RelA/p65. *Cell Death Differ.* **17**, 689–698 (2010).

74. Szydłowski, M. *et al.* PIM Kinases Promote Survival and Immune Escape in Primary Mediastinal Large B-Cell Lymphoma through Modulation of JAK-STAT and NF-κB Activity. *Am. J. Pathol.* **191**, 567–574 (2021).

75. Szydłowski, M. *et al.* Expression of PIM kinases in Reed-Sternberg cells fosters immune privilege and tumor cell survival in Hodgkin lymphoma. *Blood* **130**, 1418–1429 (2017).

76. Guo, Z. *et al.* PIM inhibitors target CD25-positive AML cells through concomitant suppression of STAT5 activation and degradation of MYC oncogene. *Blood* **124**, 1777–1789 (2014).

77. Chang, M. *et al.* PIM kinase inhibitors downregulate STAT3Tyr705 phosphorylation. *Mol. Cancer Ther.* **9**, 2478–2487 (2010).

78. Li, Z. *et al.* PIM1 Kinase Phosphorylates the Human Transcription Factor FOXP3 at Serine 422 to Negatively Regulate Its Activity under Inflammation. *J. Biol. Chem.* **289**, 26872–26881 (2014).

79. Morishita, D., Katayama, R., Sekimizu, K., Tsuruo, T. & Fujita, N. Pim kinases promote cell cycle progression by phosphorylating and down-regulating p27kip1 at the transcriptional and posttranscriptional levels. *Cancer Res.* **68**, 5076–5085 (2008).

80. Kabrani, E. *et al.* Nuclear FOXO1 promotes lymphomagenesis in germinal center B cells. *Blood* **132**, 2670–2683 (2018).

81. Sander, S. *et al.* PI3 Kinase and FOXO1 Transcription Factor Activity Differentially Control B Cells in the Germinal Center Light and Dark Zones. *Immunity* **43**, 1075–1086 (2015).

82. Szydlowski, M. *et al.* FOXO1 activation is an effector of SYK and AKT inhibition in tonic BCR signal-dependent diffuse large B-cell lymphomas. *Blood* **127**, 739–748 (2016).

83. Darwiche, N. Epigenetic mechanisms and the hallmarks of cancer: an intimate affair. *Am. J. Cancer Res.* **10**, 1954–1978 (2020).

84. Hanahan, D. Hallmarks of Cancer: New Dimensions. *Cancer Discov.* **12**, 31–46 (2022).

85. Zhang, Y., Wang, Z. & Magnuson, N. S. Pim-1 kinase-dependent phosphorylation of p21Cip1/WAF1 regulates its stability and cellular localization in H1299 cells. *Mol. Cancer Res.* **5**, 909–922 (2007).

86. Liu, Z. *et al.* Downregulation of Pim-2 induces cell cycle arrest in the G0/G1 phase via the p53-non-dependent p21 signaling pathway. *Oncol. Lett.* **15**, 4079–4086 (2018).

87. Levy, D. *et al.* Activation of cell cycle arrest and apoptosis by the proto-oncogene Pim-2. *PLoS One* **7**, (2012).

88. Mochizuki, T. *et al.* Physical and functional interactions between pim-1 kinase and Cdc25A phosphatase. Implications for the Pim-1-mediated activation of the c-Myc signaling pathway. *J. Biol. Chem.* **274**, 18659–18666 (1999).

89. Bachmann, M. *et al.* The oncogenic serine/threonine kinase Pim-1 directly phosphorylates and activates the G2/M specific phosphatase Cdc25C. *Int. J. Biochem. Cell Biol.* **38**, 430–443 (2006).

90. Wood, N. T., Meek, D. W. & MacKintosh, C. 14-3-3 Binding to Pim-phosphorylated Ser166 and Ser186 of human Mdm2 - Potential interplay with the PKB/Akt pathway and p14ARF. *FEBS Lett.* **583**, 615–620 (2009).

91. Hogan, C. *et al.* Elevated levels of oncogenic protein kinase Pim-1 induce the p53 pathway in cultured cells and correlate with increased Mdm2 in mantle cell lymphoma. *J. Biol. Chem.* **283**, 18012–18023 (2008).

92. Aho, T. L. T. *et al.* Pim-1 kinase promotes inactivation of the pro-apoptotic Bad protein by phosphorylating it on the Ser112 gatekeeper site. *FEBS Lett.* **571**, 43–49 (2004).

93. Macdonald, A. *et al.* Pim kinases phosphorylate multiple sites in Bad and promote 14-3-3 binding and dissociation from Bcl-XL. *BMC Cell Biol.* **7**, 1–14 (2006).

94. Gu, J. J., Wang, Z., Reeves, R. & Magnuson, N. S. PIM1 phosphorylates and negatively regulates ASK1-mediated apoptosis. *Oncogene* **28**, 4261–4271 (2009).

95. Tamburini, J. *et al.* Protein synthesis is resistant to rapamycin and constitutes a promising therapeutic target in acute myeloid leukemia. *Blood* **114**, 1618–1627 (2009).

96. Cao, L. *et al.* PIM1 kinase promotes cell proliferation, metastasis and tumor growth of lung adenocarcinoma by potentiating the c-MET signaling pathway. *Cancer Lett.* **444**, 116–126 (2019).

97. Zhang, F. *et al.* PIM1 protein kinase regulates PRAS40 phosphorylation and mTOR activity in FDCP1 cells. *Cancer Biol. Ther.* **8**, 846–853 (2009).

98. Lu, J. *et al.* Pim2 is required for maintaining multiple myeloma cell growth through modulating TSC2 phosphorylation. *Blood* **122**, 1610–1620 (2013).

99. Natarajan, K. *et al.* The Pim kinase inhibitor SGI-1776 decreases cell surface expression of P-glycoprotein (ABCB1) and breast cancer resistance protein (ABCG2) and drug transport by Pim-1-dependent and -independent mechanisms. *Biochem. Pharmacol.* **85**, 514–524 (2013).

100. Xie, Y. *et al.* The 44-kDa Pim-1 kinase phosphorylates BCRP/ABCG2 and thereby promotes its multimerization and drug-resistant activity in human prostate cancer cells. *J. Biol. Chem.* **283**, 3349–3356 (2008).

101. Xie, Y., Burcu, M., Linn, D. E., Qiu, Y. & Baer, M. R. Pim-1 kinase protects P-glycoprotein from degradation and enables its glycosylation and cell surface expression. *Mol. Pharmacol.* **78**, 310–318 (2010).

102. Marayati, R. *et al.* PIM kinases mediate resistance to cisplatin chemotherapy in hepatoblastoma. *Sci. Rep.* **11**, 1–14 (2021).

103. Leung, C. O. ning *et al.* PIM1 regulates glycolysis and promotes tumor progression in hepatocellular carcinoma. *Oncotarget* **6**, 10880–10892 (2015).

104. Markou, A. *et al.* PIM-1 is overexpressed at a high frequency in circulating tumor cells from metastatic castration- resistant prostate cancer patients. *Cancers (Basel).* **12**, 1–14 (2020).

105. Jiang, R., Wang, X., Jin, Z. & Li, K. Association of nuclear PIM1 expression with lymph node metastasis and poor prognosis in patients with lung adenocarcinoma and squamous cell carcinoma. *J. Cancer* **7**, 324–334 (2016).

106. Zhao, B. *et al.* PIM1 mediates epithelial-mesenchymal transition by targeting Smads and c-Myc in the nucleus and potentiates clear-cell renal-cell carcinoma oncogenesis article. *Cell Death Dis.* **9**, (2018).

107. Ledet, R. J. *et al.* Identification of PIM1 substrates reveals a role for NDRG1 phosphorylation in prostate cancer cellular migration and invasion. *Commun. Biol.* **4**, 1–12 (2021).

108. Santio, N. M. *et al.* PIM1 accelerates prostate cancer cell motility by phosphorylating actin

capping proteins. *Cell Commun. Signal.* **18**, 1–18 (2020).

109. Ai, B. *et al.* SEdb: a comprehensive human super-enhancer database. *Nucleic Acids Res.* **47**, D235–D243 (2018).

110. Ruff, S. E., Vasilyev, N., Nudler, E., Logan, S. K. & Garabedian, M. J. PIM1 phosphorylation of the androgen receptor and 14-3-3 ζ regulates gene transcription in prostate cancer. *Commun. Biol.* **4**, (2021).

111. Ha, S. *et al.* Phosphorylation of the androgen receptor by PIM1 in hormone refractory prostate cancer. *Oncogene* **32**, 3992–4000 (2013).

112. Koike, N., Maita, H., Taira, T., Ariga, H. & Iguchi-Ariga, S. M. M. Identification of heterochromatin protein 1 (HP1) as a phosphorylation target by Pim-1 kinase and the effect of phosphorylation on the transcriptional repression function of HP1. *FEBS Lett.* **467**, 17–21 (2000).

113. Yang, J. *et al.* PIM1 induces cellular senescence through phosphorylation of UHRF1 at Ser311. *Oncogene* **36**, 4828–4842 (2017).

114. Foulks, J. M. *et al.* A Small-Molecule Inhibitor of PIM Kinases as a Potential Treatment for Urothelial Carcinomas. *Neoplasia (United States)* **16**, 403–412 (2014).

115. Cortes, J. *et al.* Phase i studies of AZD1208, a proviral integration Moloney virus kinase inhibitor in solid and haematological cancers. *Br. J. Cancer* **118**, 1425–1433 (2018).

116. Raab, M. S. *et al.* The first-in-human study of the pan-PIM kinase inhibitor PIM447 in patients with relapsed and/or refractory multiple myeloma. *Leukemia* **33**, 2924–2933 (2019).

117. Iida, S. *et al.* A phase I, dose-escalation study of oral PIM447 in Japanese patients with relapsed and/or refractory multiple myeloma. *Int. J. Hematol.* **113**, 797–806 (2021).

118. Clements, A. N. & Warfel, N. A. Targeting PIM Kinases to Improve the Efficacy of Immunotherapy. *Cells* **11**, 1–12 (2022).

119. Czardybon, W. *et al.* A novel, dual pan-PIM/FLT3 inhibitor SEL24 exhibits broad therapeutic potential in acute myeloid leukemia. *Oncotarget* **9**, 16917–16931 (2018).

120. Martinelli, G. *et al.* Phase 1 / 2 study of SEL24 / MEN1703 , a first-in-class dual PIM / FLT3 kinase inhibitor , in patients with IDH1 / 2 -mutated acute myeloid leukemia : The DIAMOND-01 trial . *J. Clin. Oncol.* **40**, 7024–7024 (2022).

121. Białopiotrowicz, E. *et al.* Microenvironment-induced PIM kinases promote CXCR4-triggered mTOR pathway required for chronic lymphocytic leukaemia cell migration. *J. Cell. Mol. Med.* **22**, 3548–3559 (2018).

122. Rieger, M. A. & Schroeder, T. Hematopoiesis. *Cold Spring Harb. Perspect. Biol.* **4**, (2012).

123. Sharma, S. & Gurudutta, G. Epigenetic Regulation of Hematopoietic Stem Cells. *Int. J. Stem Cells* **9**, (2016).

124. Cico, A., Andrieu-Soler, C. & Soler, E. Enhancers and their dynamics during hematopoietic differentiation and emerging strategies for therapeutic action. **590**, 4084–4104 (2016).

125. Boller, S., Li, R. & Grosschedl, R. Defining B Cell Chromatin: Lessons from EBF1. *Trends Genet.* **34**, 257–269 (2018).

126. Novo, C. L. *et al.* Long-Range Enhancer Interactions Are Prevalent in Mouse Embryonic Stem Cells and Are Reorganized upon Pluripotent State Transition Article Long-Range Enhancer

Interactions Are Prevalent in Mouse Embryonic Stem Cells and Are Reorganized upon Pluripotent St. *CellReports* **22**, 2615–2627 (2018).

127. Pasqualucci, L. The Genetic Basis of Diffuse Large B Cell Lymphoma. *Curr. Opin. Hematol.* **20**, 336 (2013).

128. Swerdlow, S. H. *et al.* WHO Classification of Tumours of the Haematopoietic and Lymphoid Tissues The 2016 revision of the World Health Organization classi fi cation of lymphoid neoplasms. **127**, 2375–2391 (2016).

129. Reddy, A. *et al.* Genetic and Functional Drivers of Diffuse Large B Cell Lymphoma. *Cell* **171**, 481-494.e15 (2017).

130. Duan, Q., Chen, H., Costa, M. & Dai, W. Phosphorylation of H3S10 blocks the access of H3K9 by specific antibodies and histone methyltransferase. Implication in regulating chromatin dynamics and epigenetic inheritance during mitosis. *J. Biol. Chem.* **283**, 33585–90 (2008).

131. Komar, D. & Juszczynski, P. Rebelled epigenome: histone H3S10 phosphorylation and H3S10 kinases in cancer biology and therapy. *Clin. Epigenetics* **12**, 1–14 (2020).

132. Wiersma, M. *et al.* Protein kinase Msk1 physically and functionally interacts with the KMT2A/MLL1 methyltransferase complex and contributes to the regulation of multiple target genes. *Epigenetics and Chromatin* **9**, 1–12 (2016).

133. Chen, C. C. L. *et al.* H3S10ph broadly marks early-replicating domains in interphase ESCs and shows reciprocal antagonism with H3K9me2. *Genome Res.* **28**, 37–51 (2018).

134. Beacon, T. H. *et al.* The dynamic broad epigenetic (H3K4me3, H3K27ac) domain as a mark of essential genes. *Clin. Epigenetics* **13**, 1–18 (2021).

135. Kassouf, M. T., Francis, H. S., Gosden, M., Suciu, M. C. & Damien, J. Multipartite super-enhancers function in an orientation-dependent manner. (2022).

136. Hu, X. *et al.* Histone cross-talk connects protein phosphatase 1α (PP1α) and histone deacetylase (HDAC) pathways to regulate the functional transition of bromodomain-containing 4 (BRD4) for inducible gene expression. *J. Biol. Chem.* **289**, 23154–23167 (2014).

137. Feldman, J. D. *et al.* KID-1, a protein kinase induced by depolarization in brain. *J. Biol. Chem.* **273**, 16535–16543 (1998).

138. Deneen, B. *et al.* PIM3 Proto-Oncogene Kinase Is a Common Transcriptional Target of Divergent EWS/ETS Oncoproteins. *Mol. Cell. Biol.* **23**, 3897–3908 (2003).

139. Whyte, W. A. *et al.* Master Transcription Factors and Mediator Establish Super- Enhancers at Key Cell Identity Genes. *Cell* **153**, 307–319 (2013).

140. Lovén, J. *et al.* Selective Inhibition of Tumor Oncogenes by Disruption of Super- Enhancers. *Cell* **153**, 320–334 (2013).

141. McKeown, M. R. *et al.* Superenhancer analysis defi nes novel epigenomic subtypes of non-APL AML, including an RARα dependency targetable by SY-1425, a potent and selective RARα agonist. *Cancer Discov.* **7**, 1136–1153 (2017).

142. Henriques, T. *et al.* Widespread transcriptional pausing and elongation control at enhancers. *Genes Dev.* **32**, 26–41 (2018).

143. Hnisz, D. *et al.* Transcriptional super-enhancers connected to cell identity and disease. *Cell* **155**, 1–24 (2013).

144. Zhang, J. *et al.* Super enhancers—Functional cores under the 3D genome. *Cell Prolif.* **54**, 1–11 (2021).

145. Hnisz, D., Shrinivas, K., Young, R. A., Chakraborty, A. K. & Sharp, P. A. A Phase Separation Model for Transcriptional Control. *Cell* **169**, 13–23 (2017).

146. Shu, S. *et al.* Response and resistance to BET bromodomain inhibitors in triple-negative breast cancer. *Nature* **529**, 413–417 (2016).

147. Arnold, P. R., Wells, A. D. & Li, X. C. Diversity and Emerging Roles of Enhancer RNA in Regulation of Gene Expression and Cell Fate. *Front. Cell Dev. Biol.* **7**, 1–14 (2020).

148. Sabari, B. R. *et al.* Coactivator condensation at super-enhancers links phase separation and gene control. *Science (80-.).* **361**, (2018).

149. Boija, A. *et al.* Transcription Factors Activate Genes through the Phase-Separation Capacity of Their Activation Domains. *Cell* **175**, 1842-1855.e16 (2018).

150. Ahn, J. H. *et al.* Phase separation drives aberrant chromatin looping and cancer development. *Nature* **595**, 591–595 (2021).

151. Bradner, J. E., Hnisz, D., Young & A., R. Transcriptional Addiction in Cancer. *Cell* **168**, 629–643 (2017).

152. Christensen, C. L. *et al.* Targeting Transcriptional Addictions in Small Cell Lung Cancer with a Covalent CDK7 Inhibitor. *Cancer Cell* **26**, 909–922 (2014).

153. Wang, Y. *et al.* CDK7-Dependent Transcriptional Addiction in Triple-Negative Breast Cancer. *Cell* **163**, 174–186 (2015).

154. Shorstova, T., Foulkes, W. D. & Witcher, M. Achieving clinical success with BET inhibitors as anti-cancer agents. *Br. J. Cancer* **124**, 1478–1490 (2021).

155. Dębek, S. & Juszczyński, P. Super enhancers as master gene regulators in the pathogenesis of hematologic malignancies. *Biochim. Biophys. Acta - Rev. Cancer* **1877**, (2022).

156. Reich, M. *et al.* GenePattern 2.0 [2]. *Nat. Genet.* **38**, 500–501 (2006).

157. Subramanian, A. *et al.* Gene set enrichment analysis: A knowledge-based approach for interpreting genome-wide expression profiles. *Proc. Natl. Acad. Sci. U. S. A.* **102**, 15545–15550 (2005).

158. Chapuy, B. *et al.* Discovery and Characterization of Super-Enhancer-Associated Dependencies in Diffuse Large B Cell Lymphoma. *Cancer Cell* **24**, 777–790 (2013).

159. Love, M. I., Huber, W. & Anders, S. Moderated estimation of fold change and dispersion for RNA-seq data with DESeq2. *Genome Biol.* **15**, 1–21 (2014).

160. Durinck, S., Spellman, P. T., Birney, E. & Huber, W. Mapping identifiers for the integration of genomic datasets with the R / Bioconductor package biomaRt. (2009). doi:10.1038/nprot.2009.97

161. Durinck, S. *et al.* BioMart and Bioconductor : a powerful link between biological databases and microarray data analysis. **21**, 3439–3440 (2005).

162. Quinlan, A. R. & Hall, I. M. BEDTools: A flexible suite of utilities for comparing genomic features. *Bioinformatics* **26**, 841–842 (2010).

163. Wickham, H. *ggplot2: Elegant Graphics for Data Analysis*. (Springer-Verlag New York, 2016).

164. Luo, W., Friedman, M. S., Shedden, K., Hankenson, K. D. & Woolf, P. J. GAGE: Generally applicable gene set enrichment for pathway analysis. *BMC Bioinformatics* **10**, 1–17 (2009).

165. Jalili, V. *et al.* The Galaxy platform for accessible, reproducible and collaborative biomedical analyses: 2020 update. *Nucleic Acids Res.* **48**, W395–W402 (2021).

166. Altendorfer, E., Mochalova, Y. & Mayer, A. BRD4: a general regulator of transcription elongation. *Transcription* **13**, 70–81 (2022).

167. Nie, Z. *et al.* Dissecting transcriptional amplification by MYC. *Elife* **9**, 1–32 (2020).

168. Metz, J. T. & Hajduk, P. J. Rational approaches to targeted polypharmacology: Creating and navigating protein-ligand interaction networks. *Curr. Opin. Chem. Biol.* **14**, 498–504 (2010).

169. Peón, A., Naulaerts, S. & Ballester, P. J. Predicting the Reliability of Drug-target Interaction Predictions with Maximum Coverage of Target Space. *Sci. Rep.* **7**, 1–11 (2017).

170. Shi, L., Wen, H. & Shi, X. The histone variant H3.3 in transcriptional regulation and human disease. *J. Mol. Biol.* **429**, 1934–1945 (2017).

171. Demaison, C. *et al.* High-level transduction and gene expression in hematopoietic repopulating cells using a human imunodeficiency virus type 1-based lentiviral vector containing an internal spleen focus forming virus promoter. *Hum. Gene Ther.* **13**, 803–813 (2002).

172. Jenuwein, T. & Allis, C. D. Translating the Histone Code. **293**, 1074–1081 (2001).

173. Gates, L. A. *et al.* Acetylation on histone H3 lysine 9 mediates a switch from transcription initiation to elongation. *J. Biol. Chem.* **292**, 14456–14472 (2017).

174. Casillas, A. L. *et al.* Direct phosphorylation and stabilization of HIF-1α by PIM1 kinase drives angiogenesis in solid tumors. *Oncogene* **40**, 5142–5152 (2021).

175. Castillo, D. S. *et al.* E2F1 and E2F2 induction in response to DNA damage preserves genomic stability in neuronal cells E2F1 and E2F2 induction in response to DNA damage preserves genomic stability in neuronal cells. **4101**, (2015).

176. Weintraub, A. S. *et al.* YY1 Is a Structural Regulator of Enhancer-Promoter Loops. *Cell* **172**, 1573–1588 (2017).

177. Han, J. *et al.* YY1 Complex Promotes Quaking Expression via Super-Enhancer Binding during EMT of Hepatocellular Carcinoma. *Cancer Res.* **79**, 1451–1464 (2019).

178. Castro, E. De *et al.* ScanProsite : detection of PROSITE signature matches and ProRule-associated functional and structural residues in proteins. **34**, 362–365 (2006).

179. Chen, H. & Liang, H. A High-Resolution Map of Human Enhancer RNA Loci Characterizes Super-enhancer Activities in Cancer. *Cancer Cell* **0**, 1–15 (2020).

180. Alvarez-Dominguez, J. R., Knoll, M., Gromatzky, A. A. & Lodish, H. F. The Super-Enhancer-Derived alncRNA-EC7/ Bloodlinc Potentiates Red Blood Cell Development in trans. *Cell Rep.* **19**, 2503–2514 (2017).

181. Mah, L. J., El-Osta, A. & Karagiannis, T. C. γh2AX: A sensitive molecular marker of DNA damage and repair. *Leukemia* **24**, 679–686 (2010).

182. Walter, W. *et al.* 14-3-3 Interaction with Histone H3 Involves a Dual Modification Pattern of Phosphoacetylation . *Mol. Cell. Biol.* **28**, 2840–2849 (2008).

183. Winter, S. *et al.* 14-3-3 Proteins recognize a histone code at histone H3 and are required for transcriptional activation. *EMBO J.* **27**, 88–99 (2008).

184. Iiott, N. E. *et al.* Long non-coding RNAs and enhancer RNAs regulate the lipopolysaccharide-induced inflammatory response in human monocytes. *Nat. Commun.* **5**, (2014).

185. Kim, T. K. *et al.* Widespread transcription at neuronal activity-regulated enhancers. *Nature* **465**, 182–187 (2010).

186. Ren, C. *et al.* Functional annotation of structural ncRNAs within enhancer RNAs in the human genome: Implications for human disease. *Sci. Rep.* **7**, 1–15 (2017).

187. Cichewicz, M. A. *et al.* MUNC, an Enhancer RNA Upstream from the MYOD Gene, Induces a Subgroup of Myogenic Transcripts in trans Independently of MyoD . *Mol. Cell. Biol.* **38**, (2018).

188. Schaukowitch, K. *et al.* Enhancer RNA facilitates NELF release from immediate early genes. *Mol. Cell* **56**, 29–42 (2014).

189. Verheul, T. C. J., Hijfte, L. Van, Perenthaler, E., Barakat, T. S. & Dimitri, P. The Why of YY1 : Mechanisms of Transcriptional Regulation by Yin Yang 1. *Front. Cell Dev. Biol.* **8**, 1–9 (2020).

190. Zirkin, S., Davidovich, A. & Don, J. The PIM-2 Kinase Is an Essential Component of the Ultraviolet Damage Response That Acts Upstream to E2F-1 and ATM * □. **288**, 21770–21783 (2013).

191. Rampal, R. K. *et al.* Therapeutic Efficacy of Combined JAK1 / 2 , Pan-PIM , and CDK4 / 6 Inhibition in Myeloproliferative Neoplasms. *Clin. Canc* **27**, 3456–3468 (2021).

192. Kim, W. *et al.* PIM1 kinase inhibitors induce radiosensitization in non-small cell lung cancer cells. *Pharmacol. Res.* **70**, 90–101 (2013).

193. Haddach, M. *et al.* Discovery of CX-6258. A potent, selective, and orally efficacious pan-pim kinases inhibitor. *ACS Med. Chem. Lett.* **3**, 135–139 (2012).

194. Bader, A. S. & Bushell, M. DNA : RNA hybrids form at DNA double-strand breaks in transcriptionally active loci. *Cell Death Dis.* (2020). doi:10.1038/s41419-020-2464-6

195. Clozel, T. *et al.* Mechanism-Based Epigenetic Chemosensitization Therapy of Diffuse Large B-Cell Lymphoma. *Cancer Discov.* (2013). doi:10.1158/2159-8290.CD-13-0117

196. Pera, B. *et al.* Combinatorial epigenetic therapy in diffuse large B cell lymphoma pre-clinical models and patients. *Clin. Epigenetics* 1–10 (2016). doi:10.1186/s13148-016-0245-y

197. Scholze, H. *et al.* Combined EZH2 and Bcl-2 inhibitors as precision therapy for genetically de fi ned DLBCL subtypes. **4**, 5226–5231 (2020).

198. Xue, L., Wang, M., Xu, H., Yang, L. & Wang, X. Decitabine enhances cytotoxic effect of T cells with an anti-CD19 chimeric antigen receptor in treatment of lymphoma. 5627–5638 (2019).

199. Ghoneim, H. E. *et al.* De Novo Epigenetic Programs Inhibit PD-1 Blockade- Mediated T Cell Rejuvenation. *Cell* **170**, 142-157.e19 (2017).

200. Budde, L. E. *et al.* A phase I study of pulse high-dose vorinostat (V) plus rituximab (R), ifosphamide , carboplatin , and etoposide (ICE) in patients with relapsed lymphoma. (2013). doi:10.1111/bjh.12230

201. Martin, P. *et al.* Phase 1 study of oral azacitidine (CC-486) plus R-CHOP in previously untreated intermediate- to high-risk DLBCL. **139**, 1147–1159 (2022).

202. Bowen, R. C., Hahn, A. W., Butler, T. W. & Khong, H. T. Complete response to azacitidine priming and nab - paclitaxel in non - Hodgkin lymphoma resistant to biochemotherapy. 122–124 (2017). doi:10.3892/mco.2016.1090

203. Trejo-soto, P. J. *et al.* In search of AKT kinase inhibitors as anticancer agents : structure-based design , docking , and molecular dynamics studies of 2 , 4 , 6-trisubstituted pyridines. *J. Biomol. Struct. Dyn.* **1102**, 1–20 (2017).

204. Wu, P., Nielsen, T. E. & Clausen, M. H. FDA-approved small-molecule kinase inhibitors. *Trends Pharmacol. Sci.* **36**, 422–439 (2015).

205. Wu, P., Nielsen, T. E. & Clausen, M. H. Small-molecule kinase inhibitors: an analysis of FDA-approved drugs. *Drug Discov. Today* **21**, (2015).

206. Zhang, X., Song, M., Kundu, J. K., Lee, M.-H. & Liu, Z.-Z. PIM Kinase as an Executional Target in Cancer. *J. Cancer Prev.* **23**, 109–116 (2018).

207. Barros, E. M., Mcintosh, S. A. & Savage, K. I. The DNA damage induced immune response : Implications for cancer therapy. *DNA Repair (Amst).* **120**, 103409 (2022).

SEER- https://seer.cancer.gov/statfacts/html/dlbcl.html